STUDIES OF THE INTERACTIONS OF SILICON WITH H, H_2 AND O USING A NOVEL RF PROBE TECHNIQUE

BY

HONGJUN LI

B.Sc., Tsinghua University, 1986

M.Sc., Tsinghua University, 1989

A THESIS SUBMITTED IN PARTIAL FULFILLMENT OF
THE REQUIREMENTS FOR THE DEGREE OF
DOCTOR OF PHILOSOPHY

in

THE FACULTY OF GRADUATE STUDIES

Department of Chemistry

We accept this thesis as conforming
to the required standard

THE UNIVERSITY OF BRITISH COLUMBIA

October 1997

In presenting this thesis in partial fulfilment of the requirements for an advanced degree at the University of British Columbia, I agree that the Library shall make it freely available for reference and study. I further agree that permission for extensive copying of this thesis for scholarly purposes may be granted by the head of my department or by his or her representatives. It is understood that copying or publication of this thesis for financial gain shall not be allowed without my written permission.

Department of Chemistry

The University of British Columbia
Vancouver, Canada

Date Dec 23, 1997

Abstract

A radio frequency technique was developed for measuring steady state, photo-induced, free carrier densities in indirect-bandgap semiconductors. This new *in situ* technique was then used to study the effects of H-atoms on the SiO_2/Si interfacial trap densities and to study the silicon surface and bulk chemistry during gate oxide growth with a remote O_2 plasma, annealing in H_2, and the effect of the exposure of silicon substrates to atomic hydrogen. It is found that:

(1) Gate oxides with interface trap levels that are as low as those present in thermally grown oxides can be grown at temperatures below 450 °C with atomic oxygen and subsequent annealing in the presence of H_2.

(2) Boron in p-type silicon can be passivated by hydrogen, which is present in the bulk when the crystal is annealed at temperatures between 360 and 450 °C, forming a B-H complex. Dissociation of the B-H complex at temperatures above 450 °C re-activates the boron as an acceptor.

(3) Adsorption of O_2 and H_2 on freshly cleaned p-type silicon surfaces decreased the photo-generated carrier concentration which is interpreted in terms of an increase in the width of the depletion layer at the surface.

(4) Exposure of a SiO_2/Si interface to H-atoms resulted in the formation of carrier traps other than P_b centers. At temperatures below 100 °C trap formation rates were found to show a first order dependence on the H-atom concentration with an activation energy of 0.15 ± 0.02 eV. At higher temperatures, the reverse reaction and another process, which also reduces the traps formed by H-atoms, were observed. The kinetics and mechanisms of these processes are discussed in detail.

Table of Contents

List of Figures

List of Tables

Acknowledgments

I would like to thank Professor Elmer Ogryzlo for his guidance and continued enthusiasm throughout the course of this study.

My thanks also extend to:

Professor Tom Tiedje for the valuable discussions on radio frequency technique for measuring photo-induced carriers in silicon.

Dr. John Cook for giving me an opportunity to visit the Institute for Microstructural Sciences at NRC.

Dr. Dolf Landheer for the discussions on the mechanism of interfacial trap formation.

I would like to acknowledge the electronic, glass blowing and mechanical shops for their assistance in constructing the experimental apparatus necessary for the collection of the data presented in this thesis.

Chapter 1 Introduction

1.1 Semiconductors and semiconductor devices

Modern microelectronic technology is made possible by the existence of semiconductors. Semiconductors are crystalline substances whose conductivity can be controlled by doping, the deliberate addition of impurities. Dopants affect conductivity because they have a different number of valence electrons than the atoms of the host crystal. These extra electrons or missing bonding electrons that result from the presence of dopants become free charge carriers which conduct electricity. The operation of a semiconductor device is an art concerned with the manipulation of its carrier density, with the aim of controlling the device's ability to conduct and store charge.

1.1.1 Band gaps of semiconductors

The energetic relations in a semiconductor may be understood by starting from an atom. The electrons in an atom can occupy only certain energy states determined by the laws of quantum mechanics, as illustrated on the left hand side of Figure 1.1. When two atoms are close to one another their electronic wave functions can interact. The number of states of the pair remains the same, but their energies are slightly different from those of the separated atoms. When the interaction is "bonding" some energy levels are raised and some lowered, as shown in the center section of Figure 1.1. The electrons of the two atoms can then occupy only the states at lower energy when the atoms are close together than when they are apart. Since physical

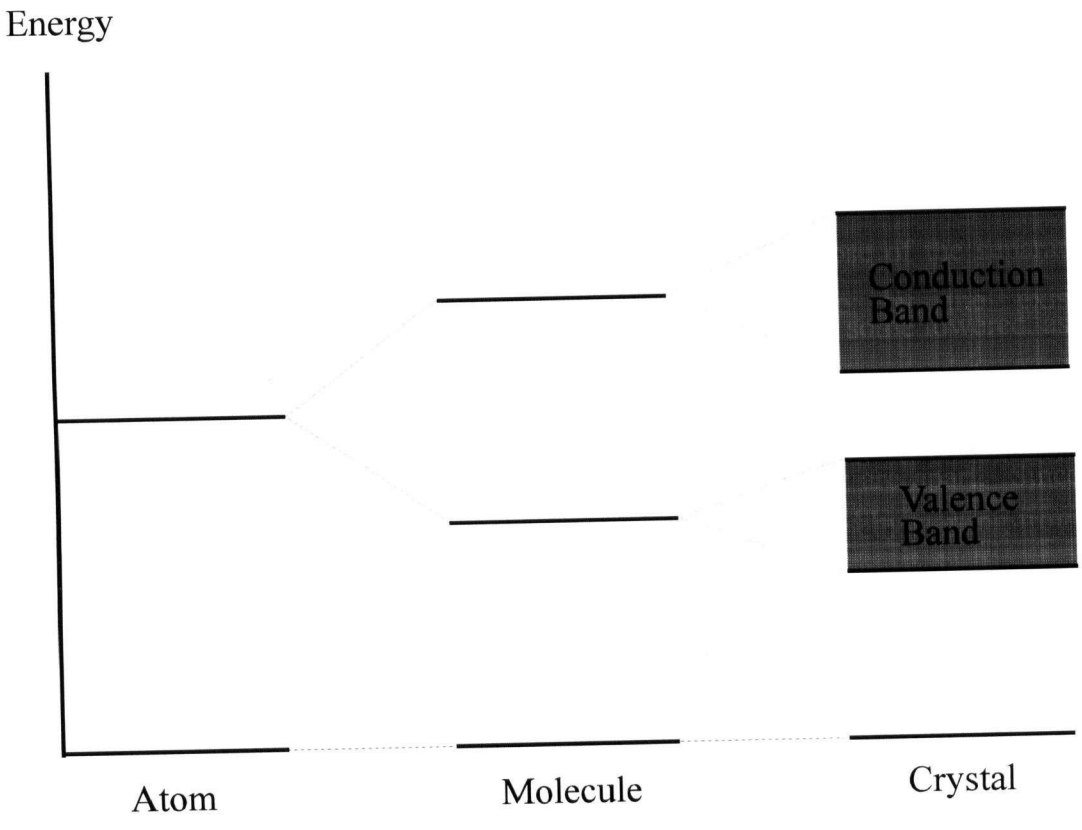

Figure 1.1 The evolution of electronic energy states from atom to molecule to crystal.

systems assume their lowest energy state, a stable state, in this case a molecule, will form.

The right hand side of Figure 1.1 shows the situation in a solid. The concepts that lead to the binding together of two atoms are extended to a much larger number of interacting atoms. The states of the various atoms interact, but there are so many of them that their energies cannot be separately shown or enumerated in any practical way. They can be characterized by their density of states, the number of states per unit volume in a small energy interval. There may be, however, a region of energy that contains no states, as shown in Figure 1.1. These groups of closely spaced energy states are called bands. The lower group of energy states is called the valence band and upper group is called the conduction band. The energy difference between the bottom of the conduction band and the top of the valence band is called the band gap, which plays a vital role in the operation of semiconductor devices.

As the energy states arise from those of the atoms, the number in each band is an integral multiple of the number of atoms. Thus, it frequently turns out that the number of electrons supplied by the atoms is just enough to fill a band exactly. Neither a completely filled band nor a band empty of electrons can conduct electricity. If the band gap is wide enough so that at room temperature the thermal energy is not high enough to excite a significant number of electrons to the conduction band, the material is an insulator. If the band gap is negative so that the valence band overlaps the conduction band, there are many electrons in the conduction band that can conduct electricity, and the material is a conductor. A material whose band gap lies between these two extremes is a semiconductor.

1.1.2 Silicon

Silicon is the fourteenth element of the periodic table; the silicon atom contains fourteen electrons. Ten of these electrons are tightly bound to the atomic nucleus and play no role in silicon chemistry and crystallography. The remaining four electrons are responsible for the bonding of silicon to its neighbors in the crystal. Bonding occurs because the electrons occupy bands lower in energy than the atomic energy levels. In a perfect crystal each silicon atom is bonded to four neighbors. Each bond consists of two electrons; four electrons from each atom are needed to form the bonds. The electrons that are responsible for bonding occupy the valence band.

When a silicon atom is replaced by an atom with five electrons available for bonding, such as a phosphorus or arsenic atom from the VA group of the periodic table, four electrons from the dopant atom enter the valence band and bond the group V atom in its place in the silicon crystal. At room temperature, the extra electron enters the next higher energy band, the conduction band, where it is free to carry electric current. The atom that donates the electron is called a donor and a crystal whose conductivity is due to electrons in the conduction band is said to be n-type.

When a silicon atom is replaced by an atom with only three electrons available for bonding, such as a boron or aluminum atom from the IIIA group of the periodic table, there are not enough electrons in the crystal to fill the valence band completely. The small deficiency in the valence band electron density amounts to a net positive charge and is called a hole. The trivalent impurities are called acceptors, and the conductivity that they produce is known as p-type. A hole is not confined to any particular site, but can move though the crystal, thereby carrying electric current and acting as a positively charged electron. The electrons and holes in

the bands move very much as free particles in space. In the absence of an electrical field, they are at rest at the edges of the bands and their velocity and energy increases with distance into the bands.

The quantity of dopant required to have a marked influence on the conductivity and produce useful electronic devices is very small. The silicon crystal contains 5×10^{22} atoms per cm^3. The doping concentrations used in devices range from around 10^{15} to 10^{20} per cm^3, or from less than one atom in ten million to a fraction of a percent. In spite of the major effect that they have on the electrical properties of the silicon, these numbers are sufficiently small so that the changes in the number of bonding electrons, which provide the forces that hold the crystal together, are negligible. The distribution of energy states and hence the band structure and the mechanical properties of the crystal are not significantly affected by doping levels in this range although there is a small change in the bandgap energy at the highest doping levels.

1.1.3 Occupation of energy bands

The density of states function, defined as the number of states per unit energy interval, in the vicinity of the energy gap, is plotted in Figure 1.2. The holes and electrons near the band edges in some aspects behave like free particles. Their energy, measured from the band edge, is kinetic energy, which is proportional to the square of their effective momentum in the crystal. The density of states in the bands is proportional to the square root of the energy measured from the band edge.

The probability that any given energy level (E) is occupied by an electron is given by the Fermi-Dirac distribution function[1]

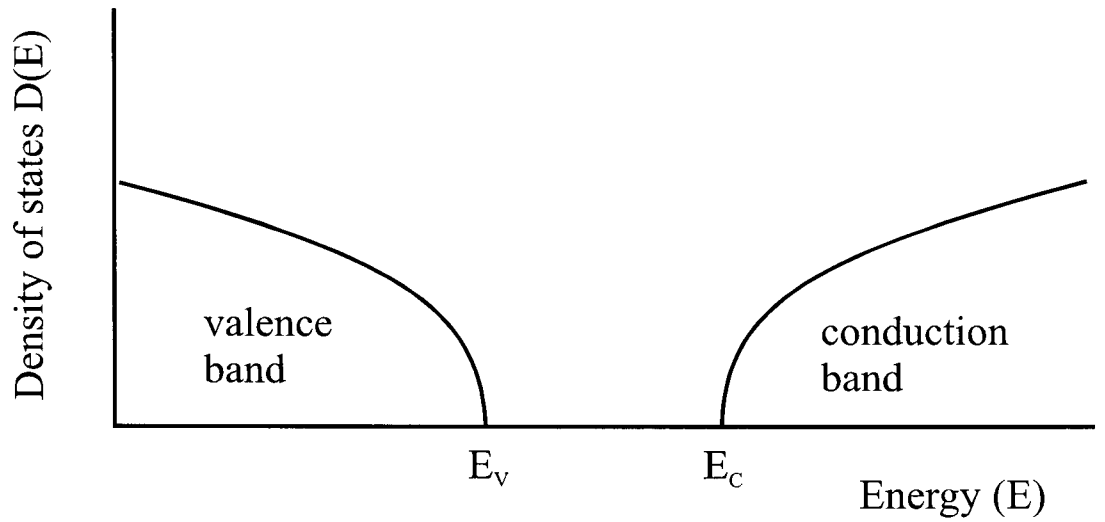

Figure 1.2 The density of states (the number of energy levels per unit energy interval) near the band gap in a semiconductor.

$$F(E) = \frac{1}{e^{\frac{E-E_F}{kT}} + 1} \qquad (1.1)$$

where E_F is the Fermi energy. The position of E_F is determined by the total number of electrons, which is fixed by the doping. At T = 0, F(E) = 1 for $E < E_F$ and F(E) = 0 for $E > E_F$. At room temperature, low energy states, those deep in the valence band of a semiconductor, are completely occupied because F(E) approaches unity when $E - E_F$ is very negative. F(E) is small for high energy states, and near E_F there is a gradual transition from high occupancy to low occupancy.

Figure 1.3 shows the Fermi function F(E), the density of states D(E), and the electron distribution N(E), which is D(E) x F(E), at room temperature. Figure 1.3 (a) shows the situation on an intrinsic semiconductor. The Fermi level is in the center of the bandgap. There are a small number of electrons in the conduction band and an equal number of holes in the valence band. Part (b) shows the situation in lightly doped p-type semiconductor where the Fermi level is near the valence band. The unoccupied states in the valence band are the holes. There are very few electrons in the conduction band because $E - E_F$ is large for those states. In (c) the semiconductor is n-doped so that the Fermi level is near the conduction band. The bottom of the conduction band is filled with electrons from donors. There are a few holes in the valence band.

1.1.4 Minority carriers and lifetimes

Electrons tend to occupy the lowest energy states available, consistent with the Pauli principle. Therefore, the conduction band in a semiconductor is ordinarily occupied by the

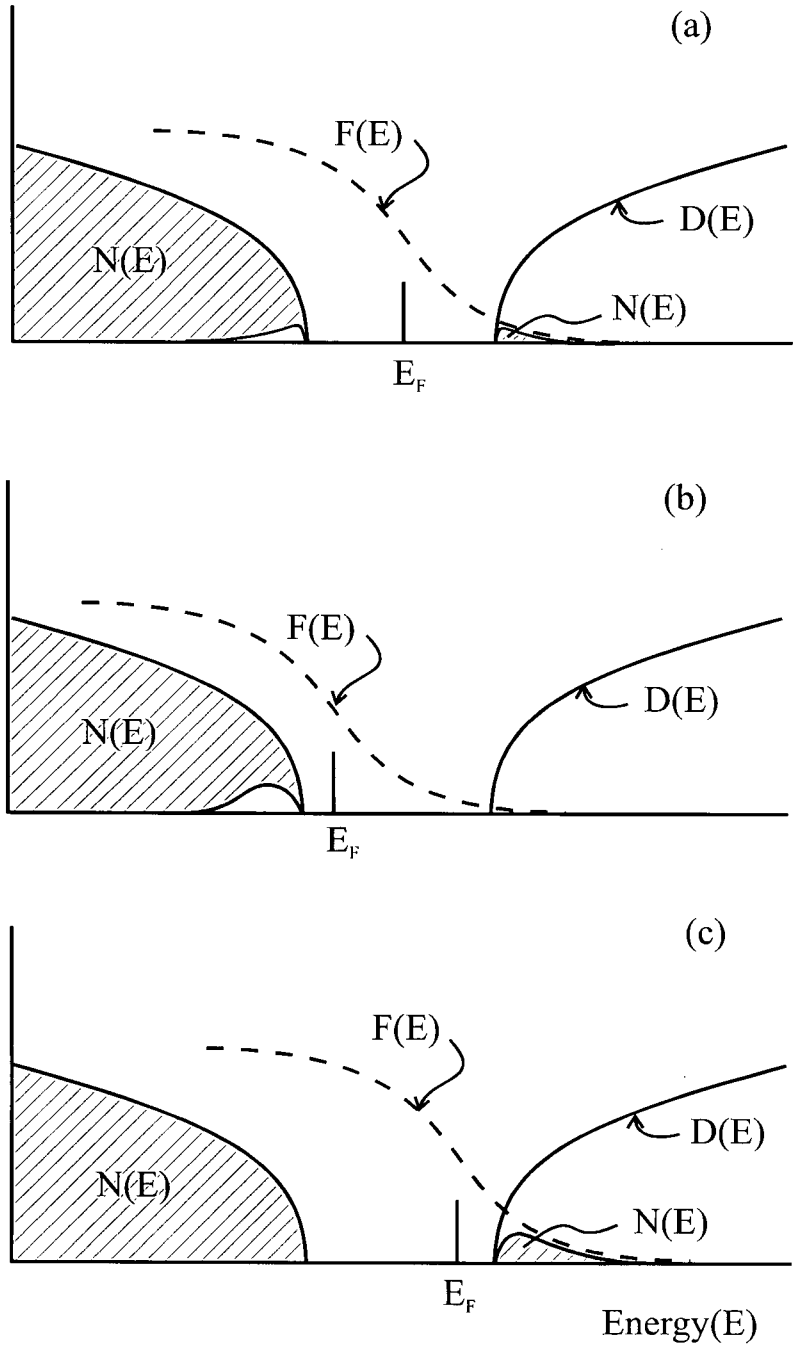

Figure 1.3 The occupancy of the bands in a semiconductor as determined by the Fermi level. The dashed line shows the form of the probability that a state is occupied by an electron (Fermi-Dirac equation). The shading shows the occupied states, the product of the density of states and the occupation probability. (a) An intrinsic semiconductor. (b) A p-type semiconductor. (c) An n-type semiconductor.

smallest possible number of electrons consistent with Fermi statistics, and conversely, the occupation of the valence band is high. This condition can be changed by the injection of energy into the semiconductor. For example, an electron in the valence band can receive energy from light with an energy that exceeds the bandgap. This excites it into the conduction band, an action that creates a hole in the valence band and an electron in the conduction band. Both of these carriers can carry current, and the increase of electrical conductivity under illumination is the well-known phenomenon of photoconductivity. However, the conductivity is transient. If the light is removed, the extra electrons fall back into the valence band, filling the hole states, in a process that is called recombination. Recombination is not instantaneous, it takes a finite and measurable time commonly designated the lifetime, which is defined as the time for the carriers to drop to 1/e of their initial value. Photoconductivity depends on a balance between the rate of excitation by radiation and the rate of recombination.

Carrier lifetimes are one of the important parameters that characterize semiconductor materials. Long lifetimes are found only in high purity material. The lifetimes of greatest interest in semiconductor devices are minority carrier lifetimes, i.e. the lifetimes of electrons in p-type materials or holes in n-type materials. The minority carrier lifetime generally decreases with increasing majority carrier concentration, as there is an increasing probability of recombination. Also, various kinds of impurities and crystalline defects that form electron states near the middle of the energy gap catalyze the recombination and decrease carrier lifetimes. Figure 1.4 shows the range of lifetimes likely to be encountered in silicon as a function of dopant level.

Although long lifetimes are desirable in most cases, there are intrinsic recombination processes in semiconductors that set upper limits on possible values of the lifetime.

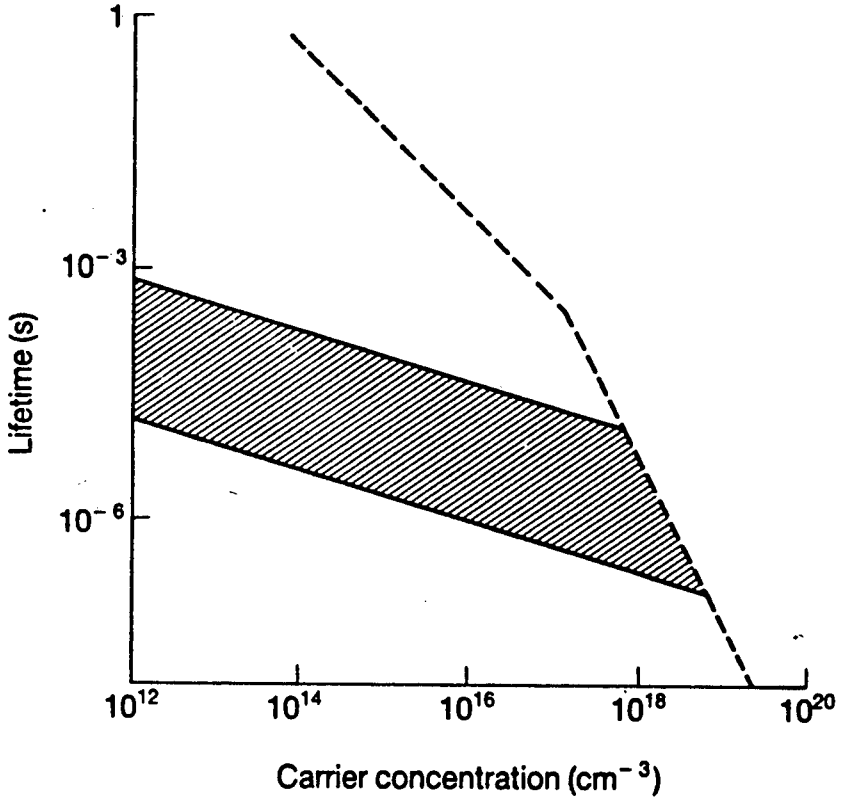

Figure 1.4 Lifetimes in silicon. The limits due to radiative recombination and Auger recombination are indicated in dashed lines. The values usually found in silicon devices lie in the shaded area (after Keyes[9]).

One of these is radiative recombination[2], in which an electron falls from an energy level in the conduction band to an empty energy level in the valence band, with the energy released creating photons:

$$e + h \rightarrow h\nu$$

where e is a free electron, h is a hole, and hν a photon. This kind of recombination is the basis of light emitting diodes and diode lasers. The other intrinsic process is Auger recombination[3], in which the recombination energy is carried away by another majority carrier:

$$e + h + e\,(\text{or } h) \rightarrow e^{*}\ (\text{or } h^{*})$$

1.1.5 The metal-semiconductor contact

Contacts are the basis of semiconductor operations in electronics. The metal-semiconductor contact is the most common contact. A simple model of metal-semiconductor contact was first described by Schottky in the 1930s[4]. Consider a metal and an n-type semiconductor that are not in contact. The potential relations are shown in Figure 1.5 (a), where ϕ_m is the metal work function, q is the charge of an electron, and χ is the electron affinity of semiconductor, i.e. the energy liberated when an electron is placed in the conduction band from the vacuum level.

Now let the metal and the semiconductor be brought into contact. The Fermi levels then coincide and the potentials are as shown in Figure 1.5 (b). Electrons have been transferred from the semiconductor into the metal, leaving a positive charge on the semiconductor and a negative charge on the metal. According to Schottky's theory, a barrier is formed at the contact which is

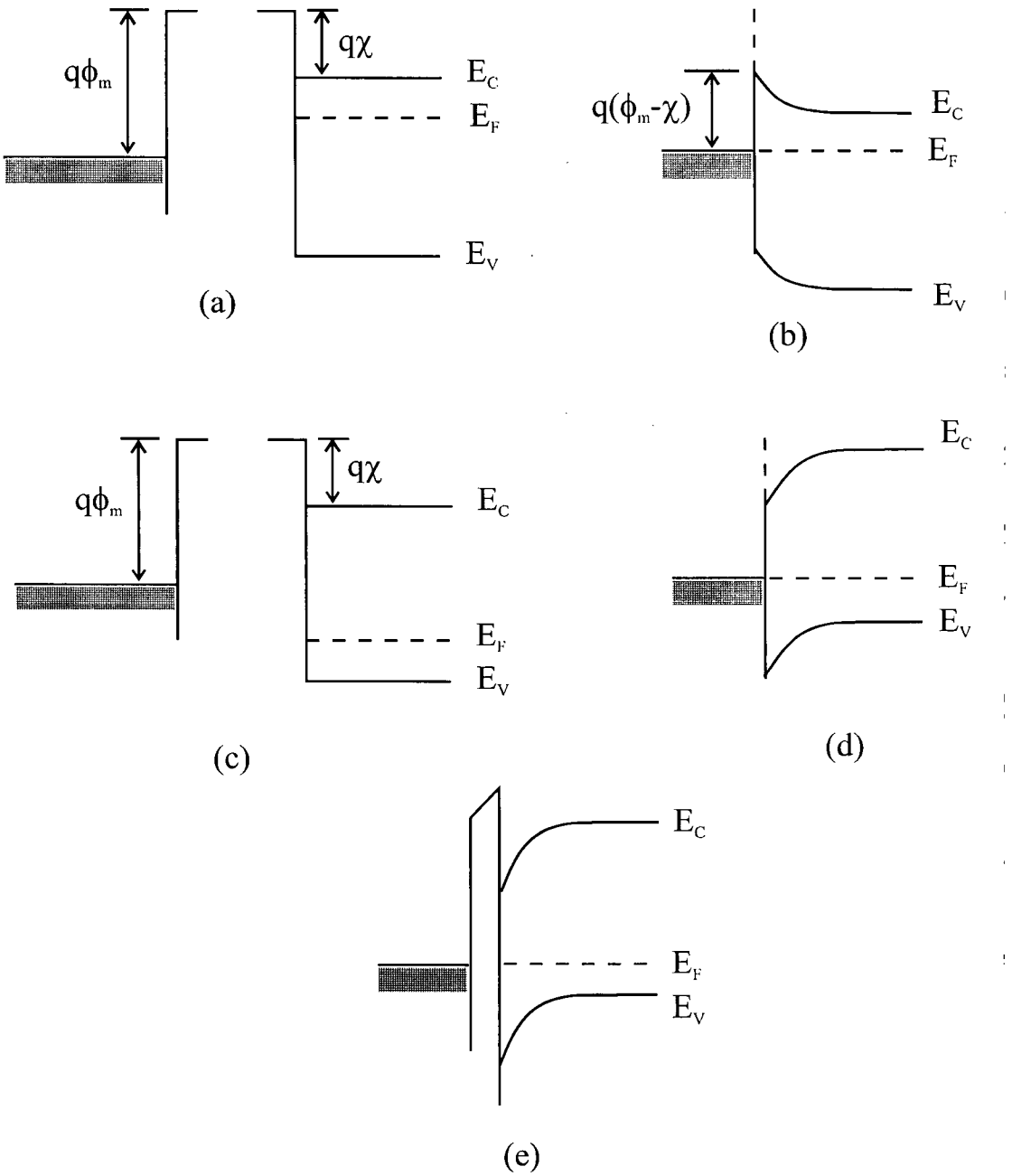

Figure 1.5 The metal-semiconductor contact. (a) Potentials in a metal and an n-type semiconductor that are not electrically connected. (b) Electrical connection aligns the Fermi levels. (c, d) The same relations with a p-type semiconductor. (e) An insulator interposed between the metal and the p-type semiconductor.

measured from the Fermi level of the metal to the conduction band of the semiconductor, and the height of the barrier is given by

$$\phi_B = \phi_m - \chi \tag{1.2}$$

The potential Φ within the semiconductor satisfies Poisson's equation

$$d^2\Phi(x)/dx^2 = Nq/\varepsilon \tag{1.3}$$

where x denotes the distance from the interface, N is the donor density in the bulk, and ε is the dielectric constant of the semiconductor. This relation defines a parabolic band bending region of width w for the metal-semiconductor junction. The solution of Equation (1.3) is constrained by the conditions $\Phi = \phi_B - (E_C-E_F)$, the displacement of the conduction band edge in the semiconductor in Figure 1.5 (b), at $x = 0$ and $d\Phi/dx = 0$ at $x = w$, and is

$$\Phi = \phi_B - (E_C-E_F) - (Nq/\varepsilon)(wx - x^2/2) \tag{1.4}$$

$$w = (2\varepsilon(\phi_B - (E_C-E_F))/Nq)^{1/2} \tag{1.5}$$

According to Equation (1.2), the height of Schottky barrier only depends on the work function of the metal and the electron affinity of the semiconductor. In practice, many metal-semiconductor and metal-insulator-semiconductor systems do not behave in this way. Measurement indicated only a weak dependence of the barrier height on the metal work function.[5] The insensitivity of the semiconductor barrier height to changing the metal is called "Fermi level pinning", referring to the fact that at the interface the Fermi level of the semiconductor is pinned at some energy level in the band gap. The details of Schottky barrier formation are not yet fully understood. It appears, however, that defects at the semiconductor surface play an important role in contact formation. Bardeen was the first to point out the

importance of surface states in determining the barrier height.[6] Such surface states may be "dangling bonds" (unsaturated valencies) at the surface or some other types of defects.[7] There is, however, still disagreement between the various proposed mechanisms explaining Fermi level pinning.[8]

The height of the Schottky barrier can not be lowered by using different work function metals due to Fermi level pinning. In practice, an "ohmic contact" (a contact without a barrier) is formed by bringing a metal into contact with a very heavily doped region of a semiconductor. The width w of the band bending region determined by Equation (1.5) is decreased by heavy doping. The thin barrier that results from such heavy doping can be penetrated easily by tunneling of electrons with little applied voltage, leading to an ohmic contact.

The analogous behavior of a p-type semiconductor is shown in Figure 1.5 (c). Here the Fermi level of the semiconductor is below that of the metal when the materials are not in contact, and when they are brought in contact charge is transferred in the opposite direction leading to the band bending shown in (d).

Next consider a thin insulating barrier placed between the metal and the semiconductor when they are in electrical contact. The potential then varies as in Figure 1.5 (e). Part of the potential difference between materials is taken up by fields in the insulator. This configuration is the basis of the Metal-Oxide-Semiconductor Field Effect Transistor (MOSFET), to be described in the next section.

1.1.6 Metal-Oxide-Semiconductor Field-Effect Transistor -- MOSFET

The famous MOSFET is one of the most important semiconductor devices. The machines that carry out the operations of a general purpose digital computer are constructed from individual logic gates, which are circuits that accept electrical input that represent digits and transmit an output that is some logical function of the input. In turn, logic gates can be formed by connecting about five MOSFETs[9]. The MOSFET is also a component in semiconductor memory circuits[10] for the storage of digital information.

As shown in Figure 1.6 a MOSFET consists of three layers: a selectively doped semiconductor material, in this case, a p-doped silicon, an insulating SiO_2 film, and a conductive metal layer. The transistor is a three-terminal device. Electrical contact regions of a conductivity type opposite to that of the substrate semiconductor type are provided at each end of the layer structure. The contacts at these ends are called the source and the drain. Another contact, called the gate, is made to the conductive layer above the insulator.

The operation of the device is based on the so called "field effect" demonstrated in the classic paper by Shockley and Pearson.[11] They showed that an external field applied to the gate could modulate the conductance in the surface region under the gate. The operation of the device will be described in terms of a transistor operated in the "enhancement mode". The basic idea involved is that the application of a positive voltage to the gate attracts electrons to the SiO_2/Si interface due to the field effect, thereby creating a conducting channel from the source to the drain. Current is driven through the channel by the application of a positive voltage to the drain. In the absence of a voltage on the gate, the source-substrate drain-substrate act as two opposite direction "bipolar transistors" in series, and almost no current flows for reasons

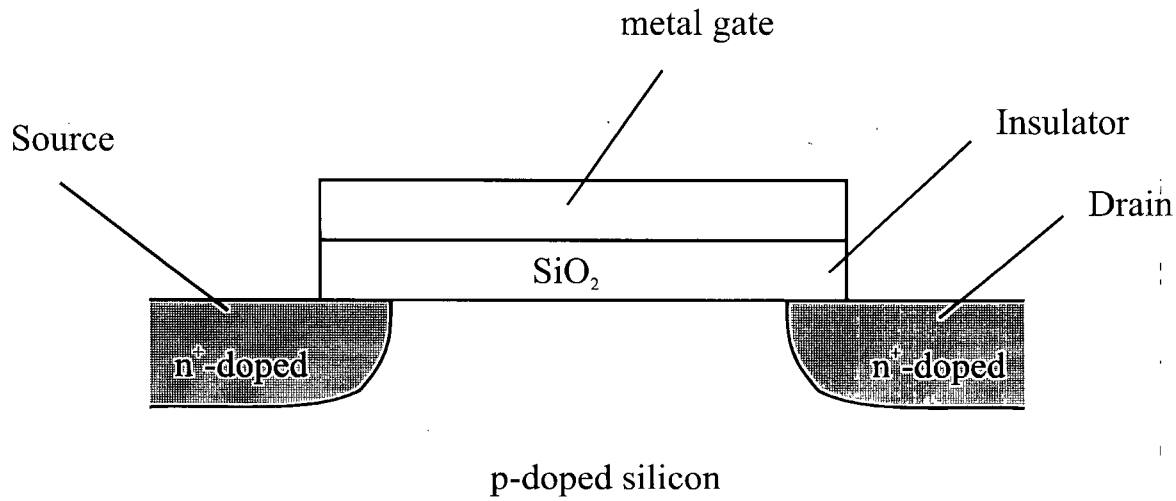

Figure 1.6 The physical structure of a metal-oxide-semiconductor field-effect transistor.

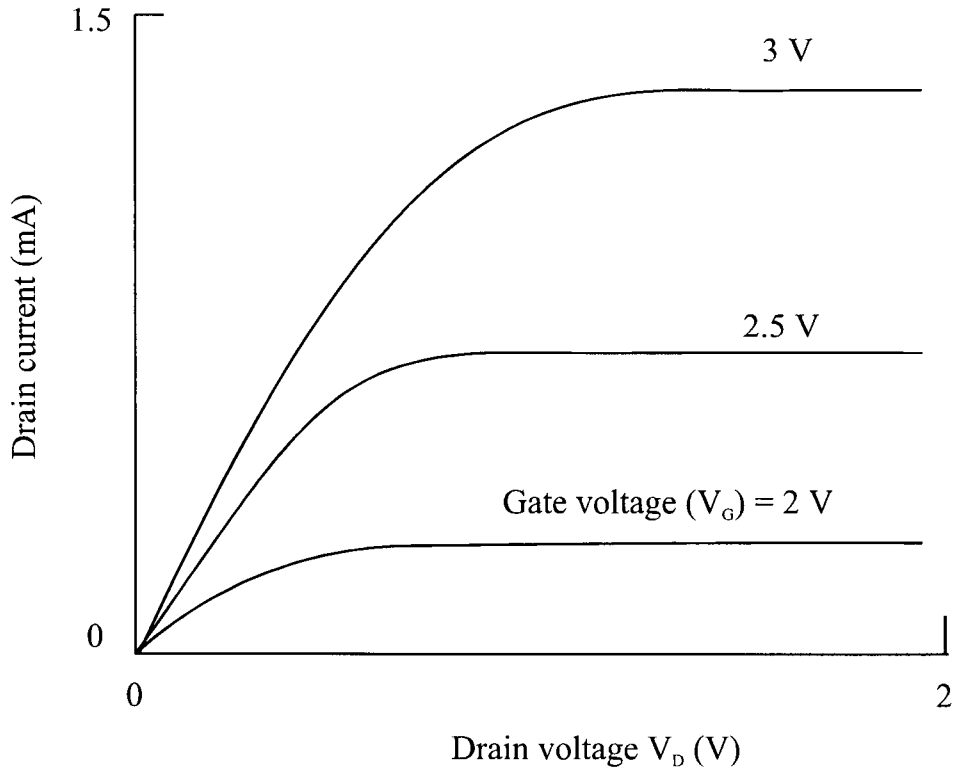

Figure 1.7 The characteristics of a FET. Drain current as a function of gate and drain voltage.

described in the next paragraph. As the positive voltage on the gate increases to a certain point, which is the threshold voltage, the electron channel forms and current flows from source to drain, increasing with increasing gate voltage, as shown in Figure 1.7.

In the absence of a gate voltage, the potential in an FET is illustrated in Figure 1.5 (e) or 1.8 (a). Both the conduction band and the valence band at the insulator-semiconductor contact are far from the Fermi level, therefore, very few holes and electrons are at the interface. There is a high impedance between the source and drain. The configuration of the potential can be varied by applying a voltage on the gate. Figure 1.8 shows some of the possibilities. (a) is the situation without applied voltage, as in Figure 1.5 (e). In (b) a negative voltage has been applied to the metal, reproducing the configuration in Figure 1.5 (a). This is known as the "flat band" condition. The effect of a more negative potential on the gate is shown in (c). The concentration of holes near the surface is greatly increased, a phenomenon known as accumulation. The effects of a positive potential on the gate are shown in (d) and (e). When, at the surface, the conduction band is bent by a positive potential so that it comes closer to the Fermi level there are an increasing number of electrons near the surface, a condition called inversion. The distance of the conduction band from the Fermi level in (d) is equal to the separation between the Fermi level and the valence band edge in the body of the semiconductor. The electron conductivity then becomes significant, and the condition (E_C - E_F) at the surface equal to (E_F - E_V) in the bulk is the definition of threshold, the point at which a connection between source and drain is established by the channel formed by the electrons drawn to the surface. The gate bias has been further increased in (e) so that the Fermi level lies within the conduction band to create a high concentration of electrons at the surface.

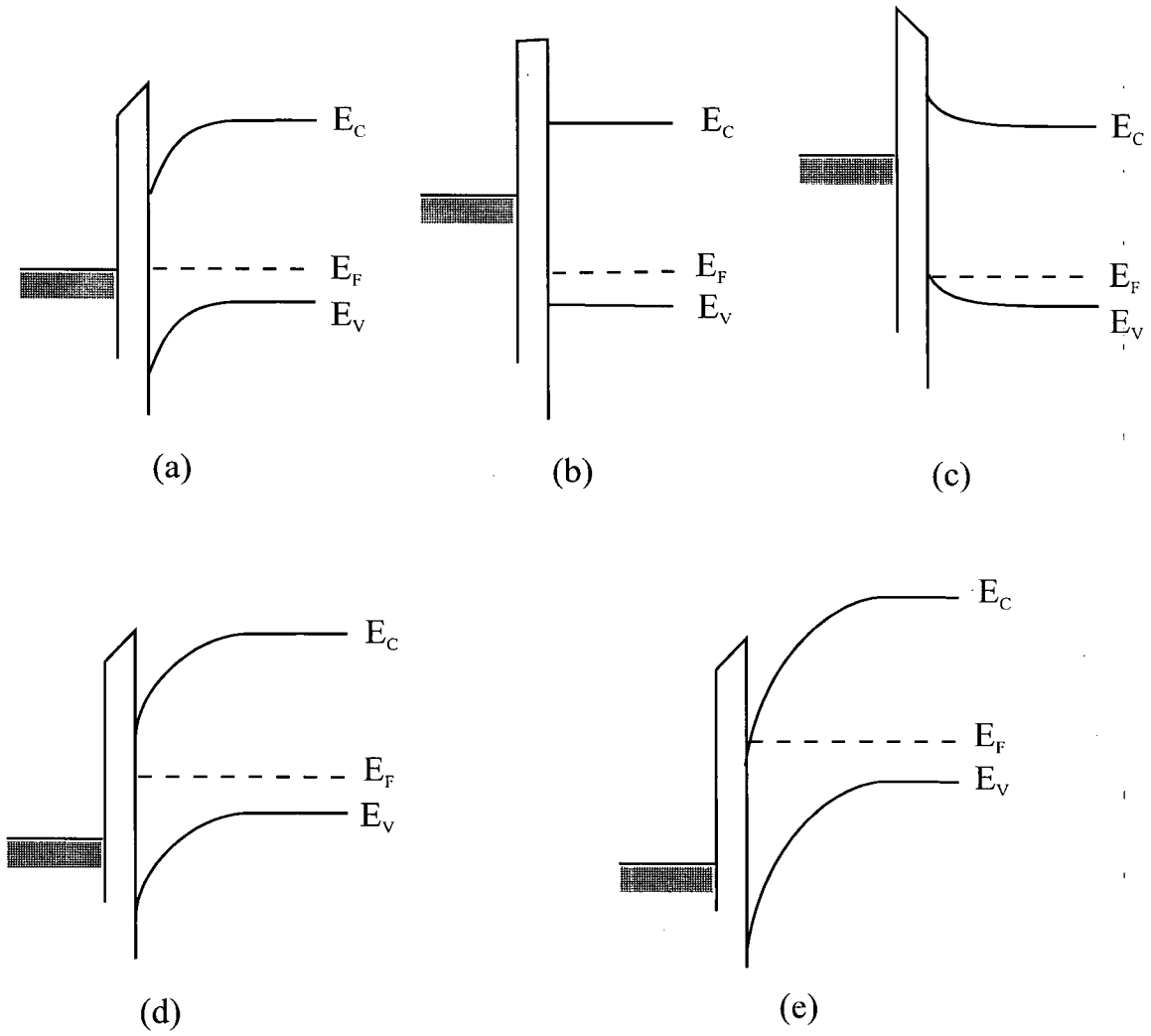

Figure 1.8 The application of potentials to the gate of an n-channel field-effect transistors. (a) Zero voltage on the gate. (b) A negative applied voltage produces the flat-band condition. (c) Accumulation of holes at the surface by a large negative potential. (d) Threshold; a positive gate voltage has raised the concentration of electrons at the surface to that of the hole concentration in the p substrate. (e) Strong inversion; the gate voltage produces a high concentration of electrons at the surface.

One important characteristic of a FET is its gain which is measured by the conductance of the channel ($\partial I/\partial V_G$, where I is the current through the channel and V_G is the gate potential). The gain of the device can be affected by traps at the interface of the insulator and the semiconductor because every charge placed on the gate is not compensated by an additional free carrier in the inversion layer; instead, some gate charge is compensated by charged interface traps. Thus interface traps reduce conductivity modulation of the inversion layer. High interface trap level densities ($> 10^{11}$ cm^{-2} eV^{-1}) also can cause increased noise as the fluctuating occupancy of interface traps modulate the inversion layer conductance. Also, charged interface traps and fixed charges influence the voltage needed to form the inversion layer.

1.2 Interface traps and their chemistry

Silicon is unique among semiconductors in that it is easy to form a layer of SiO_2 on its surface that has excellent chemical and physical properties. Especially important is the low density of surface states that can be achieved at the interface between silicon and SiO_2. Large numbers of such states, far from the band edges, exist at most interfaces between different materials. The surface states trap electrons, and the Fermi level at the surface occupies a position between the bands that is determined by the partially filled traps rather than being controllable by the gate in a FET as described in Figure 1.8. Even in the case of silicon-SiO_2, extreme cleanliness and care are needed to keep the surface trap density low enough to allow the events depicted in Figure 1.8 to occur. Such a favorable condition has not been consistently produced in any other system. The field-effect transistor has, consequently, not been successful with any other semiconductor.

1.2.1 The P_b center

For device fabrication, gate oxides are grown by thermal oxidation at around 1100 °C in 1 atm of pure and dry O_2. Electrical measurements, such as high-low frequency C-V (see section 1.3.2.1), show that as-grown thermal oxides on <111> silicon have carrier trap densities of about 10^{13} $cm^{-2}eV^{-1}$ whereas trap densities are about one order of magnitude lower[12] on <100> silicon. This is the reason why <100> silicon is widely used in device fabrication.

More than two decades ago, using electron paramagnetic resonance (EPR), the chemical nature of carrier traps at the <111> Si/SiO_2 interface was identified[13] as $\bullet Si{\equiv}Si_3$, that is, an unpaired electron centered on a silicon atom that is bound to three other silicon atoms. This structure is called a P_b center. In <100> silicon there appear to be two distinct paramagnetic P_b centers that have been labeled P_{b0} and P_{b1}.[14] The chemical structure of P_{b0} and P_{b1} are not clear, but they can also be seen by EPR. Comparing the trap density that is measured electrically with that measured with EPR, such P_b centers have been shown[15] to be the major carrier traps at the Si/SiO_2 interface after thermal oxidation.

For an as-grown Si(100) thermal oxide, the concentration of P_b centers is on the order of $10^{12}/cm^2$, which means that about 1 in 10^3 of the surface silicon atoms are P_b defect sites. For the fabrication of working devices this value is much too high. MOS technology only became possible when interface trap densities were brought down to levels of the order of 10^{10} $cm^{-2}eV^{-1}$ by annealing in H_2 at temperatures above 220 °C. This passivation by H_2 is believed to involve the binding of a hydrogen atom to the trivalent silicon atom, resulting in the formation of a H-Si bond

$$P_b + H_2 \rightarrow P_b\text{-}H + H \qquad (1.6)$$

Annealing a <111> Si/SiO_2 interface in H_2 in the temperature range 230-260 °C, Brower[16] showed that the rate of this passivation reaction for P_b centers with H_2 is first order in H_2. The temperature dependence of the rate constant was observed to obey the Arrhenius equation with an activation energy of 1.66 eV and a preexponential factor of 1.94×10^{-6} cm^3/sec.

Passivation of both P_{b0} and P_{b1} in <100> silicon can also be described by reaction (1.6). The passivation rate constants were determined by Stesmans.[17] He found an activation energy of 1.51 eV for P_{b0} and 1.57 eV for P_{b1}, which are close to the value that Brower obtained for P_b centers. A 0.15 eV Gaussian spread of the activation energy was introduced by Stesmans to account for the fact that the decay of P_{b0} and P_{b1} is not exponential with time. Decay of the P_b centers in <111> silicon was found to be exponential[16].

This passivation reaction (1.6) can be reversed by vacuum annealing at temperatures over 500 °C[18]. Using EPR, Bower and Myers[16,19] have studied the dissociation of hydrogen-passivated P_b centers in <111> silicon by vacuum annealing at temperatures ranging from 500 to 595 °C. Their results provided evidence for the following reaction [19]:

$$P_b\text{-}H \rightarrow P_b + H \qquad (1.7)$$

This dissociation process was found to be first-order in the P_b-H density. An activation energy of 2.56 eV and a preexponential factor of 1.2×10^{12} sec^{-1} was obtained for reaction (1.7).

1.2.2 Carrier traps generated by hydrogen

Despite the identification of the above reactions and the reasonable agreement regarding the activation parameters, and despite its importance to integrated circuit fabrication, the passivation and depassivation at gate oxide interfaces in MOSFET devices remains a poorly

understood phenomenon because of its complexity. Much of the evidence has come from the study of hot-electron-[20] or radiation-induced[21] interfacial states in gate oxides. The mechanism by which these states arise is still controversial. There is no question that it is at least a two step process. In the first, hydrogen is released from defect sites in the oxide. In the second, this mobile species moves to the Si/SiO_2 interface where it produces interface states.

Brower[19] argued from theoretical considerations that P_b passivation by atomic hydrogen according to the reaction

$$P_b + H \rightarrow P_b\text{-}H \qquad (1.8)$$

as well as depassivation according to the reaction

$$P_b\text{-}H + H \rightarrow P_b + H_2 \qquad (1.9)$$

should both occur, with essentially no energy barrier, in the presence of atomic hydrogen. If the energy barriers for each of these reactions were exactly zero, one would expect that if reactions (1.8) and (1.9) occur with equal probability, the steady state concentration of P_b centers during atomic hydrogen exposure would reach half the value of the intrinsic P_b density at the Si/SiO_2 interface. For <111> silicon, one would expect to be able to produce about $5x10^{12}$ cm^{-2} P_b centers by atomic hydrogen exposure. However, experiments performed by Cartier and co-workers[22] showed that a maximum steady-state P_b density of only $3\text{-}6x10^{11}$ cm^{-2} can be achieved by exposing a <111> Si/SiO_2 interface to atomic hydrogen at room temperature. Exposure of either the well-passivated thermally-oxidized surface ($\sim 10^{10}$ traps/cm^2), or a vacuum annealed surface (10^{12}) traps/cm^2) to atomic hydrogen results in approximately the same steady state density of P_b states. They conclude that both reactions may be thermally activated with reaction (1.8) about six times faster than reaction (1.9).

Furthermore, Cartier and co-workers[22] found that the P_b density measured with EPR is about only 1/10 of the total number of electrically active interface states measured by the high-low-frequency capacitance method. The majority of interface states produced by atomic hydrogen are carrier traps other than the well-known P_b centers. Cartier and Stathis[23] showed that atomic hydrogen can generate up to 10^{13} /cm^2 interface states. They believe that these states are different from P_b centers in the following aspects, although this remains a controversial point[24]: (a) Cartier and Stathis found that these new interface states could not be detected by EPR[23]. (b) The distributions of these states evolve in a very similar fashion to those reported during hot electron stress or irradiation. They are strongly asymmetric with respect to the middle of the bandgap, showing only one peak above midgap, a distribution that is not compatible with those reported for silicon dangling bonds. The nature of the majority traps created by H-atoms at the Si/SiO_2 interface remains unknown. De Nijz et al[25] have proposed that these other traps are H-atoms which are trapped by oxygen atoms bound to two silicon atoms at the Si/SiO_2 interface. Absorption of H at such stretched ≡Si-O-Si≡ sites is also indicated in some theoretical studies.[26]

The new kind of traps produced by atomic hydrogen can be represented by the reaction

$$H + P \rightarrow T \qquad (1.10)$$

where P is the trap precursor and T is the carrier trap created by H-atoms. The trap density was shown[27] to increase linearly with the H-atom dose with no indication that the trap density saturates at values below 10^{13} eV^{-1} cm^{-2}. The (111) interface degrades roughly 2.5 times faster than the (100) interface, possibly due to a higher precursor site density at the (111) interface.

The measured temperature dependence of the trap production rates yields an activation energy of 0.20 eV for reaction (1.10) in the temperature range from -50 to 100 °C.

1.3 Measurement of surface states

In section 1.1.1, we described the formation of broad bands of energy states in crystals due to the interaction of a vast number of atomic orbitals. A few of the energy band structures of GaAs and Si are shown in Figure 1.9, where the potential energy is plotted against the momentum in the crystal.[28] GaAs is called a direct band-gap semiconductor because the maximum in the valence band and the minimum in the conduction band occur at the same momentum. Thus an electron at the bottom of the conduction band can make a transition to vacant levels in the valence band without a change in momentum. In contrast, Si is an indirect band-gap semiconductor. Its valence band maximum and conduction band minimum occur at different momentum values. Therefore, a transition between the bands requires a change of momentum.

A transition from conduction band to valence band is called direct recombination. One type of direct recombination is radiative recombination in which a photon is emitted that carries away the energy of the band-gap. If a change of momentum is required, then the possibility of a radiative recombination is very low. Another type of direct recombination is Auger recombination in which the energy is transferred to a third carrier. Direct recombination in which the recombination energy is liberated to lattice vibrations (phonons) is too slow to be important in most semiconductors. A transition via localized energy levels in the bandgap[29] (due to impurity or defects) is called indirect recombination. These states act as stepping stones between the conduction band and the valence band. Because the transition probability depends

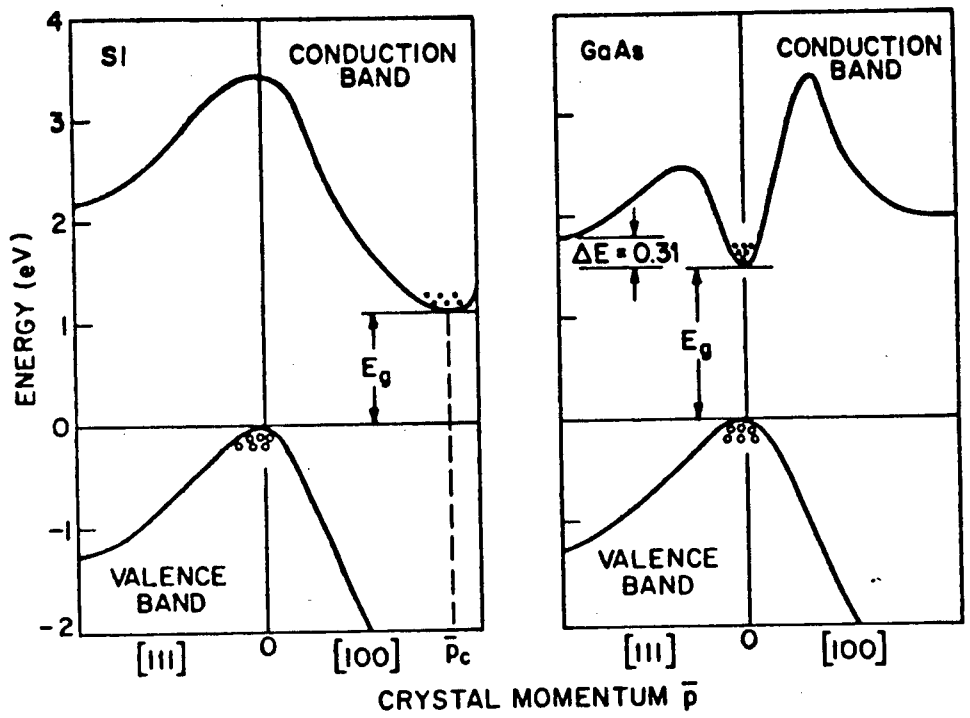

Figure 1.9 Energy band structures of Si and GaAs in the direction specified on the axis. Circles (°) indicate holes in the valence bands and dots (•) indicate electrons in the conduction bands (from Sze[28]).

on how much energy must be liberated to the lattice in any step, these intermediate states can substantially enhance the recombination process. Indirect recombination via deep-level (i.e. near mid gap impurity states) is often called Shockley-Read-Hall (SRH) recombination,[30] and because the energy liberated during the recombination event is dissipated by lattice vibrations or phonons, indirect recombination is also called multiphonon recombination.

1.3.1 Lifetime measurements for direct-bandgap semiconductors

When excess carriers are introduced into a direct band-gap semiconductor electrically or by a constant flux of incident photons with energy greater than the band gap, radiative and non-radiative carrier recombination will bring the system into a steady state, at which point the carrier injection rate is equal to the recombination rate. If the deep-level states are changed somehow, recombination will be redistributed among the radiative and non-radiative processes to reach a new steady state, since the SRH recombination rate depends on the concentration of the recombination centers. The photoluminescence from the radiative recombination process in a direct band-gap semiconductor can therefore be used as a measure of the density of carrier recombination centers, such as interfacial dangling bonds.

1.3.2 Techniques for indirect-band gap semiconductors

For indirect band-gap semiconductors, such as silicon, the radiative recombination process is extremely weak, so photoluminescence cannot be used to measure the density of deep level states. There are, however, a number of alternative techniques that can be used to measure the densities of these recombination catalysts.

1.3.2.1 MOS capacitance measurement

Interfacial traps are defects located at the Si-SiO_2 interface which have energy levels within the silicon bandgap. These defects can exchange charge with the silicon. Specifically, they can interact with the silicon conduction band by capturing electrons and with the valence band by capturing holes.

The occupancy of interfacial traps can be changed by the gate bias as illustrated in Figure 1.10 for a p-type substrate. In (a), no gate bias is applied and band bending is caused by charged interface traps, producing the Fermi level pinning discussed in section 1.1.5.1. Interface trap levels below the Fermi level are full, and those above are empty. In (b) a negative gate bias has been applied, moving the valence band edge at the silicon surface toward the Fermi level. Interface trap levels empty by capturing holes until the equilibrium condition illustrated in (b) is reached. In (c) a positive gate bias fills more of the interface energy levels.

Interface traps can be detected through Metal-Oxide-Semiconductor (MOS) capacitance measurements. For an ideal MOS capacitor without interface traps, the total capacitance is the series combination of the oxide capacitance and the silicon capacitance. Since interface traps can hold an electron for some time after capture, that is, interface traps store charge, a capacitance parallel to the silicon capacitance is added. In this method, the MOS capacitance is measured by superimposing a small ac voltage on the gate bias. If the frequency of the ac voltage is low, the response of the interface traps is immediate, and the capacitance due to interface traps will contribute. If the frequency is so high that interface traps can not respond, then interface traps will not contribute capacitance to the high frequency measurement. By comparing the low and high frequency measurement[31], the interface trap density near the Fermi

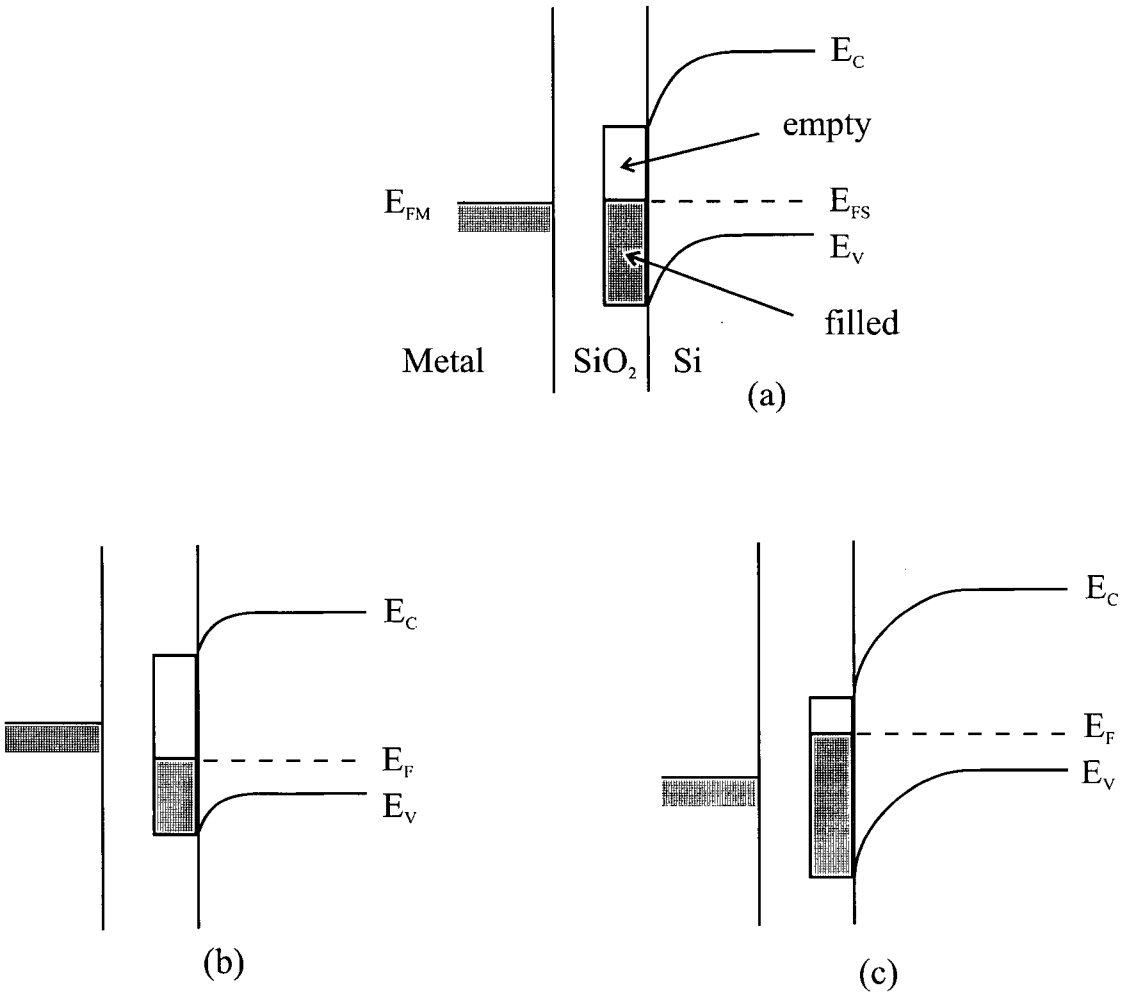

Figure 1.10 Band-bending diagram showing how interface traps change occupancy with gate bias. The sample is p-type. (a) No gate bias; (b) negative bias; (c) positive bias.

level can be extracted. Interface trap density is obtained as a function of position in the bandgap by repeating this procedure for different values of gate bias.

It should be noticed that the detection of interface trap density by capacitance measurement needs the fabrication of a MOS capacitor, so it can not be used as an *in situ* technique.

1.3.2.2 Photoconductive decay techniques

As the name implies, electron-hole pairs are created by optical excitation, and their decay is monitored as a function of time following the cessation of the excitation. The conductivity, which is determined by the free carrier concentrations, is usually monitored, and the simplest way is to measure photoconductive decay with ohmic contacts.[32]

The carrier decay can also be monitored without sample contacts. One such technique was developed by Tiedje et al,[33] in which an rf bridge circuit is capacitively coupled to the wafer by two flat electrodes that are vacuum pressed against one side of the wafer. The photoconductivity, produced by a 60-ns burst of near-infrared light from a GaAs laser diode array, is measured by comparing the phases of the input rf signal and the one reflected back from the wafer. The rf bridge method has proved to be very useful in the development of high-efficiency solar cells.[34] In one variation of this contactless technique the photoconductivity is monitored by microwave reflection.[35]

These contactless measurements cannot be used as a "continuous" technique either, because about 10^4 light pulses must be accumulated in order to achieve an acceptable signal to

noise ratio. In the current work it is our aim to develop a continuous contactless technique for monitoring changes in interfacial states.

1.4 Trends in device fabrication

1.4.1 The integrated circuit

After its invention in 1947 by John Bardeen and Walter Brattain of the Bell Telephone Laboratories, the transistor quickly replaced the relay and the vacuum tube in computers, because of the transistor's high reliability, low power dissipation, and small size. The historical development of transistor fabrication is illustrated by techniques (a) to (d) for pn junction formation presented in Figure 1.11. Initially the "grown junction method" (a) was used. Later the alloy junction method (b) was invented and then this was superseded by the diffused mesa junction method (c) due to the more precise dopant control by solid-state diffusion. All these methods were used to fabricate isolated devices. Although monolithic integrated circuits were made using mesa technology, interconnections had to be made from element to element. The introduction of the planar process (d) by Hoerni[36] in 1960 laid the foundation for modern integrated circuits.

The planar process was so successful that all monolithic circuits are made by this method today. The discovery by Froth and Derrick[37] that a thin layer of SiO_2 can effectively mask against the diffusion of impurities made possible precise control of both the depth of a diffused junction and its location on the silicon wafer. The location of devices could be delineated by covering the silicon with SiO_2 and then exposing the silicon to the diffusing

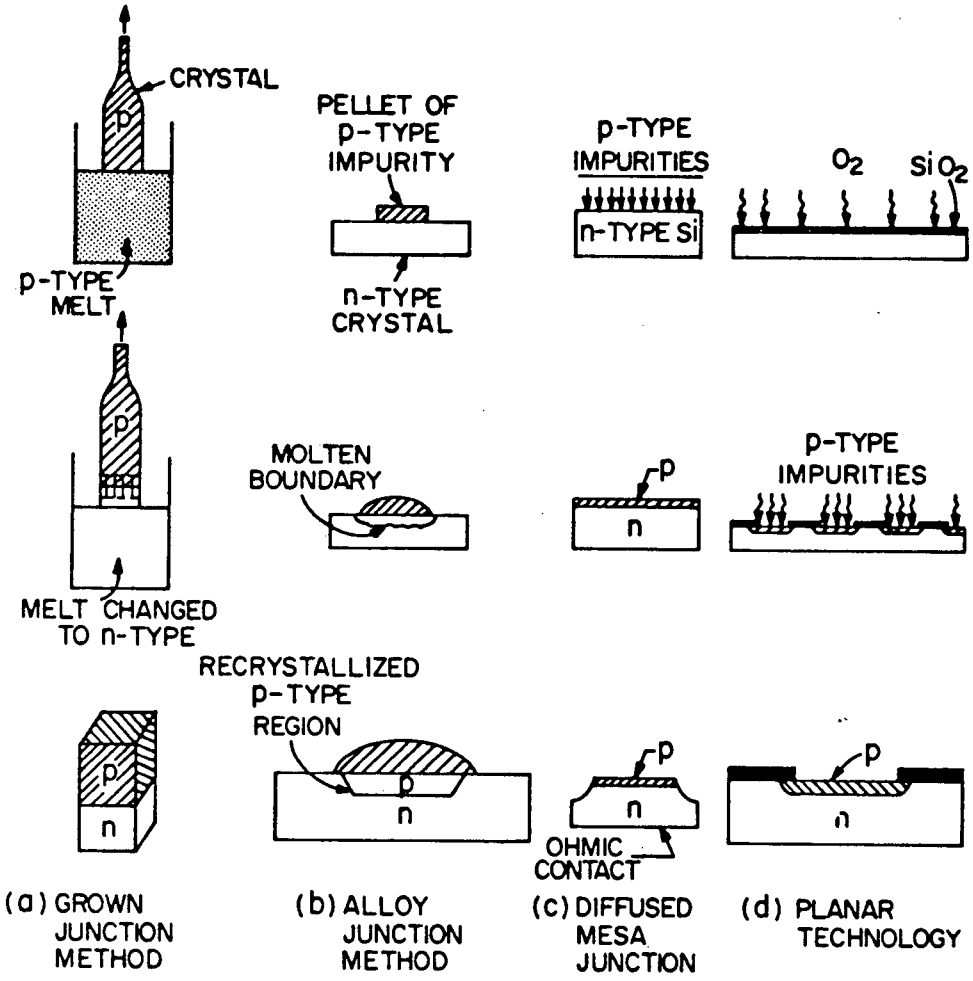

Figure 1.11 Methods of fabricating pn junctions (from Keyes[9])

dopant only in selected areas, defined by photolithography, where the SiO_2 had been removed. Interconnections between devices are made by evaporating a metal over the SiO_2, making contact with the diffused regions through holes cut in the SiO_2. The metal is then cut into a particular pattern by photolithography and etching. The integrated circuits made this way contain a large number of interconnected devices, making the cost per device decrease dramatically.

Since the invention of planar process technology, the feature size of devices has been decreasing steadily so that more devices can be made on a single chip. This process of miniaturization was clearly delineated by the evolution of acronyms that describe the increases in scale of integration. The early integrated circuit consisted of a few transistors interconnected on a chip. The abbreviation IC was introduced to characterize the new technology. The realization that the method could be extended to hundreds of components led to the term Large Scale Integration (LSI) being coined. When the number of devices on a chip exceeded thousands the adjective Very was added and it became Very Large Scale Integration (VLSI). Nowadays, more than ten million devices can be fabricated on a single chip, with the minimum dimension of structures below one micron. The description becomes Ultra Large Scale Integration (ULSI). The trend of miniaturization will probably continue for some time to come. The decrease in cost per device is the economic force driving the advances in the technology.

1.4.2 The challenge of miniaturization

Ultra-large scale integration (ULSI) of microelectronic devices has resulted in aggressive scaling of device dimensions into the submicron range. However, operating voltages have not

always been scaled accordingly, resulting in high electric fields in devices. These high fields as well as a clear trend toward even smaller device dimensions in the future have increased concern over the reliability of materials used to fabricate these devices. It is not clear that the materials and device as whole can continue to perform to original specifications over an extended period of time. Of particular concern is the reliability of the Si/SiO_2 interface which is vital to metal-oxide-semiconductor (MOS) device operation. At high electric fields, high-energy or "hot" carriers are injected across this interface and into the SiO_2 gate dielectric film where they create physical defects that act as electrical traps. These hot carrier-induced traps can lead to degraded device performance or even complete device failure.

Another concern that has arisen due to shrinking device dimensions is the thermal budget, or time-temperature product, of the microelectronic device fabrication process. In submicron devices, junction depths and dopant profiles must be carefully controlled and preserved. Conventional microelectronic processing involves several high-temperature processes such as thermal oxidation and various thermal annealing cycles. Temperatures often exceed 800-1000°C. At such high temperatures, considerable dopant transport can occur, altering device properties such as threshold voltage or destroying the device all together. The challenge, therefore, is to develop alternatives to conventional, high-temperature processing while at the same time satisfying increasing demands on materials performance for ULSI technology.

Several potentially viable low thermal-budget processing approaches for the formation of gate oxides have been identified. Rapid thermal oxidation[38] and/or plasma-enhanced chemical-vapor deposition[39] are among them. Oxygen plasmas can also be used to create thin oxides at greatly reduced temperatures, but these have been found to usually have a high carrier

trap density at the SiO_2/Si interface which makes them unacceptable for use in integrated circuits. In the last few years it has been shown[40] that acceptable SiO_2/Si interfaces can be formed by first exposing a clean silicon surface to a somewhat remote oxygen plasma briefly for the formation of an Si-SiO_2 interface, followed by plasma-enhanced chemical-vapor deposition of an oxide layer. However, this approach has not been optimized and the properties of the Si-SiO_2 interface grown by low temperature plasma oxidation is not known before annealing in hydrogen. Another unknown is the effect of hydrogen incorporated during the annealing process. It has been found that device degradation during operation has something to do with the presence of hydrogen.

1.5 The objectives of this research project

Photoluminescence from radiative recombination processes can be used as an *in situ* measurement of interfacial traps for direct-bandgap semiconductors. There is no such *in situ* technique for the monitoring of interfacial traps in indirect-bandgap semiconductors. The first objective of this research was to develop a technique for the measurement of interface traps in indirect-bandgap semiconductors which can be used during low temperature processing of silicon. Using such an *in situ* probe, we then proposed to study the properties of the Si-SiO_2 interface during its formation by exposing silicon surfaces to a remote oxygen plasma at low temperatures and subsequently to H_2 at elevated temperatures and to H-atoms from a remote H_2 plasma. Since hydrogenic species are known to be released by hot electrons during device operation, and it has been shown that simultaneously with its release a rapid degradation of the interface occurs,[41] we felt that it was crucial to understand the hydrogen chemistry at the

interface. We therefore also proposed to expose silicon samples with a layer of SiO_2 grown by standard thermal oxidation techniques at 1100 °C, to hydrogen atoms produced by a remote hydrogen plasma, and to monitor the interface trap density during all these processes.

Chapter 2 *In Situ* monitoring of the steady state carrier concentrations in silicon

2.1 Introduction

Because silicon is an indirect band gap semiconductor, it does not emit light, and hence photoluminescence, which has been used to follow the change in surface states on III-V semiconductors[42,43], cannot be used as an *in situ* probe for this semiconductor. A technique developed by Tiedje[33], which measures the decay time of photon induced conductivity by an RF coupling technique offers the possibility for an alternative contactless technique for *in situ* monitoring of the carrier losses at the silicon surface or interface and on bulk traps. In their apparatus, photoconductivity was produced by 60-ns bursts from a near-infrared laser, and the lifetimes of the minority carriers were determined with a 100 MHz radio-frequency (RF) bridge circuit capacitively coupled to the silicon wafer. To achieve an acceptable signal to noise ratio, about 10^4 light pulses had to be averaged in about 1 minute.

From conversations with Professor Tiedje, we concluded that greater sensitivity could be achieved with inductive coupling, and true continuous monitoring could be achieved by following the steady state carrier concentrations created by a continuous wave incident light source. The technique which we developed[44] for this purpose is shown in Figure 2.1. It consists of a RF coil, which is inductively coupled to the silicon chip, and the same radio frequency bridge circuit used by Tiedje. The pulsed light source was replaced with a CW He-Ne laser which was chopped at a reference frequency in order to distinguish the conductivity produced by the laser from the intrinsic conductivity of the semiconductor when it is detected by the lock-in amplifier.

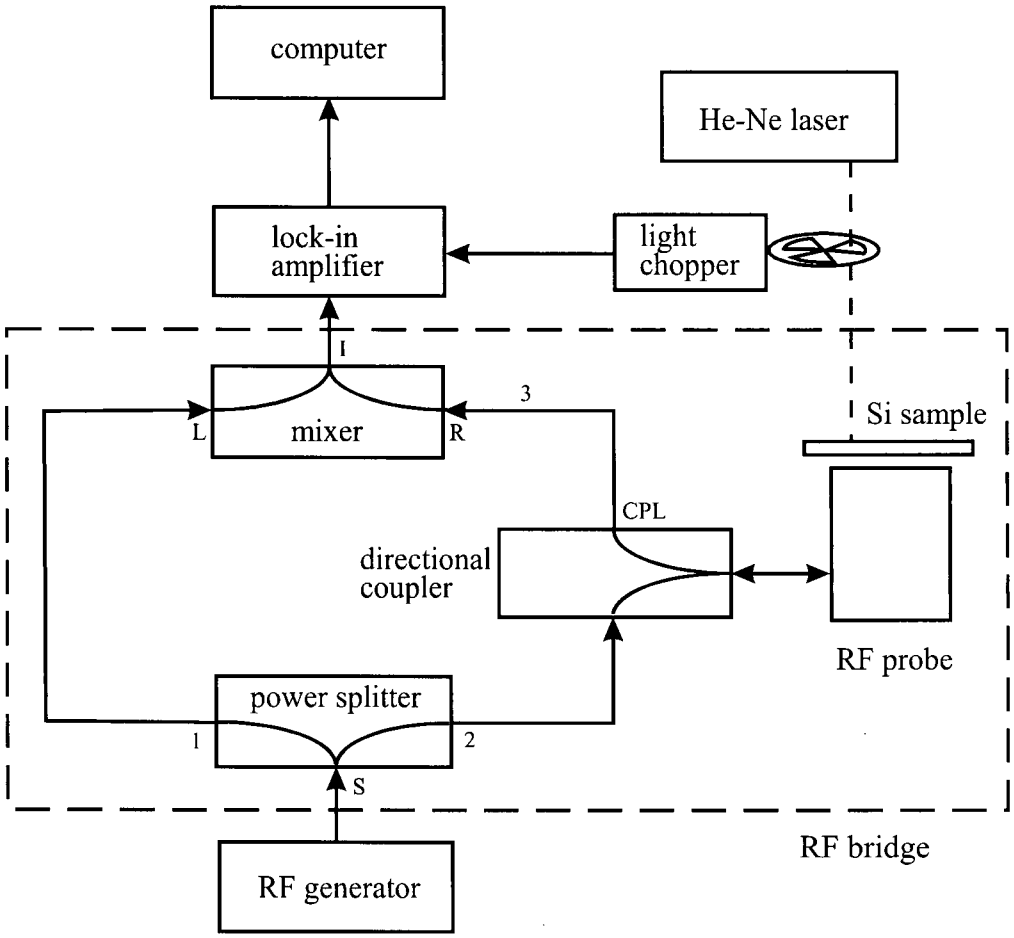

Figure 2.1 Block diagram of the contactless technique for *in situ* monitoring of steady state carrier concentrations in silicon.

2.2 The RF probe

The key element in this RF bridge is the compact coil which we will call the RF probe. The sensitivity of the whole system is largely determined by the configuration of this probe. It consists of a helical resonator designed according to the specifications of MacAlpine[45]. It was constructed out of copper with a shielding tube and a helically wound wire as illustrated in Figure 2.2. The resonator coil was soldered to the shield at point e, with the other end terminating level with the top of the shield. An electrical "tap" connected to a coaxial cable was soldered to the helical coil at a carefully chosen point along its length (point t). The input RF power was connected through the coaxial cable and the shield was grounded.

Four different high Q resonator coils were constructed with the general structure depicted in Figure 2.2 and tested for sensitivity. The dimension of the most sensitive probe is:

The outside diameter of the shield D_{out} = 21.3 mm

The inner diameter of the shield D_{in} = 17.4 mm

The length of the shield B = 33.2 mm

The diameter of the copper wire τ = 1.7 mm

The diameter of the coil d = 9.6 mm

The total number of coil turns N = $12^1/_4$

The distance of the soldered point e to the bottom of the shield f = 2.0 mm

The position of the coaxial cable tap was $1^2/_3$ turns from the bottom.

The RF probe was placed underneath the sample, against the outside bottom of the reactor tube with about 2 mm of Pyrex between the sample and the probe.

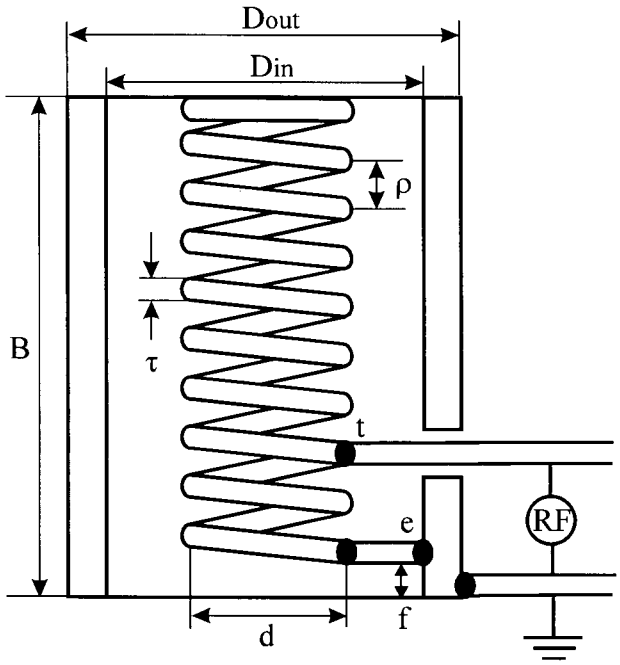

Figure 2.2 Schematic of the RF probe used in the contactless technique for *in situ* monitoring of steady state carrier concentrations in silicon.

2.3 The RF bridge

All of the components that were interconnected in this RF circuits had a 50 Ω impedance so that they were "matched". As shown in Figure 2.1, RF power from an RF generator (HP model 3200B VHF Oscillator, frequency range 10 to 500 MHz, RF output > 150 mW) was fed into port S of a power splitter (Mini Circuits ZFSC-2-1) and came out of ports 1 and 2 as two identical output signals. Signal 1 had the form $V_1\sin(\omega t)$, in which V_1 was the peak to peak voltage of the radio frequency signal and ω is the frequency. It was connected directly to a frequency mixer (Mini Circuits ZFM-2H) to serve as a reference signal. This was one arm of the RF bridge. The other arm of the RF bridge consisted of the circuit from port 2 of the power splitter to port R of the frequency mixer. Signal 2, of the same form as signal 1, was fed into the RF probe and was reflected back as signal 3, which had the form of $V_2\sin(\omega t + \Delta\phi)$, in which V_2 is the signal voltage and $\Delta\phi$ is the phase shift. A directional coupler (Mini Circuits ZFDC-10-2) was used to separate the incoming and reflected signal 2 and 3. The phase shift $\Delta\phi$ of the reflected signal was determined by the conductivity of the silicon sample σ, which could be expressed as

$$\sigma = q\,(n\,\mu_n + p\,\mu_p) \qquad (2.1)$$

where q is the magnitude of electronic charge, n and p are the free electron and hole concentrations, and μ_n and μ_p are the electron and hole mobilities, respectively. The frequency mixer performed the phase comparison by multiplying signals 1 and 3. The output V_{out} was therefore composed of a DC and an AC signal:

$$V_{out} = V_1\sin(\omega t) \times V_2\sin(\omega t+\Delta\phi)$$

$$= V_1 V_2 \cos(\Delta\phi) - V_1 V_2 \cos(2\omega t + \Delta\phi) \quad (2.2)$$

The DC signal $V_1 V_2 \cos(\Delta\phi)$ is a function of the conductivity of the silicon sample σ and could be measured with a voltage-meter at port I of the frequency mixer.

2.4 The injection and measurement of carriers

A 10 mW, 633 nm (1.96 eV) He-Ne laser beam, with a beam diameter of 2 mm was directed at the silicon chip. The laser beam was chopped at 200 Hz, and therefore free electrons and holes were "injected" into the silicon sample at that frequency. According to equation (2.1), when the beam was on the silicon chip, the conductivity of the sample increased by $\Delta\sigma$ due to the injected electron concentration Δn and hole concentration Δp, we have

$$\Delta\sigma = q (\Delta n \mu_n + \Delta p \mu_p) \quad (2.3)$$

Since an equal number of electrons and holes are formed,

$$\Delta n = \Delta p \quad (2.4)$$

Then equation (2.3) becomes

$$\Delta\sigma = q \Delta n (\mu_n + \mu_p) \quad (2.5)$$

For a p-doped semiconductor, at low level photo-injection, the laser beam intensity was such that the concentrations of injected carriers (n) were always much higher than the minority carrier concentration and much lower than the majority carrier concentration in the absence of radiation. Hence, at low level photo-injection, the injected carriers concentration is equal to the minority carrier concentration. In the case of p-type silicon,

$$\Delta n = n \quad (2.6)$$

In this circumstance, equation (2.5) means that the photoconductivity produced by the laser beam $\Delta\sigma$ was proportional to the photogenerated minority carrier concentrations "n" in p-type silicon.

Provided that the loss of carriers occurs with a time constant much shorter than its chopping frequency (200Hz), the conductivity change $\Delta\sigma$ induced by the laser beam superimposes a square wave on the output DC signal from the frequency mixer. The amplitude of the square wave was found to be small compared to the DC signal. A lock-in amplifier (EG&G Princeton Applied Research model 5102) detected the square wave signal by comparison with the chopping frequency at 200 Hz and amplified it. The lock-in amplifier filtered out the background DC signal and signals at frequencies other than 200 Hz, hence isolating the changes induced by illumination as the output.

A PC AT computer was used for data acquisition. The typical sampling rate was 2/second.

It was found that the largest signal was obtained when the beam struck the portion of the silicon near the inside of the copper shield in which the RF-coil was located. The relative position of the laser beam spot and the probe was therefore optimized, and then any silicon chip of the same shape and size could be placed over the probe, and the signal was not greatly affected by a small change in the sample position.

2.5 The resonance frequency of the RF bridge

When the conductivity of a silicon chip changes, one arm of the RF bridge is altered, so that the resonance frequency of the bridge is different. That frequency lies between 230 to 250

Mhz for the probe we constructed. However, the exact resonance frequency varies with the conductance of the Si sample. This variation with sample resistivity is shown in Figure 2.3. It can be seen that the resonance frequency shifts towards lower frequencies and the peak in the DC signal goes through a minimum as the resistivity is varied between 2.2 and 5.8×10^3 ohm·cm.

When this RF bridge technique was being used for monitoring the photo-induced steady state carrier concentrations, the reading was taken from the output of the lock-in amplifier rather than the frequency mixer, because the signal arising from the laser induced photoconductivity is only a few per cent of the background DC signal. By detecting the output at 200 Hz, the lock-in amplifier measures only the laser injected carriers. This is the difference between resonance curves with and without photogenerated carriers. To illustrate the magnitude of the change in the output from the mixer as a function of input frequency when the conductivity of the Si sample is changed, the difference of the two resonance curves for two Si samples with two different doping levels, with conductivities of 0.067 and 0.45 $ohm^{-1} \cdot cm^{-1}$, and the output from the lock-in amplifier are presented in Figure 2.4.

The similarity of these two curves demonstrates that the lock-in amplifier isolated the photoconductivity signal from the rest.

When continuously monitoring photoconductivity, the frequency of the RF power was fixed at a value for which the "lock-in signal" reached its maximum. For P-type silicon chips with a resistivity of 15 ohm·cm, this resonance frequency occurred at 240.36 MHz. The DC signals from the frequency mixer for silicon samples with differing conductivities at this frequency are listed in Table 2.1.

Figure 2.5 is a plot of the "mixer signal" against $\ln(\sigma)$. The straight line fit to the data

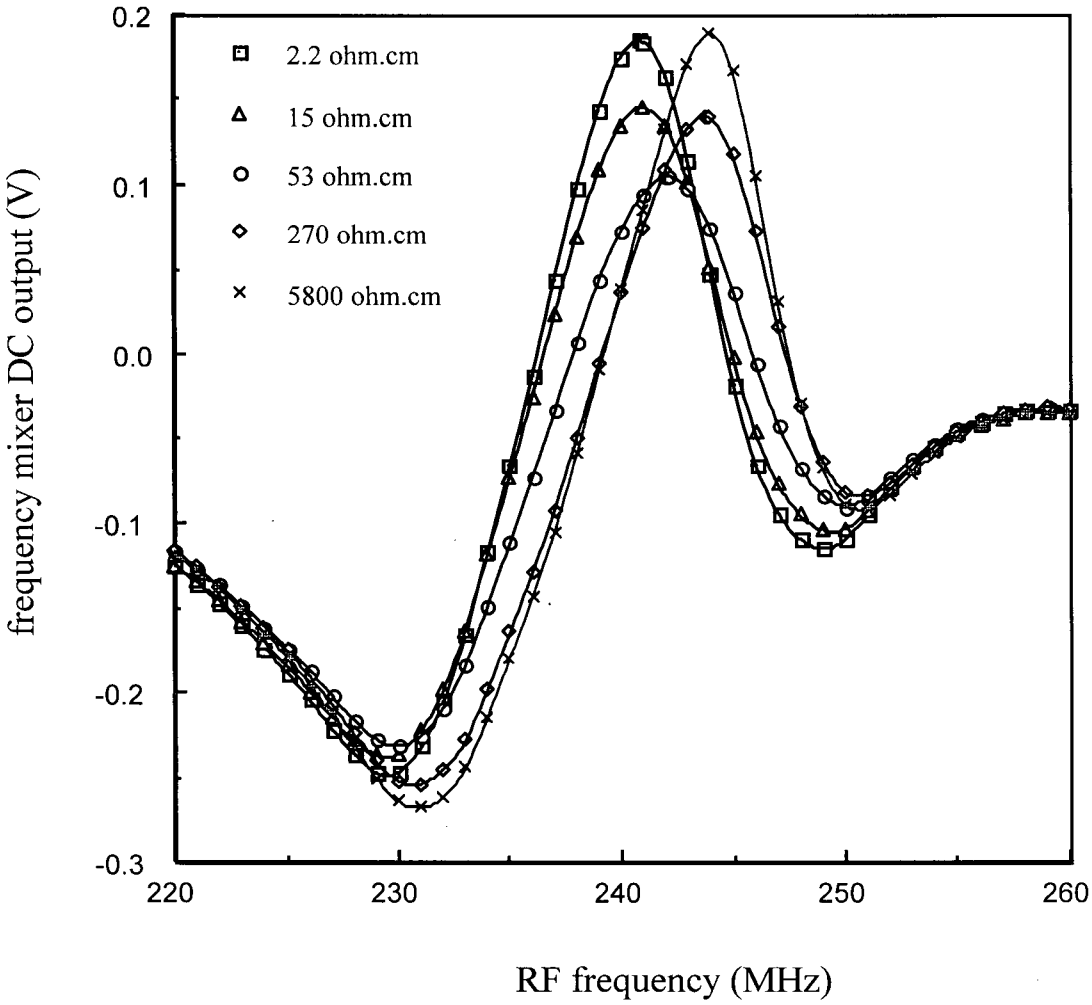

Figure 2.3 The resonance frequencies of different resistivity silicon samples.

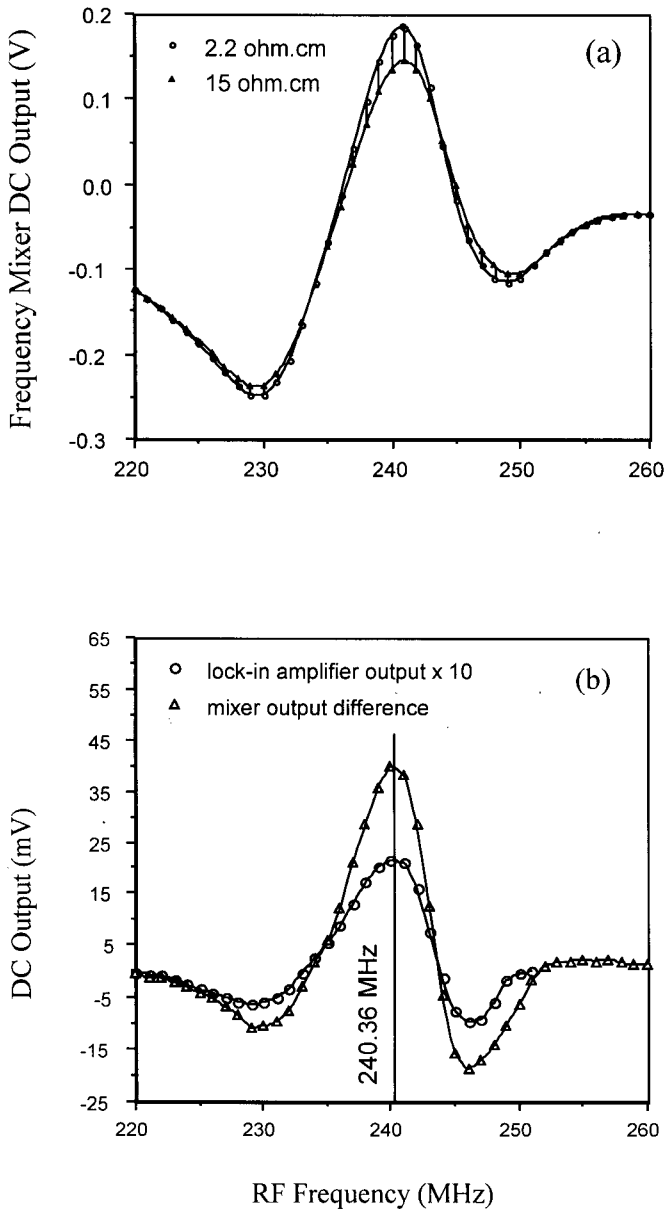

Figure 2.4 (a) D.C output from the frequency mixer for a 2.2 Ω·cm sample and a 15 Ω·cm sample. (b) A plot of the difference between the curves in (a) and a plot of the output of the lock-in amplifier.

Table 2.1 The DC signal values from the frequency mixer for silicon samples with different conductivity at 240.36 MHz.

conductivity σ ($ohm^{-1} \cdot cm^{-1}$)	resistivity ρ (ohm·cm)	DC signal from frequency mixer S_m (V)
0.45	2.2	0.18
0.067	15	0.14
0.019	53	0.082
0.0037	270	0.050

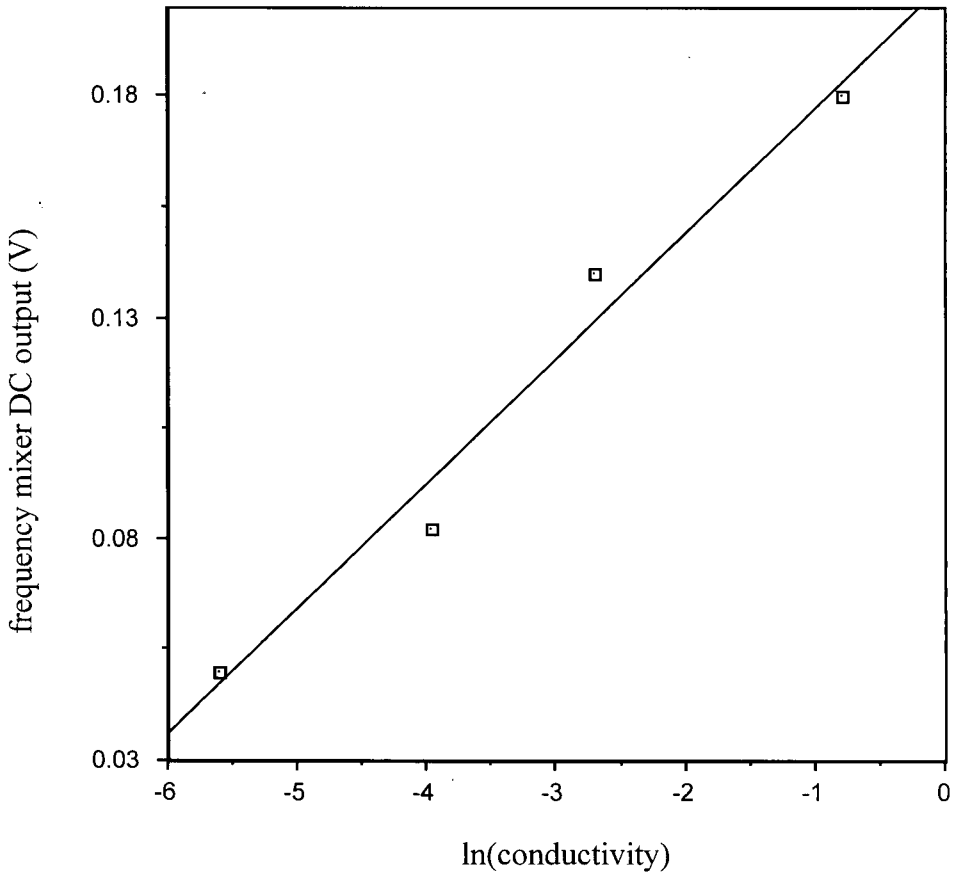

Figure 2.5 Plot of "mixer signal" against ln(σ) at 240.36 MHz.

shown in Figure 2.5 indicates that the mixer signal and the conductivity σ are related by the equation:

$$S_m = A + B * \ln(\sigma) \tag{2.7}$$

where S_m stands for "mixer signal". A and B are constants. Since the lock-in amplifier output is equal to the change in the mixer signal ΔS_m for a conductivity change of $\Delta\sigma$, provided $\Delta\sigma$ is small, the lock-in signal:

$$S_l = \Delta S_m$$

$$= \frac{d}{d\sigma} S_m * \Delta\sigma \tag{2.8}$$

In view of equation (2.7), equation (2.8) becomes

$$S_l = \frac{B}{\sigma} * \Delta\sigma \quad \text{and}$$

$$S_l \propto \frac{\Delta\sigma}{\sigma} \tag{2.9}$$

For p-type silicon at low level injection, from equations (2.5) and (2.6), equation (2.9) becomes

$$S_l = B\, q\, (\mu_n + \mu_p) * \frac{n}{\sigma}$$

$$\propto \frac{n}{\sigma} \tag{2.10}$$

If there is no significant change in conductivity, then the output signal of the lock-in amplifier is, therefore, proportional to the minority carrier concentration.

2.6 The effect of laser beam intensity

Because silicon is an indirect band gap semiconductor, the direct radiative recombination of free electrons and holes is insignificant, and direct recombination occurs only

through the relatively slow "Auger" recombination[46]. The photo-injected carriers are therefore lost on bulk defects and on interfacial defects. Under these circumstances the rate of change of the minority carrier concentration can be expressed by the following equation provided the majority carrier concentration is unchanged:

$$\frac{d[C]}{dt} = k_i j - k_b [t_b] [C] - k_s [t_s] [C] \qquad (2.11)$$

where [C] is minority carrier concentration in silicon, k_i is the coefficient for photo-injection of carriers, j is the laser beam intensity, k_b and k_s are the rate coefficients for carrier loss on bulk and interfacial traps, $[t_b]$ and $[t_s]$ are the bulk and interfacial trap densities, respectively. The first term on the right side of equation (2.11) is the carrier photo-injection rate, the second and third term are loss rates on bulk and interfacial traps, respectively. When a steady state is achieved:

$$\frac{d[C]_{ss}}{dt} = 0 \qquad (2.12)$$

and equation (2.11) can be solved for the steady state minority carrier concentration

$$[C]_{ss} = \frac{k_i * j}{k_b[t_b] + k_s[t_s]} \qquad (2.13)$$

For p-type silicon the minority carriers are electrons (n) and equation (2.13) can be written:

$$n = \frac{k_i * j}{k_b[t_b] + k_s[t_s]} \qquad (2.14)$$

where n = electron concentration. At a fixed temperature k_b and k_s are constants, n is a function of both $[t_b]$ and $[t_s]$. This RF bridge technique can therefore be used to monitor interfacial traps.

Equations (2.10) and (2.14) predict that the output signal of the lock-in amplifier should be proportional to the laser beam intensity j. To test for this relationship, the laser beam intensity was reduced by placing neutral density filter No. 1 or No. 3 in the optical path, which

reduced the laser beam intensity by 87 and 42 percent, respectively. The sample was p-type silicon with a resistivity of 540 ohm·cm. The results are presented in Table 2.2 and Figure 2.6. It can be seen that below 5 mV the output signal of the lock-in amplifier was linearly related to the laser beam intensity. There was a "saturation" effect above 5 mV. According to equation (2.9), at high injection level when photo-injected carriers concentrations were higher then the majority carrier concentration, $\Delta\sigma/\sigma \rightarrow 1$. Thus increasing the laser beam intensity does not cause any further increase in the lock-in output signal. Most of the experiments in this thesis were performed in the linear region. Otherwise, the results were calibrated with a curve like the one in Figure 2.6.

2.7 The effect of changes in temperature

A change in the temperatures of the Si substrate was also found to shift the resonance frequency of the RF probe. Figure 2.7 compares the resonance frequencies of a silicon chip of resistivity 15 ohm·cm with a 170 Å thick thermal oxide on the surface at 22 °C and at 180 °C. The resonance frequency shifted towards higher frequencies with rising temperatures up to 160 °C. The lock-in signal changes with temperature for the same sample are presented in Table 2.3

Table 2.2 The frequency mixer DC signal output changes with laser beam intensity.

	laser beam intensity (arbitrary unit)	mixer output signal (mV)
laser off	0	0
with no filter	1	9.54
with neutral density filter No. 1	0.13	1.48
with neutral density filter No. 3	0.58	6.45

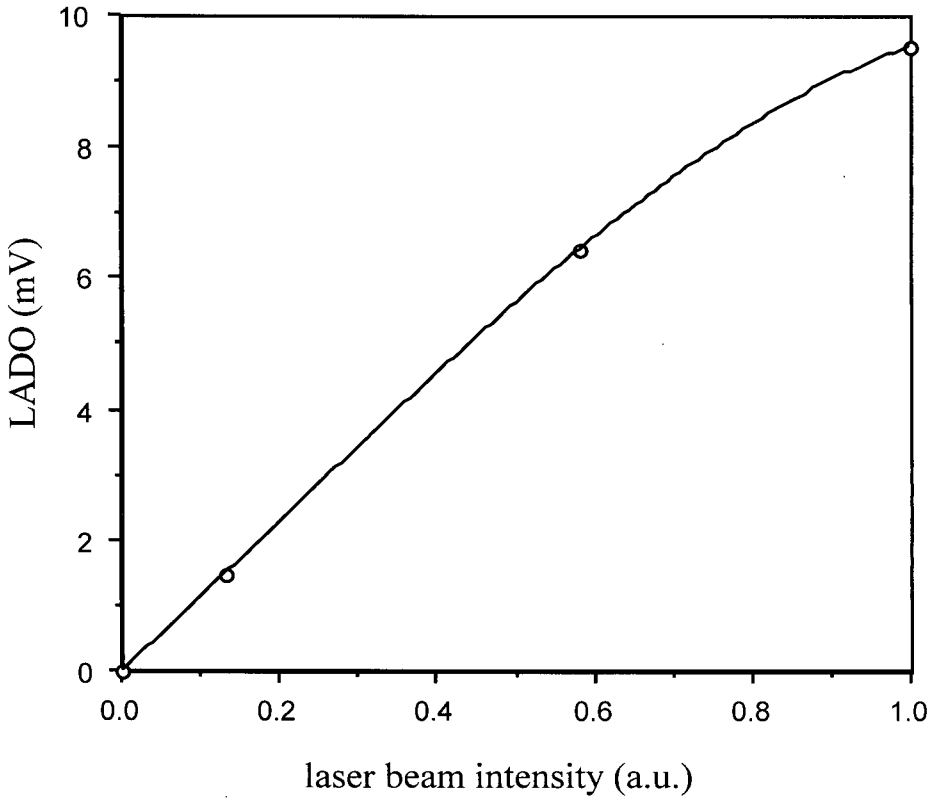

Figure 2.6 Lock-in amplifier output changes with laser beam intensity.

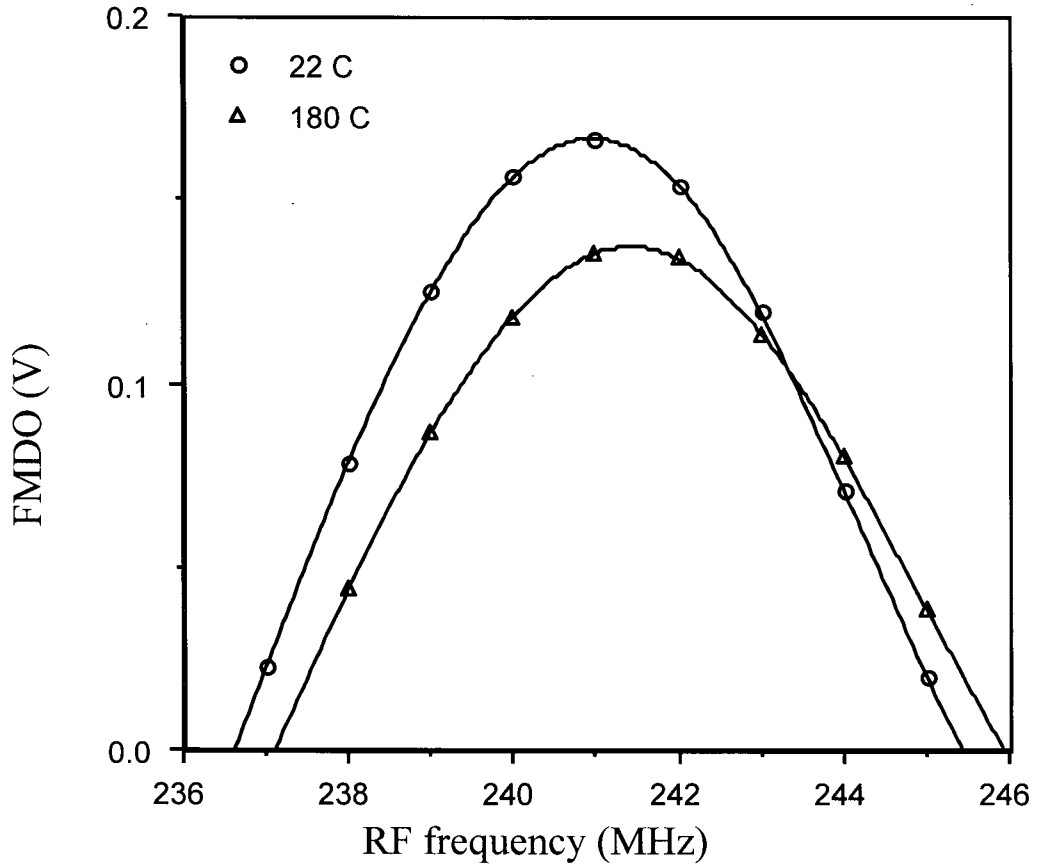

Figure 2.7 Resonance frequencies of a silicon chip of resistivity 15 ohm·cm at 22 °C and at 180 °C

Table 2.3 DC output from the frequency mixer as a function of sample temperature.

silicon sample temperature (°C)	mixer output signal (mV)
21	2.28
33	2.53
55	2.96
77	3.35
97	3.68
119	4.02
137	4.21
159	4.32
177	4.35
202	4.32
222	4.32

and Figure 2.8. The mixer output signal increased with temperature and leveled at 160 °C. Above 250 °C, the lock-in signal quickly dropped to below the detection limit of the RF bridge. The reason for this temperature effect is not clear.

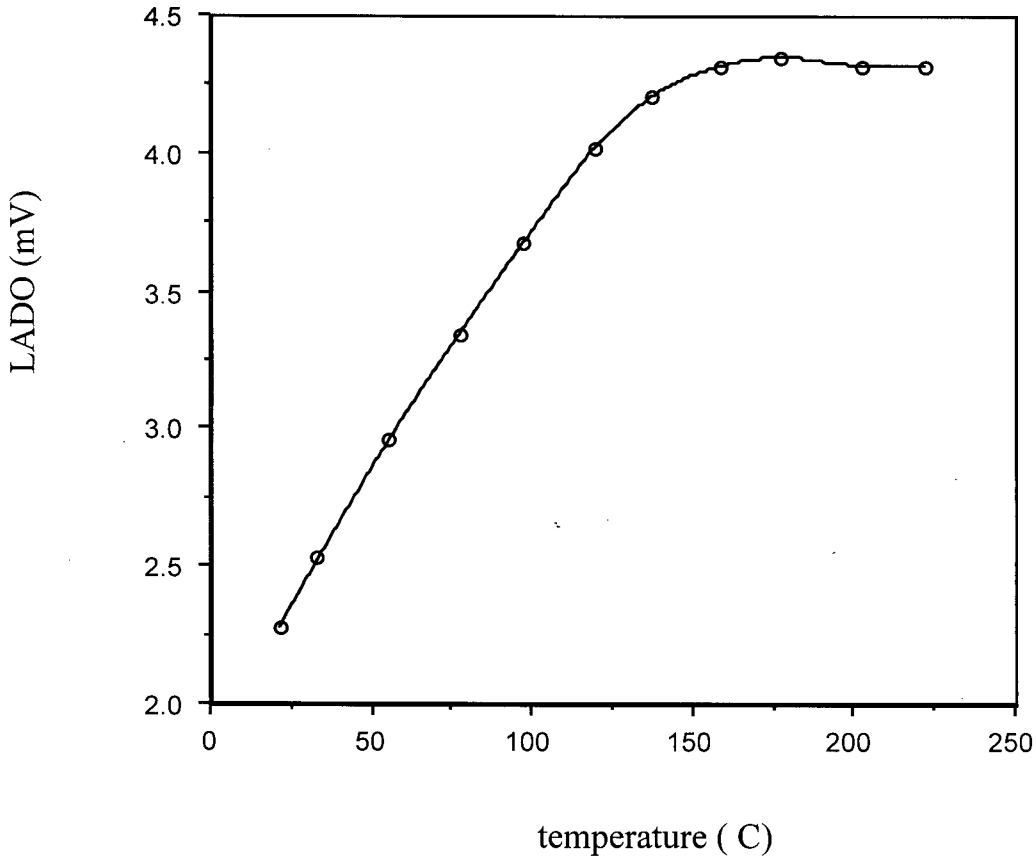

Figure 2.8 Lock-in amplifier output as a function of temperature.

Chapter 3 Experimental

3.1 Apparatus

A schematic of the discharge-flow system used to expose silicon to atomic oxygen and atomic hydrogen is presented in Figure 3.1. The core of the apparatus consisted of a microwave cavity for the creation of atoms, a reaction chamber for monitoring the change in the silicon samples, and a Mass Spectrometer (MS) chamber for monitoring the gaseous species from the reaction chamber.

3.1.1 Reactor for treatment with atomic oxygen and atomic hydrogen

The reactor was constructed of Pyrex except for the discharge region which was made of quartz. The tube was 24 mm in inner diameter in the reaction region and 10.5 mm in the discharge region. Two light traps were added between the discharge region and the reaction region to keep the discharge radiation from impinging on the sample. The end of the tube on the gas inlet side was bent to protect the Cajon O-ring from the discharge radiation. The Pyrex reaction chamber was integrated into the remaining CF-Flange vacuum system with the aid of a $1^1/_2$ inch Glass-to-Metal adapter. The melting point of Pyrex limited the temperature to below 530°C. The reactor was replaced with one constructed entirely from quartz for the thermal oxidation of silicon samples at a temperature of 1100°C.

Gas pressures were measured using a capacitance manometer (Edwards Barocel Series 600) with a pressure range of 10^{-3} to 10 Torr. A cold cathode pressure gauge (HP Model 421)

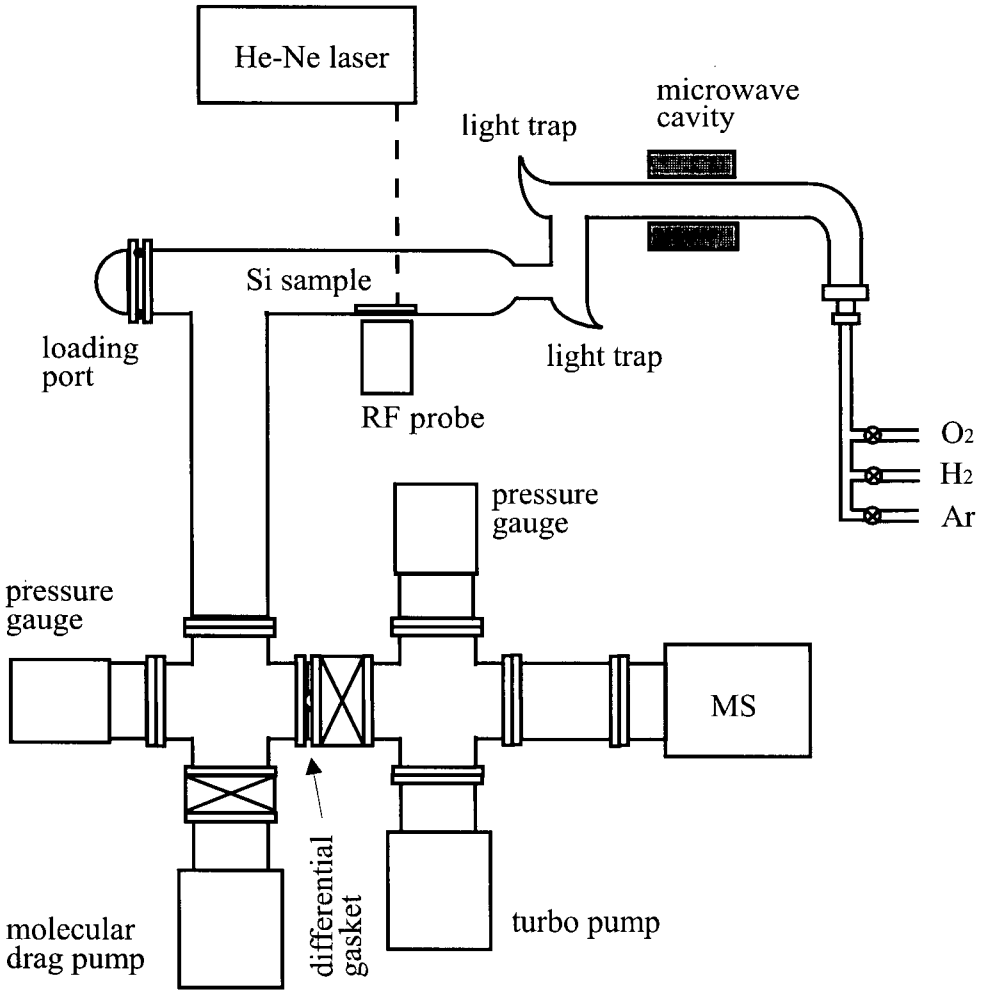

Figure 3.1 Apparatus for silicon oxidation and surface passivation.

was used to measure the pressure in the range of 10^{-2} to 10^{-10} Torr.

The flow system was pumped by a molecular drag pump (Alcatel MDP 5010, 7.5 liters/second nitrogen pumping speed) backed by a rotary pump (Sargent Welch Model No. 1376, 300 liters/minute pumping speed). The base pressure of the reaction system was typically 10^{-6} Torr and the gas pressure was a few hundreds mTorr. The molecular drag pump has the advantage of a high pumping speed and a high maximum operating pressure at the inlet (about 100 mTorr) in continuous operation. This permitted a fast gas flow rate for the discharge-flow system so that the atomic species from the discharge have less time to decay before reaching the sample, keeping the concentrations of atoms high in the sample region. When a pressure higher than 100 mTorr was needed, the molecular drag pump was removed. The system was then pumped directly by the rotary pump. The pumps were isolated from the remaining system by a butterfly valve.

Argon, oxygen, and hydrogen were connected to the system with a Cajon reducing union. Argon and oxygen flow rates were controlled with bellows metering and regulating needle valves (Nupro SS-4BMG). Fine control of the hydrogen flow rates were achieved with a Granville-Philips series 203 variable leak valve. Diaphragm valves (Nupro SS-DLS4) or ball valves (Nupro B-4P4T) were used to shut the gas lines off completely. The gas lines were 1/4 inch copper tubing. A helical coil constructed of part of the copper gas line was immersed in liquid nitrogen and served as a cold trap to remove water vapor from the feed gases. The flow rates were measured for each gas by pumping at a fixed pressure, suddenly isolating the system from the pump and measuring the rate of pressure increase in the closed system. The system volume was determined to be 600 mL by measuring the dimensions of the reaction chamber.

Argon or oxygen was used to bring the system up to atmospheric pressure after

completing an experiment and to provide a positive pressure of gas while loading and unloading samples. This was done in an effort to avoid the introduction of air or moisture into the system.

An E.M.I. Microtron 200 microwave generator, which was coupled to the gas through a quarter wave cavity, was used to create a glowing discharge. The discharge region was cooled with compressed air to prevent overheating and to reduce atom losses on the hot walls. The microwave generator was operated at 2.45 GHz, between 30 and 100 watts.

3.1.2 The sample holder and temperature measurement

The design of the sample holder is illustrated in Figure 3.2. The sample holder was attached with concentric, Cajon type, O-ring fittings to the loading port cap and another Cajon fitting was used to attach the cap to the system. The silicon samples were laid horizontally on the bottom of the Pyrex tube reactor. To hold the samples in place, the 6 mm diameter Pyrex sample retainer was bent downward so that its tip just touched the silicon sample. The bending of the sample retainer was done with great care so that a small pressure was applied to the samples by the elasticity of the three Cajon O-ring fittings. A 1 mm diameter flexible high-temperature thermocouple probe (Cole-Parmer H-08514-96, K type, maximum temperature 1100°C) was inserted into the sample holder for measuring the sample temperature. The tip of the sample retainer was blown very thin to minimize the amount of Pyrex between the sample and the thermocouple.

The sample was heated by wrapping a heating wire around the sample region indicated in Figure 3.2 for temperatures below 200°C. Better insulation was needed for the heated region at higher temperatures. In the temperature range from 200 to 500°C, the RF probe underneath

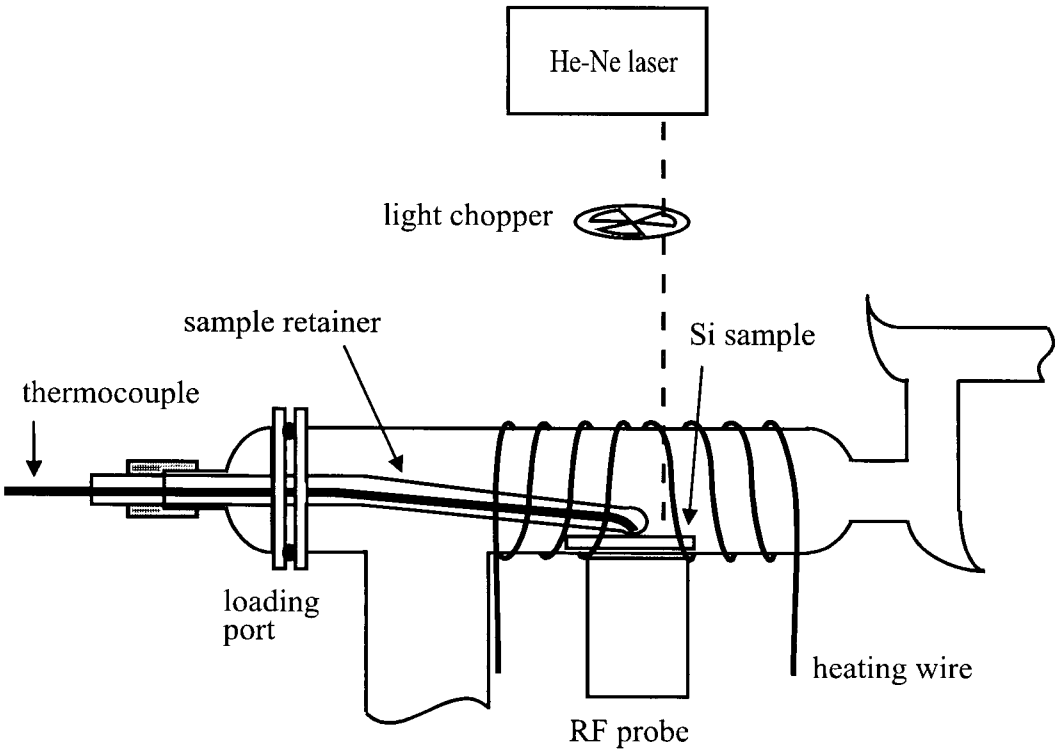

Figure 3.2 Sample retainer used for silicon oxidation and surface passivation. It was also used to monitor the sample temperature.

the sample was removed, aluminum foil was wrapped around the heated region for insulation. Above 500°C, a high temperature tube furnace was used to raise the temperature up to 1100°C.

The reaction system was designed with only two openings, the loading port and gas inlet, to minimize the possibility of leaking. For the titration of oxygen atoms, gases like nitrogen dioxide needed to be introduced into the system at the sample position. This was done by replacing the sample retainer with Pyrex tubing which served as another gas inlet. The inlet tubing was bent at the end so that the added gas was introduced in the same direction as the total gas flow.

3.1.3 The mass spectrometer

The mass spectrometer vacuum chamber was constructed of $1^1/_2$ inch stainless steel tube fittings with $2^3/_4$ inch CF-Flanges (Figure 3.3). The system was pumped by a turbomolecular pump (Edwards EXT70, pumping speed 52 liters/second nitrogen) backed by a rotary pump (Sargent-Welch model No. 1402, pumping speed 160 liters/minute) permitting the system to be pumped down to a base pressure of 10^{-7} Torr. A pneumatic valve (Kurt J. Lesker model No. SA0075PVTE) was employed in between the turbomolecular pump and the rotary pump to prevent backstreaming of hydrocarbon vapors from the rotary pump oil if the power failed. Dry nitrogen could be admitted into the system with a solenoid vent-valve (Edwards TAV5) attached to the vent port on the turbomolecular pump, functioning as another measure for power failure protection or when the pump was switched off. 24 V d.c. power was supplied by a turbomolecular pump controller.

A gate valve (MDC electropneumatic, model No. GV-1500V-P) connected the MS chamber to the reaction chamber. The gasket between the gate valve and flange on the side of reaction chamber is a "differential gasket", which was a copper plate with a pin hole ~ 100 micrometer in diameter in the center to leak a small amount gases from the reaction chamber into the MS chamber. Since the gas is swept past this pinhole, sampling is rapid, and diffusion on the low pressure side of the pinhole is rapid because of the low pressure there. There are two reasons that this arrangement is better than one in which the differential gasket is on the MS side. One reason is that it takes less time for gases in the reaction chamber to diffuse to the differential gasket. Furthermore, if the differential gasket is on the MS side, it takes a long time to pump the remaining gases out through the small pinhole after the gate valve is shut off. When the pressure in the reaction chamber is 500 mTorr, the pressure in the MS is $2x10^{-5}$ Torr due to the leak through this differential gasket.

The mass spectrometer was a quadrupole mass analyzer (MKS partial pressure transducer (PPT) residual gas analyzer) with a mass range of 1 to 200 atomic mass units and a maximum operating pressure of $1x10^{-4}$ Torr. Its ionization chamber was set close to the gate valve connecting the MS chamber and the reaction chamber so that the gas flow passed through the ionization chamber to minimize the response time and increase the sensitivity.

The pressure of the system was measured with an ionization gauge (Leybold-Heraeus COMBITRON CM330). The pressure could also be read from the quadrupole mass sensor in the range of $1x10^{-4}$ to $2x10^{-9}$ Torr.

A PC computer (IBM 486DX33) was used to control the mass spectrometer and to display the MS spectrum. The software was supplied by MKS which runs under a DOS

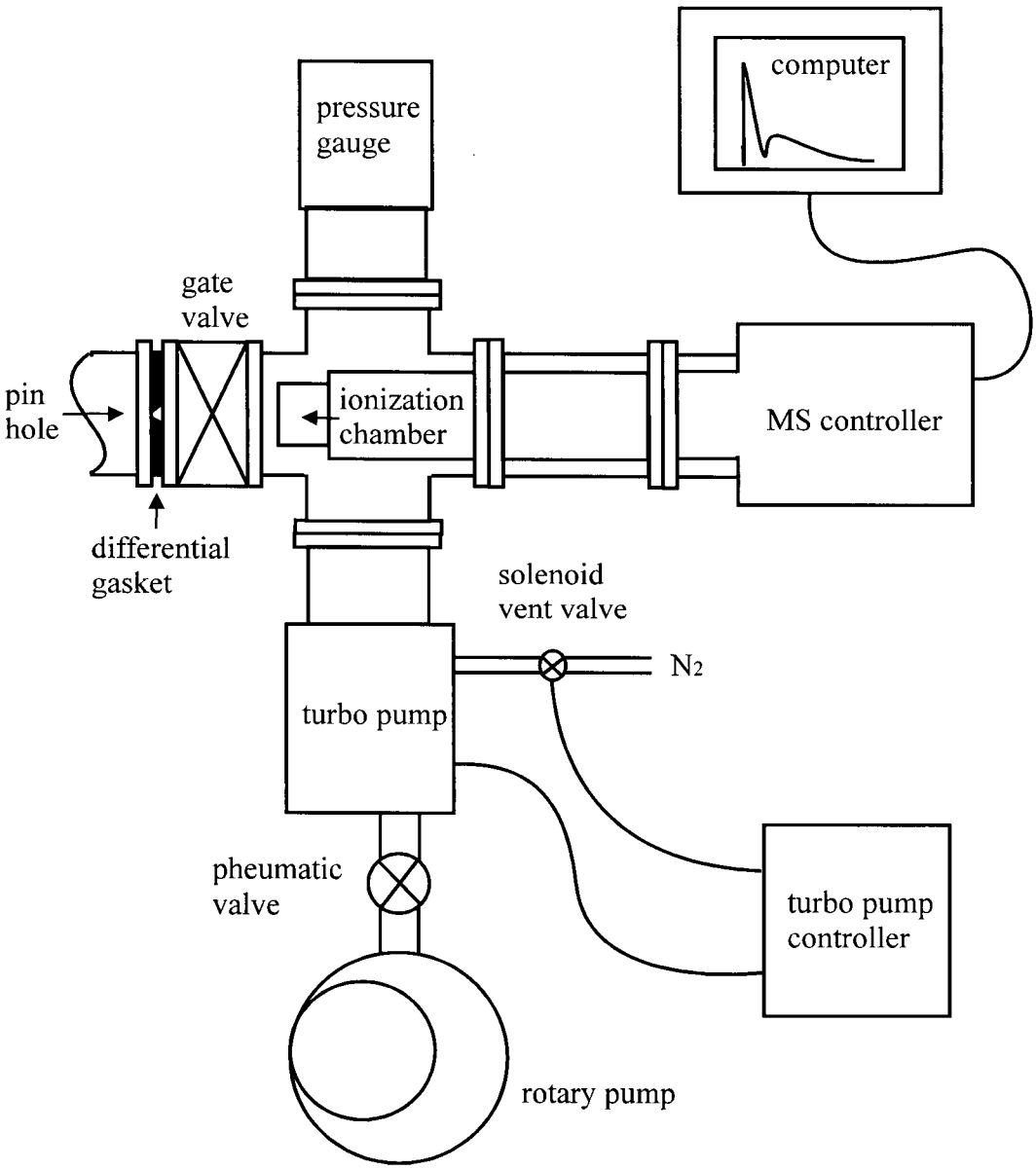

Figure 3.3 The mass spectrometer system.

operating system.

3.2 Chemicals

3.2.1 Silicon samples

3.2.1.1 Czochralski grown silicon

Most single crystal silicon produced for the semiconductor industry is grown by the Czochralski technique[47]. Silicon is first melted in a quartz crucible and a suitably oriented seed crystal is inserted into the melt. When its end is molten, the seed is slowly withdrawn pulling with it a single crystal which grows by progressive freezing at the liquid-solid interface. Then the single crystal ingot is cut into wafers and polished.

All Czochralski silicon samples used for oxidation and surface passivation were cut from boron-doped single crystal wafers with a (100) surface orientation. The resistivities, wafer thicknesses and sizes are listed in Table 3.1. Also included in the table is a code number for each wafer which will be used to identify the samples studied. Both sides of Wafer CZ0 were covered with a 170 Å layer of thermal oxide which was grown at about 1100 °C in pure O_2.

3.2.1.2 Float-zone silicon

Single crystal silicon grown by the Czochralski technique can be further purified by the float zone technique[48]. A rod of silicon is held in a vertical position and rotated slowly. A small zone of the crystal is kept molten by means of a radio-frequency heater which is moved so that this floating zone traverses the length of the bar. A seed crystal is provided at the

Table 3.1 Float zone (FZ) and Czochralski (CZ) grown silicon wafers. All surfaces are (100).

wafer number	resistivity (Ω·cm)	dopant concentration (cm^{-3})	wafer thickness (mm)	wafer size (inch)	oxide cap (Å)
FZ	~4200	~$1x10^{12}$	0.50	3	none
CZ0	13-17	~$9x10^{14}$	0.70	6	170
CZ1	1-3	~$8x10^{15}$	0.35	$2^1/_4$	none
CZ2	8-10	~$1x10^{15}$	0.30	2	none
CZ3	20-40	~$5x10^{14}$	0.35	2	none
CZ4	70-130	~$1x10^{14}$	0.25	2	none

starting point where the molten zone is initiated and arranged so that its end is just molten. As the zone traverses the rod, the silicon is recrystallized and impurities removed with the zone by the fact that impurities have higher solubilities in the melt. Float zone silicon samples have few impurities and thus fewer carrier traps in the bulk.

Float zone silicon wafers of (100) orientation were used for oxidation and surface passivation. The resistivity, wafer size, and thickness of the FZ-wafer used in this studies are also listed in Table 3.1.

3.2.1.3 Determination of resistivities and dopant concentrations

The resistivity (ρ) was measured using the four point probe method[49]. The measurement was made by bringing an array of four equally spaced tungsten carbide electrodes in contact with the surface to be measured. A current (I) of a few tenth of a milliamp was passed through the two outermost electrodes and the resulting voltage drop (V) across the inner two electrodes was measured. The calculated sheet resistance (V/I) was then multiplied by the film thickness (t) to yield a value of resistivity in units of ohm-cm

$$\rho = F\, t \frac{V}{I} \qquad (3.1)$$

where F is a correction factor that depends on the sample geometry. The instrument was calibrated with a wafer of known resistivity. Conversion curves for each type of dopant are available which then relate the film resistivity to dopant concentration.

3.2.2 Gases

Ultra high purity helium, argon, oxygen, and hydrogen supplied by Linde were used. The purity was quoted as 99.999%, with a maximum moisture of 5 ppm. The purity of the nitrogen dioxide used for titrating the O-atoms is about 99.5% (liquid phase).

3.3 Wafer cleaning

Samples cut from the various single crystal silicon wafers were dipped in a solution of 2% hydrofluoric acid (Aldrich, A.C.S. reagent) for 60 seconds, followed by rinsing in deionized water and blow-dried in nitrogen. The surface was not put through the common RCA[50] chemi-oxidation and HF removal cycle since it was shown that reproducible results could be achieved whether the oxide is grown chemically, thermally, or naturally[34]. Depending on the objective of the experiment, the oxide on the polished side of the sample could be removed by floating the sample on the surface of an HF solution while the oxide on the other side was left intact. Because clean silicon surfaces of freshly cleaved edges were hydrophobic, surface tension helped to keep the sample floating on the surface of the HF solution.

Attenuated total reflection (ATR) IR spectra of silicon surfaces after dilute HF treatment have demonstrated that surface dangling bonds are terminated with H-atoms and not F-atoms[51], and the (1x1) symmetry formed in LEED patterns[50] of such HF washed silicon (100) surfaces indicates that these surfaces are terminated with silicon dihydride. This is in agreement with IR spectra in which the SiH_2 peak is the highest[51] . The hydrogen termination after an HF wash is stable and protects the surface from being oxidized for several hours even in air[52].

3.4 Atomic oxygen oxidation of silicon

3.4.1 Production of O atoms

Microwave discharges have long been used to generate O-atoms. In our experiments the molecular oxygen to be dissociated was passed directly through the discharge without inert gas dilution. The microwave generator supplied 100 watts of power to the quarter wave cavity. The pressure of O_2 was chosen to be 500 mTorr to maximize the O-atom concentrations and to minimize the sputtering of the quartz walls. A high gas flow rate was required in order to transport the atoms from the discharge to the sample. A long transit time would result in a drop in the O atoms concentration through atom recombination. The flow rate was measured to be 115 sccm (where sccm stands for standard cubic cm per minute, i.e. cm^3min^{-1} at 1 atm and 25 °C). Assuming plug flow conditions, the gas flow rate inside the 10.5 cm diameter flow tube was greater than 30 m/sec. This is 3 cm/ms, i.e. 0.33ms/cm. Taking into account the large diameter of the reaction vessel the gas took about 10 ms to travel the 17 cm from the discharge region to the silicon sample.

3.4.2 Titration of oxygen atoms

Nitrogen dioxide is introduced downstream of the microwave plasma discharge at the silicon sample position to titrate the oxygen atom concentration by the following chemical reactions[53].

$$NO_2 + O \rightarrow NO + O_2 \qquad (2.15)$$

$$O + NO \rightarrow NO_2^* \rightarrow NO_2 + h\nu \qquad (2.16)$$

Reaction (2.15) is very fast so that NO_2 rapidly consumes a stoichiometrically equivalent number of oxygen atoms. Reaction (2.16) emits yellowish-green chemi-luminescence which can be seen in a dark room but does not consume a significant number of O-atoms. The end point of the titration can be taken as either the extinction of the light from reaction 2.16, at which point $[NO_2] = [O]$, or the point at which the intensity of the emitting light reaches its maximum. At this latter end point, half the O-atoms have been titrated making the light intensity from reaction (2.16) a maximum because the concentrations of O and NO are equal and the concentration of NO_2 introduced is exactly half of the initial oxygen atoms concentration at the sample position generated by the upstream microwave discharge.

At the maximum emission end point, NO_2 introduced in our system was 46 mTorr indicating P_O = 92 mTorr. Assuming NO_2 and O atoms behave as ideal gases, this pressure corresponded to about $4x10^{-9}$ mol·cm^{-3} or $2x10^{15}$ atoms·cm^{-3} and 8% O_2 dissociation at room temperature.

3.4.3 The measurement of oxide thickness

The height of the Si-O stretching peak at 1070 cm^{-1} in transmission FTIR (Bomem M120 with a HgCdTe detector cooled with liquid nitrogen) spectrum was used to measure the oxide thickness since it has been shown to be linearly related to the oxide thickness[54]. The spectrum of the same sample with oxide removed served as the reference in order to subtract background absorption. The peak of this absorption band in the thin oxide grown with atomic oxygen was found to be at 1050 cm^{-1}. This is about 20 cm^{-1} lower than the peak observed for the 170 Å thermal oxide. The thickness was calibrated with the 170 Å thermal oxide and the

coefficient was found to be 6.37 x 10^3 Å /Absorbence unit, which is in good agreement with Bardwell.[55]

3.4.4 Oxidation Procedure

Experiments were carried out in the following manner. 12x7 mm samples were cut from silicon wafers. Prior to being oxidized, all samples were cleaned in 2% HF solution, rinsed in deionized water, blown dry with N_2 and then loaded into the reaction tube with the polished side facing up. The sample holder was then placed in position while the system was flushed with O_2. The positive pressure of O_2 helped to prevent air or moisture from entering the system during the loading procedure. The system was pumped down to the desired pressure of 500 mTorr and O_2 was flowed through the system for about 30 minutes to allow the flow to stabilize and flush out any impurities. This process was monitored with the mass spectrometer and the decrease and then stabilization of the H_2O peak, and the disappearance of the N_2 peak indicated that the reaction chamber was clean. The apparatus was brought up to the desired operating temperature with the heating wire connected to a Variac. The discharge was ignited with a Tesla coil and the atoms flowed for the desired period of time. Steady state carrier concentrations were monitored *in situ* with the RF probe placed underneath the sample for temperatures below 250°C. Because the RF probe becomes insensitive above 250°C, for experiments performed at higher temperatures, the steady state carrier concentrations were measured after the sample was cooled down to room temperature. Once the oxidation was complete, the discharge was shut off and the system was cooled and brought up to atmospheric pressure with O_2.

The system was flushed with Ar to keep it clean when not used. The reaction tube was washed at regular intervals with dilute HF solution and then rinsed with distilled water to clean the walls. To prevent contamination from metal ions, the tube was not degreased with hot KOH before the HF wash.

3.5 Atomic hydrogen treatment

3.5.1 Production of H atoms

A microwave discharge was used to generate H-atoms. Because the effect of H-atoms on the carrier traps was very rapid it was found necessary to produce very small H-atom concentrations in order to make the rate of this process measurable by the RF probe. The following measure was taken to reduce the H-atom concentrations. The H_2 passed through the discharge was reduced to below 10^{-3} Torr and diluted with 30 mTorr of argon. The power of the microwave generator was reduced to 30 watts. Phosphoric acid, which has been used in this laboratory[55] for reducing the wall recombination rate was not applied. The presence of the phosphoric acid in the discharge region might introduce a variable amount of water into the gas stream which could complicate the reactions. The flow rate of the Ar/H_2 mixture was measured to be 13.5 sccm. Assuming plug flow conditions, the gas flow rate inside the system was about 65 m/sec.

Low H-atom concentrations are very difficult to measure. We had to assume that the H-atom concentration is proportional to the H_2 partial pressure since at these low pressures we expect the percentage dissociation to remain constant. The H_2 peak in the mass spectrum was therefore monitored as a measure of the H-atom pressure in the reaction chamber.

3.5.2 Typical procedure for exposure to H-atoms

The procedure followed in the H-atoms treatment was essentially the same one used in atomic oxygen oxidation discussed in section 3.4.4. Once the sample was loaded, the system was flushed with 30 mTorr Ar until the N_2 peak disappeared on the mass spectrum. Argon was then shut off and the system was pumped down to a base pressure below 10^{-5} Torr. The desired flow of H_2 was admitted into the system and then a flow of argon was added to make the total pressure 30 mTorr. Once the temperature was stabilized, the microwave discharge was ignited. Steady state carrier concentrations were monitored in situ with the RF probe. The experiment was terminated by shutting off the power to the discharge.

Chapter 4 Results and discussion (I): Oxidation and H_2 annealing of Si(100)

4.1 The Si/SiO_2 interface

P-type silicon substrate CZ0 (see Table 3.1) was subjected to the following processing steps, and the effect of each was monitored with the RF probe. The results are presented in Figure 4.1.

(1) The thermal oxide coating was removed from one side of the wafer with an HF wash at room temperature.

The steady state carrier concentration drops by about 1/3, i.e. the H-terminated surface that results from an HF wash has about the same level of carrier traps as the thermal oxide covered surface.

(2) The H-terminated surface was exposed to atomic oxygen for 5 minutes at 404 °C.

The steady state carrier concentration dropped to a level that was below the detection limit of the RF probe, while a ~15 Å layer of silicon dioxide formed on the surface (see section 4.2). No recovery of the steady state carrier concentration was observed to result from further exposure to O-atoms at any temperature between 25 °C and 450 °C.

(3) The oxidized surface was then annealed in 3 Torr of H_2 for 30 minutes at 414 °C.

The steady state carrier concentration recovered to a level 2.5 times as high as the H-terminated silicon surface.

(4) The exposure of this oxidized and annealed surface to oxygen atoms at room temperature resulted in an initial drop of the steady state carrier concentration, but as the exposure was continued for longer than 5 minute, the steady state carrier concentration rose to

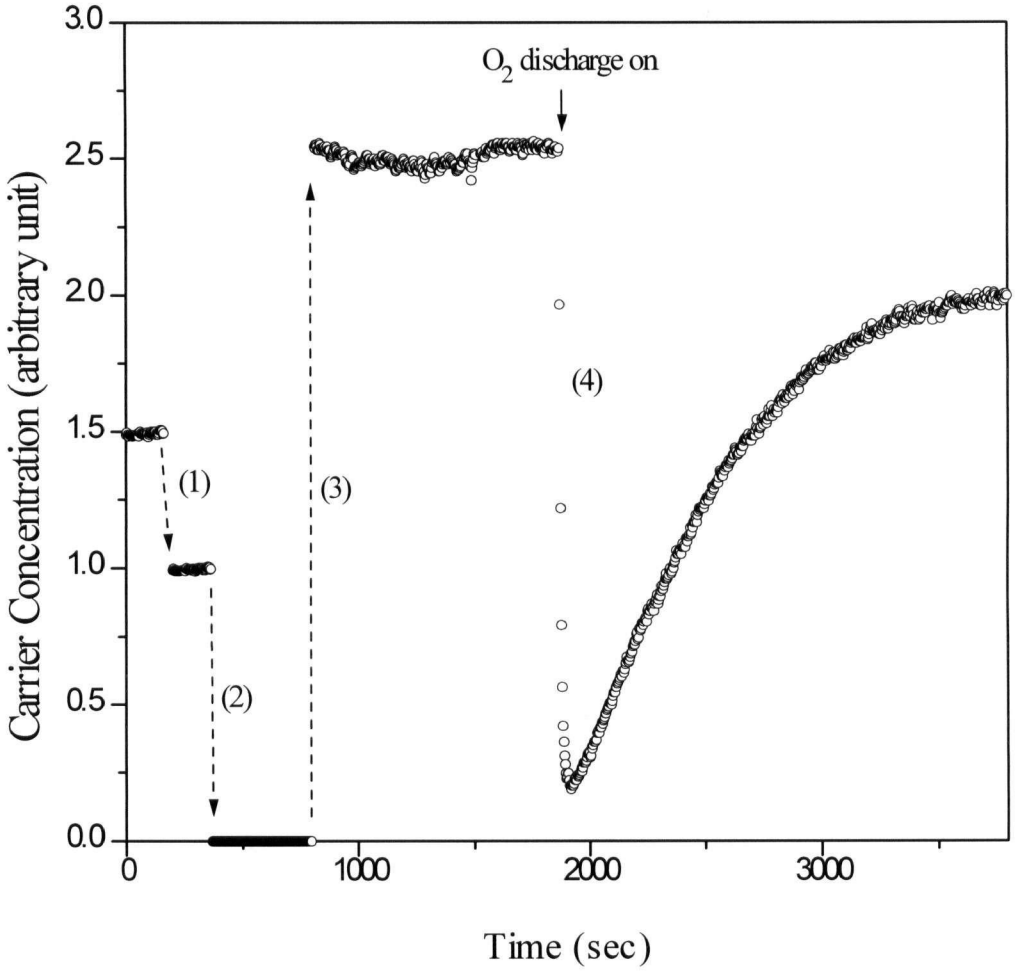

Figure 4.1 The carrier concentration change of silicon sample CZ0 (with 170 Å thermal oxide on both sides) after (1) the thermal oxide on the polished side was washed off with a dilute HF solution at room temperature (the other side was still covered with oxide), (2) O-oxidation at 404°C for 5 min. and (3) annealing in 3 Torr of H_2 at 414°C for 30 min., and (4) during exposure to oxygen atoms at room temperature after the H_2 anneal.

above ¾ of the value that it had after the H_2 anneal.

The effect of exposure of a freshly HF washed, intrinsic, float-zone silicon sample to oxygen atoms is similar to the effect on a p-type Czochralski grown sample, as illustrated in Figure 4.2. After exposure to O-atoms at 450 °C (O_2 pressure 1.0 Torr, microwave power 100 watt) for 11 minutes, the steady state carrier concentration was about 1/4 of its initial value. An H_2 (5 Torr) anneal at 450 °C for 30 minutes raised the passivation level by a factor of 10, to about 2.2 times its value after the HF wash. The same effect was observed by exposure of this oxidized and annealed surface to oxygen atoms at room temperature. Only the final level of recovery was lower, i.e. about the same as the H-terminated surface at the beginning. The rise that is labeled process (1) in Figure 4.2 appears to be caused by the desorption of gases from the surface. This will be discussed in Chapter 6.

In preliminary work we found that the effect of exposure of an H-terminated surface to the products just outside the glowing region of a radio frequency discharge is very similar to the effect of an exposure to the down-stream products of a microwave discharge. The growth of a layer of silicon dioxide at temperatures between 25 to 450 °C creates a high density of interfacial traps. Annealing in H_2 removes these traps and improves the passivation so that it becomes as good as a thermal oxide.

4.2 Thickness of the silicon dioxide layers

As shown in Figure 4.3, the oxide grown with the down stream products of a microwave discharge in O_2 reaches a thickness limited by the oxidation temperature in about five minutes. The maximum thickness of the oxide does not increase very much with temperature. It only

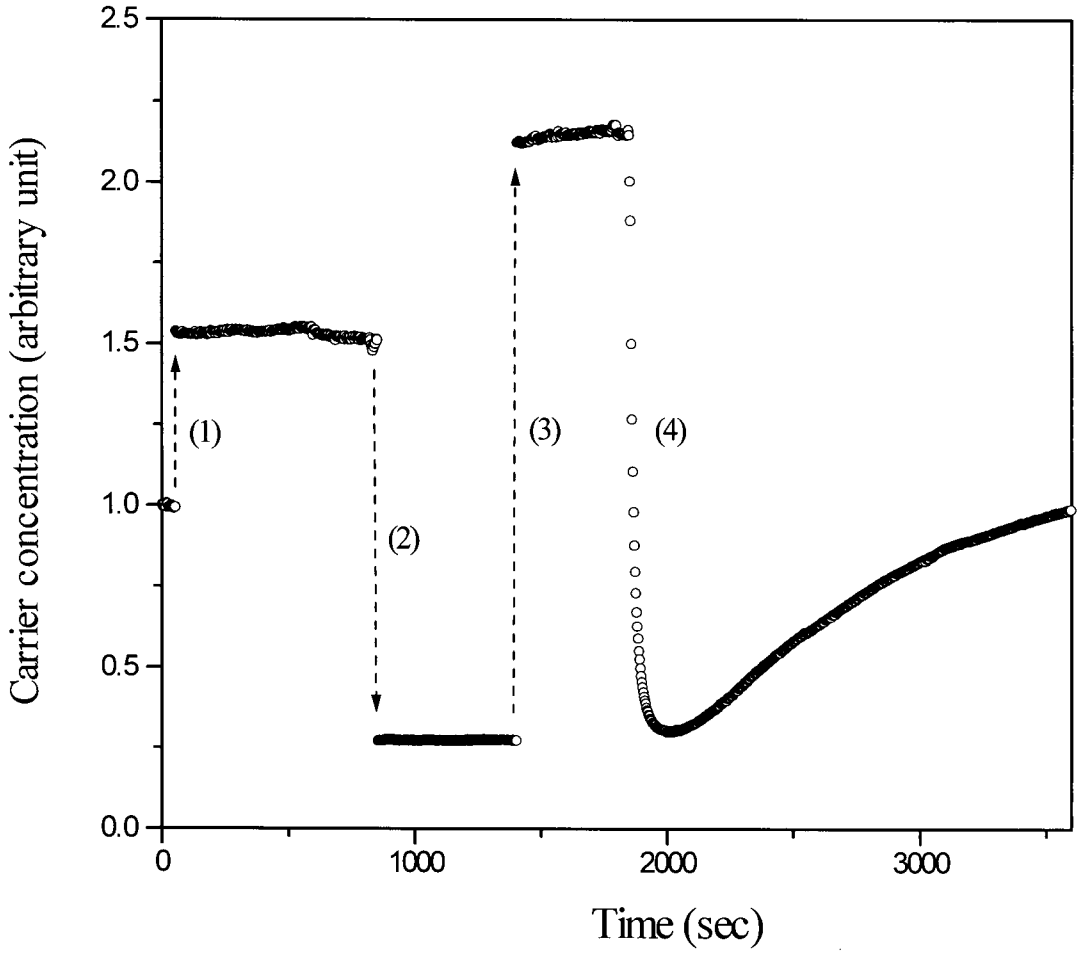

Figure 4.2 The carrier concentration change of silicon sample FZ (intrinsic, float-zone) after (1) annealing in H_2 at 470°C for 20 min., (2) O-oxidation at 450°C for 11 min., and (3) annealing in H_2 at 450°C for 30 min., and (4) exposure to oxygen atoms at room temperature.

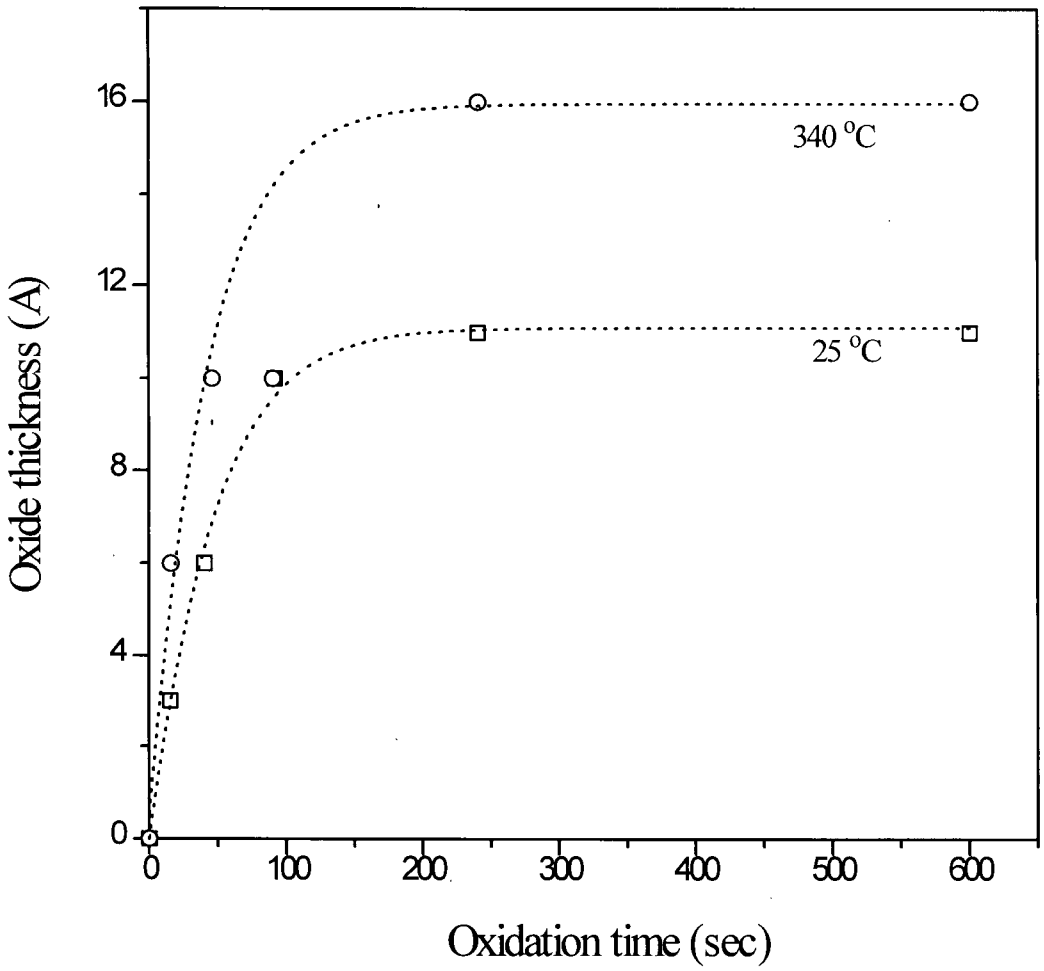

Figure 4.3 Plot of silicon dioxide thickness against oxidation time for surface oxidation of silicon with gaseous atomic oxygen at room temperature and 340 °C.

increased from 11 Å to 16 Å when the oxidation temperature was raised from room temperature to 340 °C.

As demonstrated in Figure 4.4, the thickness of the oxide grown in close proximity to a radio frequency discharge is also limited by the oxidation temperature. However, the maximum thickness of the oxide increases faster with temperature than it does with a remote microwave discharge. Within experimental error, the thickness that can be reached increases with the oxidation temperature. The charged species that are present when the plasma is near the silicon surface might contribute to the growth of a thicker oxide when the radio frequency discharge is in close proximity.

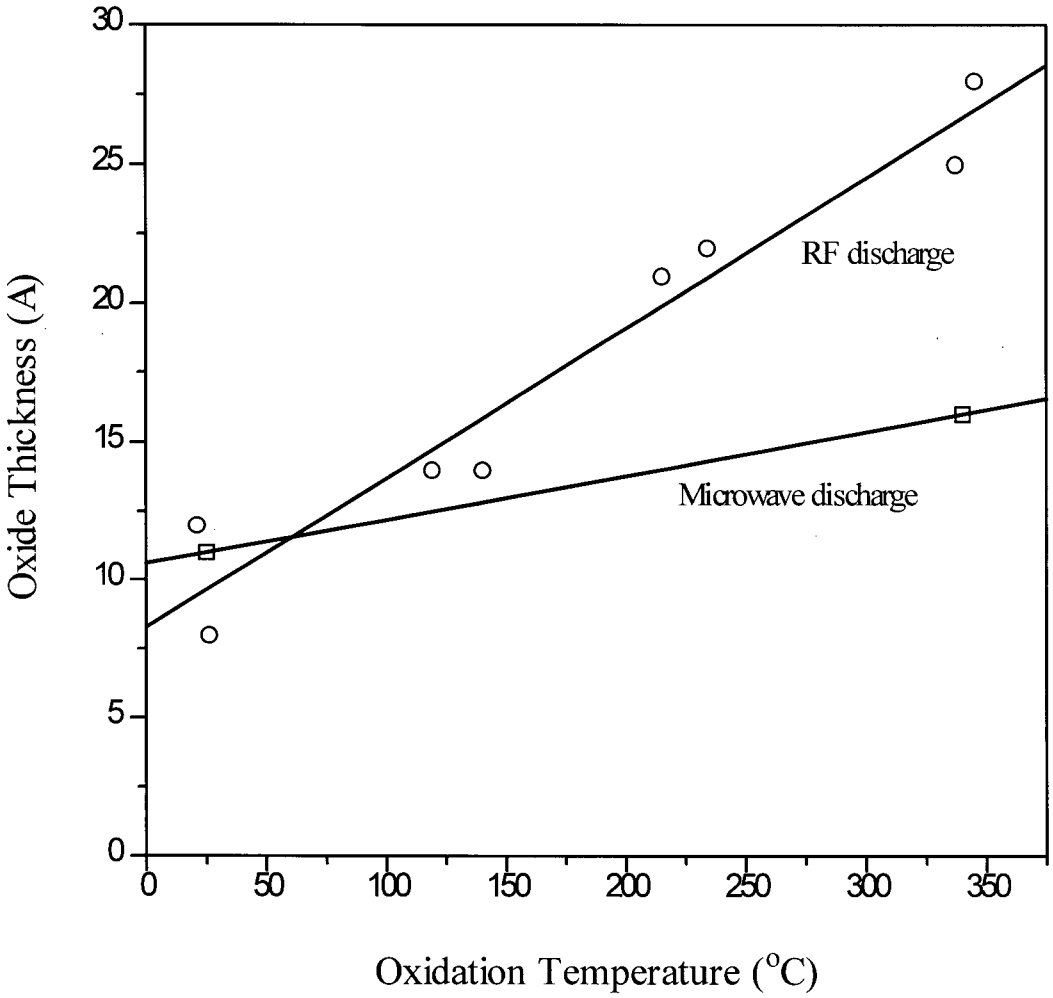

Figure 4.4 Maximum oxide thickness limited by the oxidation temperature for microwave discharge and radio frequency discharge oxidation of silicon.

Chapter 5 Results and discussion (II): Annealing of p-type silicon in H_2

As shown in section 4.1, annealing at 450 °C in the presence of hydrogen is a very effective way of removing interfacial traps. In order to optimize the passivation levels, silicon sample CZ0 (p-type, 13-17 ohm·cm resistivity, with 170 Å thermal oxide on both sides) was annealed at 450 °C in 5 Torr of hydrogen. The change in steady state carrier concentration with annealing time is presented in Figure 5.1. Since the RF probe does not give a measurable signal at temperatures higher than 250 °C, the sample was cooled to 25 °C for each point, so that the steady state carrier concentration could be recorded before it was heated up again to obtain the later points on the curve. Over a period of three hours, the steady state carrier concentration rose an order of magnitude, and then fell to a level that was much lower than the initial value.

Since both bulk and the interface losses contribute to the steady state carrier concentration, it is necessary to identify the source of the change. If the annealing at 450 °C was passivating carrier traps at the Si/SiO_2 interface only, for the first 85 minutes, and then creating interfacial traps more rapidly after 85 minutes, removing the surface oxide with an HF wash at different points along the curve in Figure 5.1 would always yield the same steady state carrier concentration, i.e. that characteristic of an H-terminated surface. On the other hand, if the changes were in the bulk only, removing the oxide would make the steady state carrier concentration drop by about the same percentage (i.e. not always to the same value). When the annealed sample was stripped of the oxide layer at t = 0, t = 90 minutes and t = 110 minutes, the steady state carrier concentration of all three samples fell 20-30%, i.e. the drop characteristic of an untreated oxide covered sample. Therefore, we conclude that the change that occurs in the

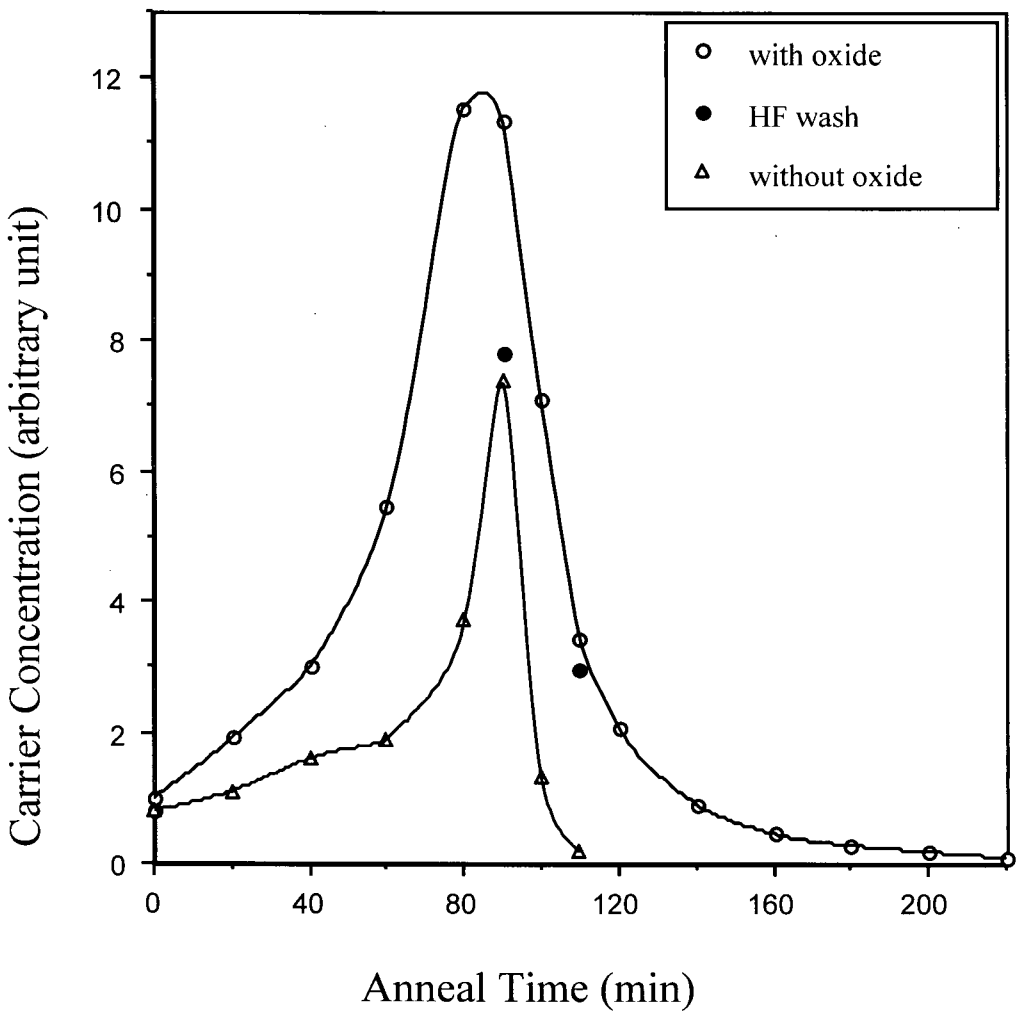

Figure 5.1 Annealing of silicon sample CZ0 in 5 Torr H_2 at 450 °C with and without oxide on its surfaces. The two (•) symbols indicate the level of carrier concentration of the oxide covered sample after the oxide was removed with an HF wash at the indicated times along its anneal process.

annealing process is principally in the bulk. This conclusion is supported by the fact that the annealing of silicon sample CZ0 with the thermal oxide removed produced the same effect as that observed for an oxide covered sample. This is shown in Figure 5.1. The steady state carrier concentration went through a series of values which coincides with the three HF washed points of the annealed oxide covered sample, i.e. it does not matter whether the surface oxide is removed before or after the anneal.

A measurement of the resistivity along the annealing curve in Figure 5.1 also confirmed that the change is in the bulk. The initial resistivity of the silicon sample was 13 Ω·cm. After annealing in 5 Torr of H_2 at 450 °C for 85 minutes, when the steady state carrier concentration was at its peak, the resistivity rose to 380 Ω·cm. Further annealing dropped the resistivity, just as it dropped the steady state carrier concentration. The resistivity fell to 18 Ω·cm after 210 minutes of annealing. For p-type silicon, the resistivity is determined by the concentration of the dopant boron. The corresponding boron densities for resistivities of 13 and 380 Ω·cm are $9x10^{14}$ and $3x10^{13}$ cm^{-1} respectively[56]. The change of resistivity indicates that the dopant boron is "passivated" during the first 85 minutes' annealing and is "reactivated" or "depassivated" with further anneal. The fact that no effect was observed during the H_2 annealing of an intrinsic float-zone grown silicon (FZ) at 450 °C in 5 Torr H_2 confirms the proposal that these changes are due to the passivation and depassivation of the dopant. In earlier work shallow acceptors in silicon have been neutralized by atomic hydrogen at low temperatures (<400 °C)[57] and by annealing in H_2 at high temperatures (>900 °C).[58]

The passivation of boron in a p-type silicon decreases the conductivity of the sample. As described by equation (2.10), the signal measured by our RF probe is inversely proportional to the conductivity of the sample. Therefore, the probe measures an apparent increase in the

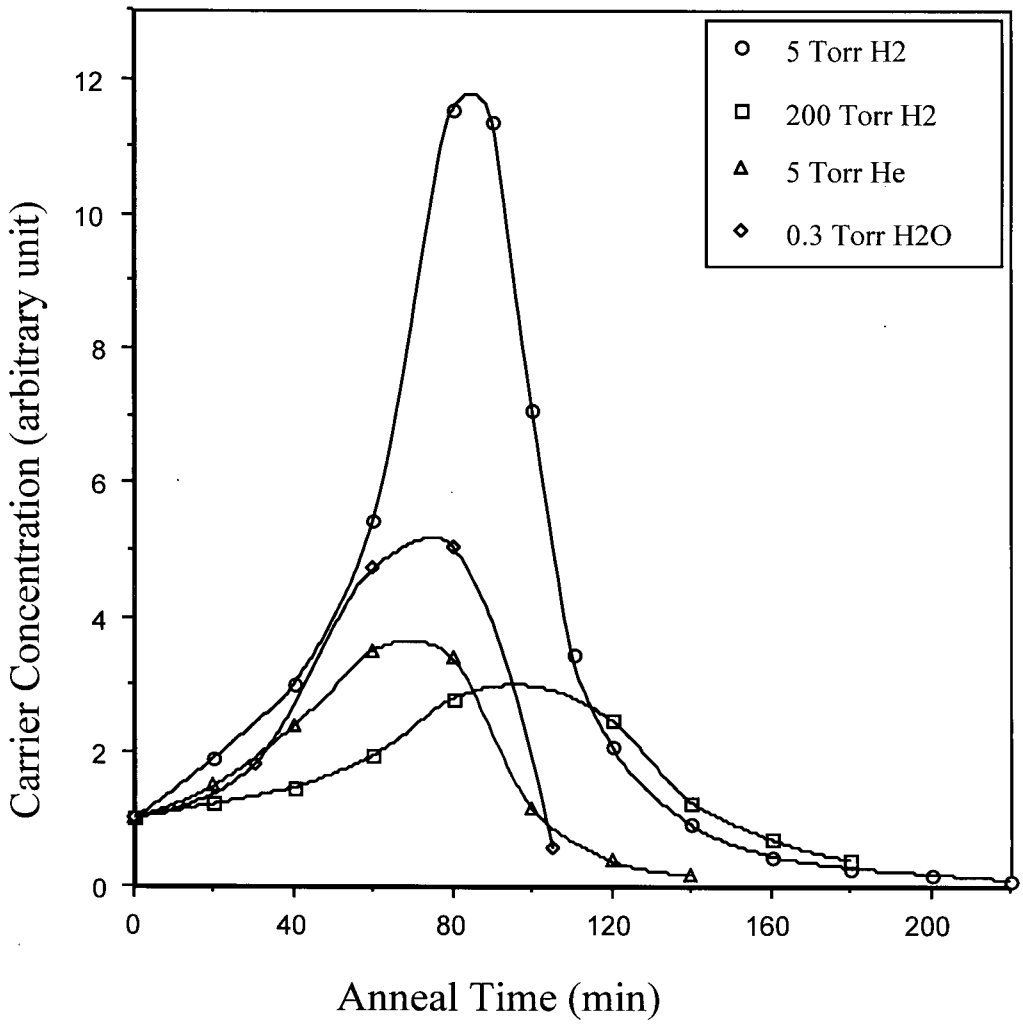

Figure 5.2 Annealing of silicon sample CZ0 (p-type, 13-17 ohm·cm resistivity, with 170 Å thermal oxide on both sides) at 450 °C in 5 Torr H_2, 200 Torr H_2, 5 Torr He, and 0.3 Torr H_2O.

steady state photogenerated carrier concentration during the passivation of boron by hydrogen.

It is important to note that similar curves were obtained when the ambient hydrogen pressure was altered, or hydrogen was replaced with helium, as illustrated in Figure 5.2. The experiment with H_2O was carried out to test the possibility that the change during the annealing process is due to the impurity moisture in the ambient gases. However the results of the water experiment indicate this is not true, as shown in Figure 5.2. It takes about the same length of time, 70-100 minutes, for the steady state carrier concentration to reach the peak maximum at the same temperature. The increase in signal with annealing was, however, largest in the experiment recorded in Figure 5.1, i.e. for the oxide covered sample annealed in the presence of H_2. The similar effect of different annealing gases tells us that the boron passivation and depassivation is not due to diffusion of the ambient species, but is due to changes within the silicon bulk itself. Recall, however, that all of our oxide covered samples have been pre-annealed with H_2.

The passivation and depassivation of dopant was further studied by altering the annealing temperature. The result of annealing the silicon sample CZ0 in 5 Torr H_2 at temperatures between 360 °C and 450 °C are presented in Figure 5.3, and the result of annealing in 1 atm He at 475 °C, 500 °C, and 520 °C is presented in Figure 5.4. The passivation of boron starts at about 360 °C, and the rate increases as the annealing temperature rises. The depassivation of boron does not occur at temperatures below 425 °C within a period of 200 minutes. At 450 °C and above, the steady state carrier concentration rises at first, reaches a maximum in about 85 minutes, and then it falls to a level lower than the initial value. At 520 °C, only a slow depassivation of boron was observed.

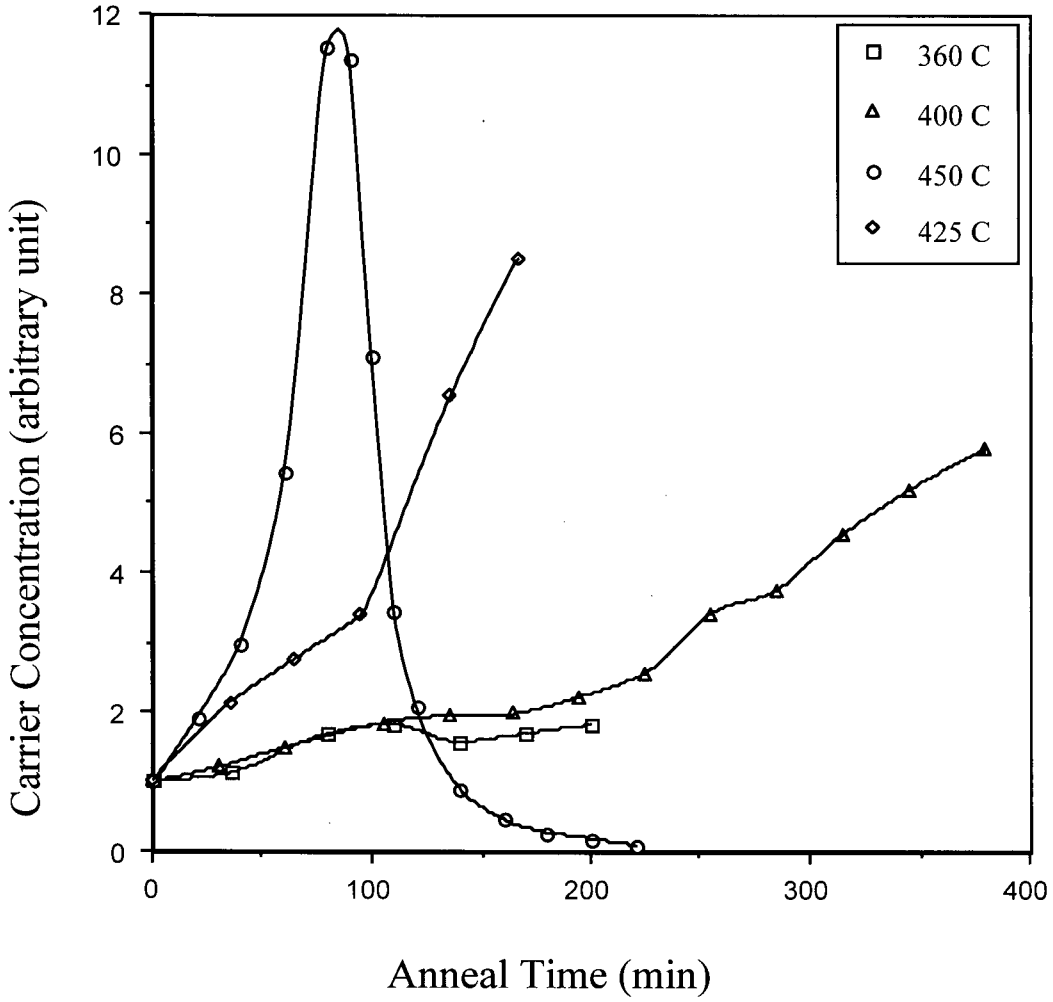

Figure 5.3 Annealing of silicon sample CZ0 (p-type, 13-17 ohm·cm resistivity, with 170 Å thermal oxide on both sides) in 5 Torr H_2 at 360 °C, 400 °C, 425 °C, and 450 °C.

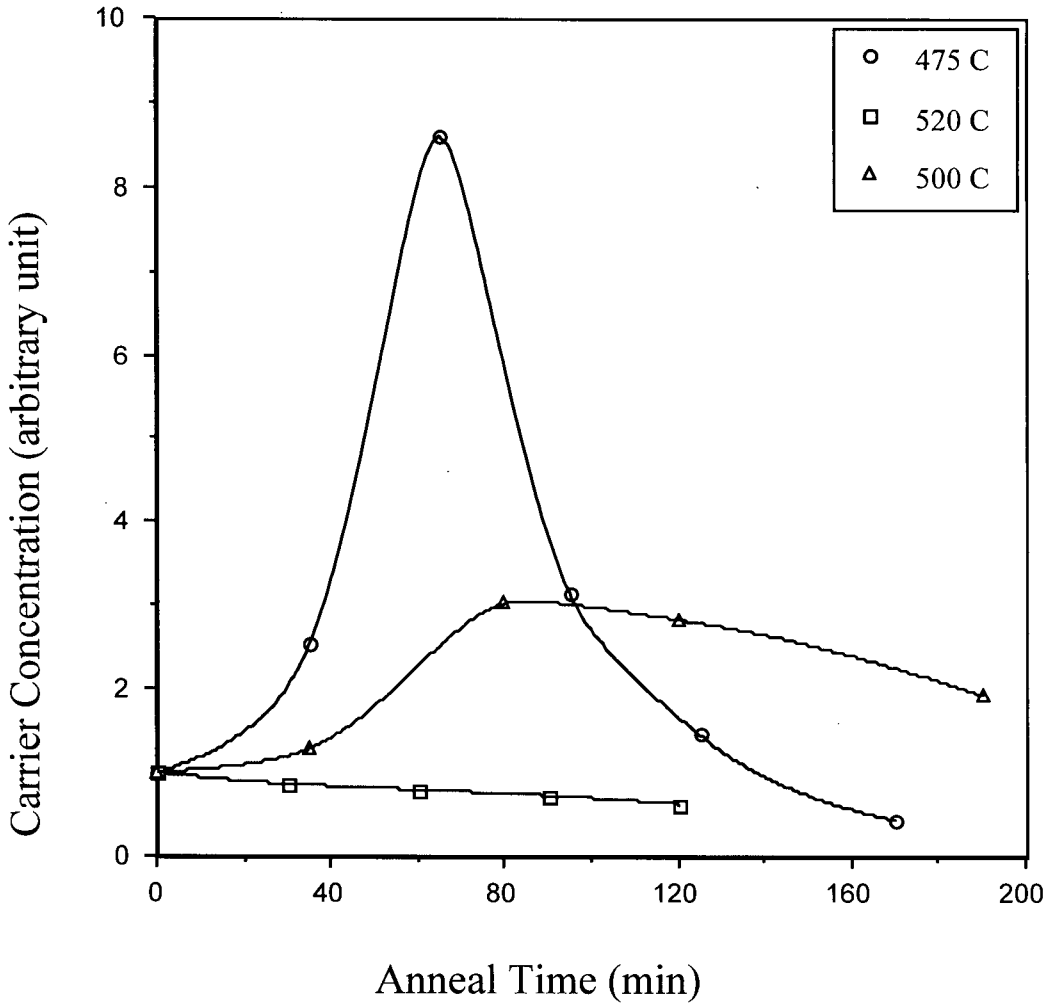

Figure 5.4 Annealing of silicon sample CZ0 (p-type, 13-17 ohm·cm resistivity, with 170 Å thermal oxide on both sides) in 1 atm He at 475 °C, 500 °C, and 520 °C.

From the observations described above, we conclude that the passivation of boron in p-type silicon is due to the formation of a boron-hydrogen complex, which "inactivates" the dopant. The source of hydrogen is the hydrogen that is already present in the bulk. The form of the hydrogen is undetermined. At temperatures higher than 500 °C, the boron-hydrogen complex is dissociated, and hydrogen is driven out of the bulk or turned into another form, making the dopant boron "active" again.

Chapter 6 Results and discussion (III): Adsorption on the HF washed silicon surface

6.1 Results

When a freshly HF washed FZ silicon sample (intrinsic, float-zone grown, with a resistivity of 4200 Ω·cm) was first heated in the presence of 50 mTorr argon, the steady state carrier concentration dropped in the first few minutes, but then it went through a minimum and started to rise, as illustrated in Figure 6.1. The concentration reached a maximum in about 600 seconds and then fell slightly while the temperature was continuously raised to 195 °C. After that the temperature was decreased slowly to 25 °C and the steady state carrier concentration rose to a new plateau. Further cycles of heating and cooling produced the same plateaus at about 3.5 and 2.2 on the arbitrary scale shown in Figure 6.1.

After the initial changes that occur as the temperature is being raised (200 - 600 s in Figure 6.1) the changes that are recorded are consistent with an explanation proposed by Gothscho et al[59] to explain a similar behavior in GaAs. When the temperature is raised the Auger recombination becomes more rapid. If the rate at which the photogenerated carriers are formed remains unchanged, then the steady state carrier concentration decreases as the temperature is raised. This explains the "repeatable" changes that occur after the initial changes that occur when a new sample is introduced.

In order to understand the initial "abnormal rise" of the steady state carrier concentration when the freshly HF washed silicon sample was first heated, as shown in Figure 6.1, a freshly washed silicon sample was annealed in 5 Torr of argon at 200 °C for 15 minutes, and then

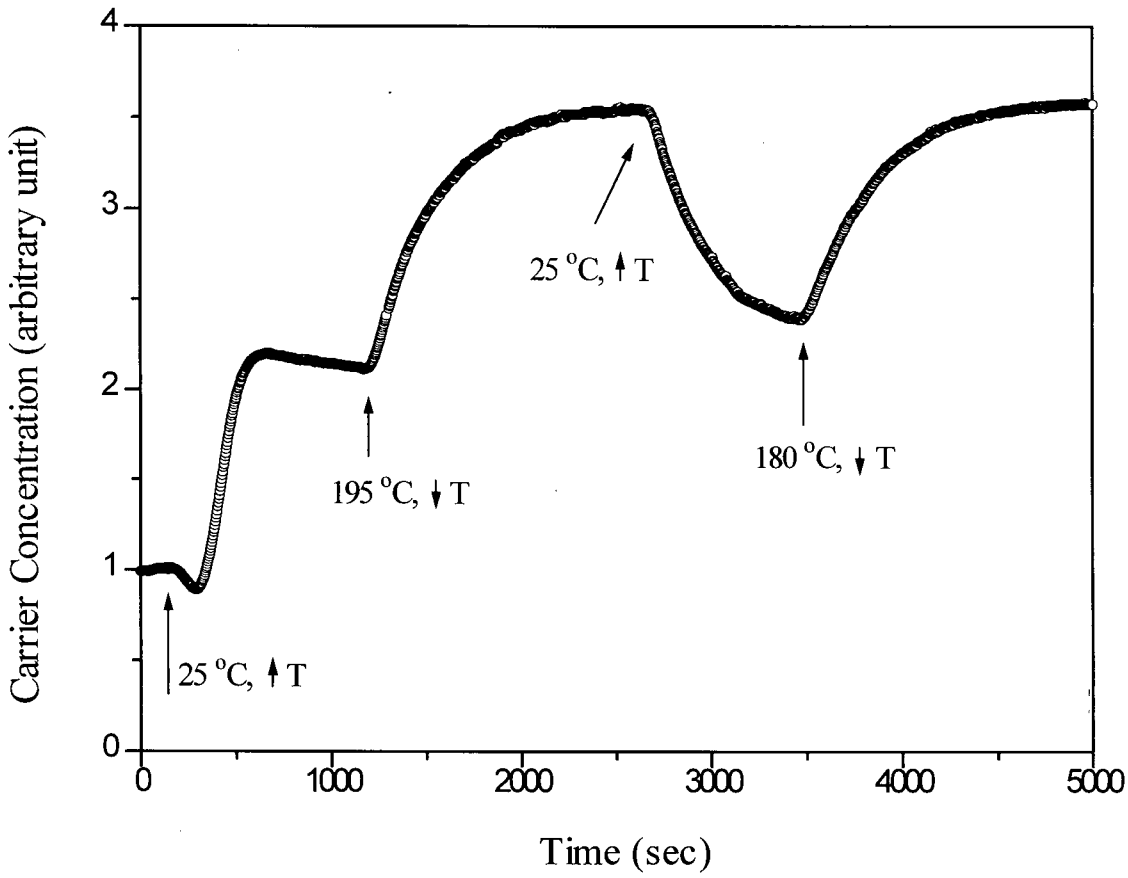

Figure 6.1 Effect of heating (↑T) and cooling (↓T) a freshly HF washed silicon sample FZ (intrinsic, float-zone grown) in the presence of 50 mTorr Ar.

exposed to various gases at room temperature. The results of the experiments are present in Figure 6.2. The anneal raised the steady state carrier concentration to a level twice as high as the initial value, as it did in Figure 6.1. Subsequent exposure of this substrate to 5 Torr of oxygen dropped the steady state carrier concentration to a level about 1.5 times the initial value. An increase of the oxygen pressure to 10 Torr dropped the steady state carrier concentration to an even lower level. Switching to 5 Torr of argon made the steady state carrier concentration rise again. Another anneal in 5 Torr of argon at 200 °C for 15 minutes recovered the steady state carrier concentration to almost the same level as the first anneal.

From the above experiments it can be seen that the adsorption of oxygen lowers the steady state carrier concentration. The rise that occurs in Figure 6.1 during the initial heating is therefore probably due to the desorption of oxygen adsorbed on the freshly washed silicon surface during the transfer of the sample through air.

As can be seen in the second half of Figure 6.2, the adsorption of hydrogen was also detected when the sample was annealed first. H_2 was found to have an effect very similar to oxygen, with a decrease in carrier concentration which is larger than that due to the adsorption of oxygen.

The adsorption and desorption were observed at higher temperatures as well as at room temperature. Presented in Figure 6.3 are the results of an experiment performed at 200 °C. Exposure of the freshly washed silicon surface to 3.5 Torr of oxygen decreased the steady state carrier concentration to about half of the initial value. The thermal desorption of the oxygen recovered the signal to a level that was about 80% of the initial value when oxygen was replaced with 0.2 Torr helium. The adsorption and desorption could be repeated by introducing oxygen

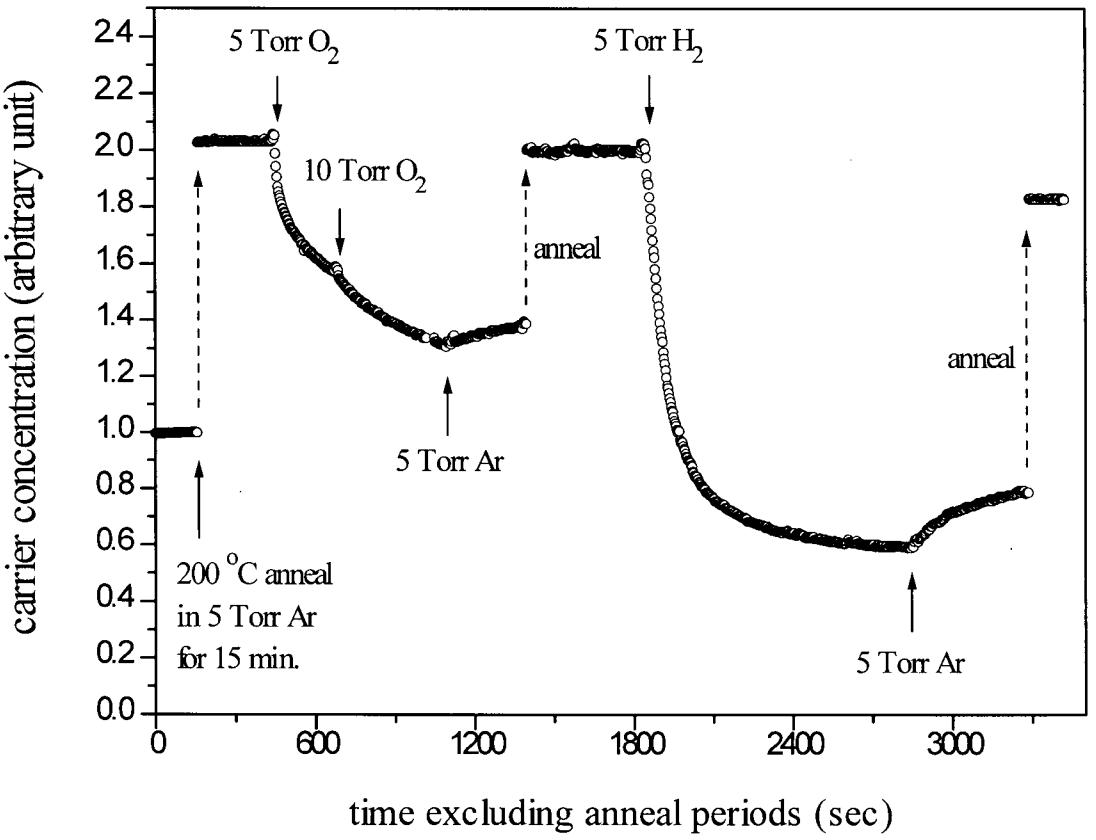

Figure 6.2 Exposure of a freshly HF washed silicon sample FZ (intrinsic, float-zone grown) to O_2 and H_2 at room temperature after an anneal at 200 °C in the presence of 5 Torr of Ar for 15 minutes.

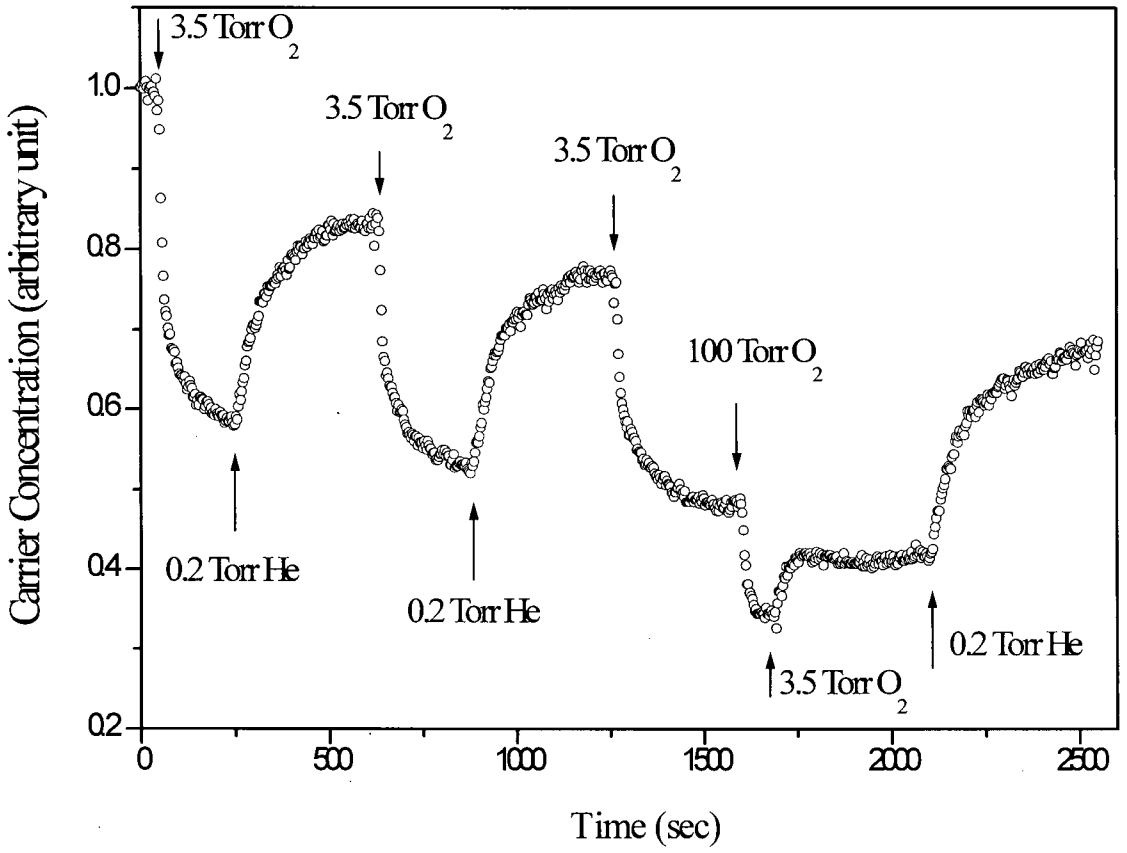

Figure 6.3 Exposure of a freshly HF washed silicon sample CZ0 (p-type, 13-17 ohm·cm resistivity) to O_2 and He at 200 °C.

and helium into the system alternately. However, the recovery of the carrier concentration as a result of desorption was always lower than the previous one. Higher pressures of oxygen made the steady state carrier concentration fall to a lower level. The deterioration of the surface during the consecutive exposure to oxygen indicates that the adsorption is not purely physi-sorption.

Adsorption of O_2 on surfaces of p-type InP has similar effects on photoluminescence[60], which is a measure of steady state free carrier concentrations in direct bandgap semiconductors. A "dead-layer" model[61] has been proposed to explain the effects of adsorption on III-V semiconductors. It applies equally well to our observations.

6.2 The "dead-layer" model

As described in section 1.1.5.1, when a semiconductor and a metal are brought into contact, electrons flow in or out of the semiconductor until an equilibrium is reached. An equilibrium is also established between a semiconductor and surface states in the bandgap. At this point the surface states are filled with electrons up to the Fermi level, as shown in Figure 6.4.

A consequence of this process is that an electrical field is now present in the near-surface region of the semiconductor, reflecting the charge separation that has taken place. This field is represented by a bending of the band edges of the semiconductor, as illustrated in Figure 6.4. The near-surface zone that has been depleted of free carriers due to the field, hence is called the depletion region. Its thickness, the depletion width W, is described by equation (1.5).

The dead-layer model treats the depletion region as a nonemissive zone or a dead-

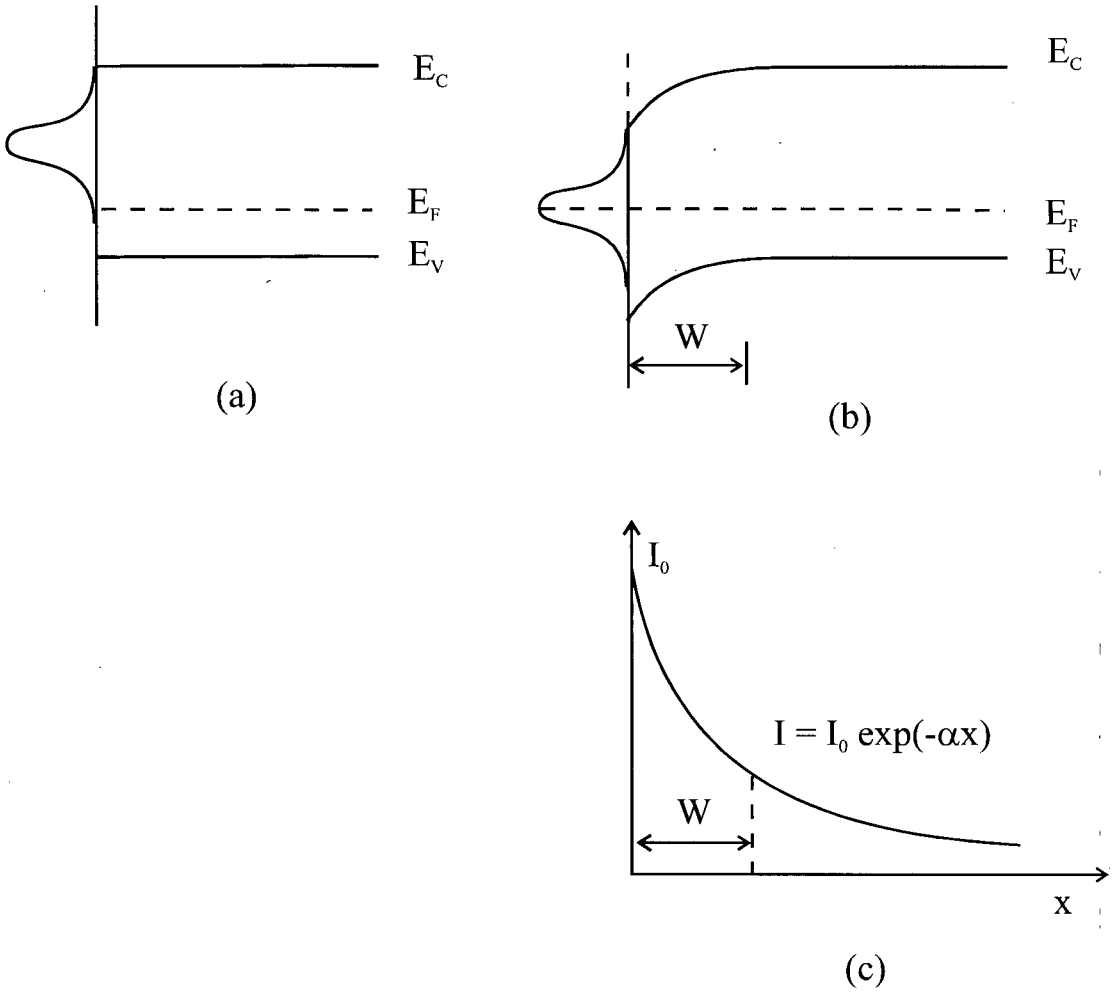

Figure 6.4 Semiconductor-gas interface (a) before and (b) after establishment of equilibrium. Shown are the valence band E_V and conduction band E_C edges of the p-type semiconductor, the Fermi level E_F, and a hypothetical distribution of surface states. (c) The profile of excitation radiation intensity. W is the depletion width.

layer, in which free carriers are depleted, hence little radiative recombination occurs. Light absorbed in this layer has little contribution to the free carrier concentrations. If the excitation radiation entering the semiconductor is absorbed exponentially (Beer-Lambert law) with absorption coefficient α, the fraction penetrating through a dead layer of thickness W is $\exp(-\alpha W)$. The steady state free carrier concentration C_{SS} should be

$$C_{SS} = C_{SS}^{FB} \exp(-\alpha W) \qquad (6.1)$$

where C_{SS}^{FB} is the flat band, no dead layer, steady state carrier concentration.

Adsorption can alter the depletion width in a manner that reflects the Lewis acidity or basicity of the species. For example, adsorption of a Lewis basic molecule might cause electron density trapped in surface states to be shifted back into the semiconductor bulk, thereby reducing the depletion width in a p-type semiconductor. Conversely, an adsorbed Lewis acid might draw additional electron density into surface states from the semiconductor bulk, expanding the depletion width.

For a p-type semiconductor, adsorption of O_2 will increase the depletion width if it is a Lewis acid. According to equation (6.1), this drops the steady state carrier concentrations as we have observed. However, the adsorption of H_2 dropped the steady state carrier concentrations more than the adsorption of O_2. It is hard to explain this in terms of Lewis acid or base behavior. Further studies are clearly required to fully understand the effects of adsorption of stable molecules on silicon surfaces.

Chapter 7 Results and discussion (IV): Processes generated by atomic hydrogen

In preliminary experiments we found that when a Si (100) wafer with a 170 Å thermal oxide layer was exposed to the products of a discharge in H_2, the laser-generated steady-state carrier concentration dropped to undetectable levels within the time constant of the instruments (< 0.1 second). The process was comparably rapid when the H_2 discharge was some distance upstream from the sample so that only room temperature H-atoms reached the wafer sample. When the sample was exposed to the down-stream products of an Ar discharge, the steady state carrier concentration also dropped as shown in Figure 7.1, however, the rate at which the steady state carrier concentration dropped was orders of magnitude slower. Since there is always some hydrogenic impurity present in the Ar, this latter observation is consistent with the view that diffusion of H-atoms through the 170 Å SiO_2 layer is very rapid and that in all these systems we are observing the formation of carrier traps created by atomic hydrogen at the Si/SiO_2 interface.

In order to slow the process down to the point at which the rate of change could be measured with our detector, we decreased the H-atom concentration by diluting the H_2 passing through the discharge with argon and by decreasing the power of the microwave generator. The rate became measurable when the partial pressure of H_2 was less then 10 % of the argon.

7.1 Trap production at room temperature

The rate of creation of carrier traps at the SiO_2/Si interface on sample CZ0 (p-type, 13-17 ohm·cm resistivity, with 170 Å thick thermal oxide on both sides) was determined as a function of the partial pressure of hydrogen atoms in order to determine the order of the reaction

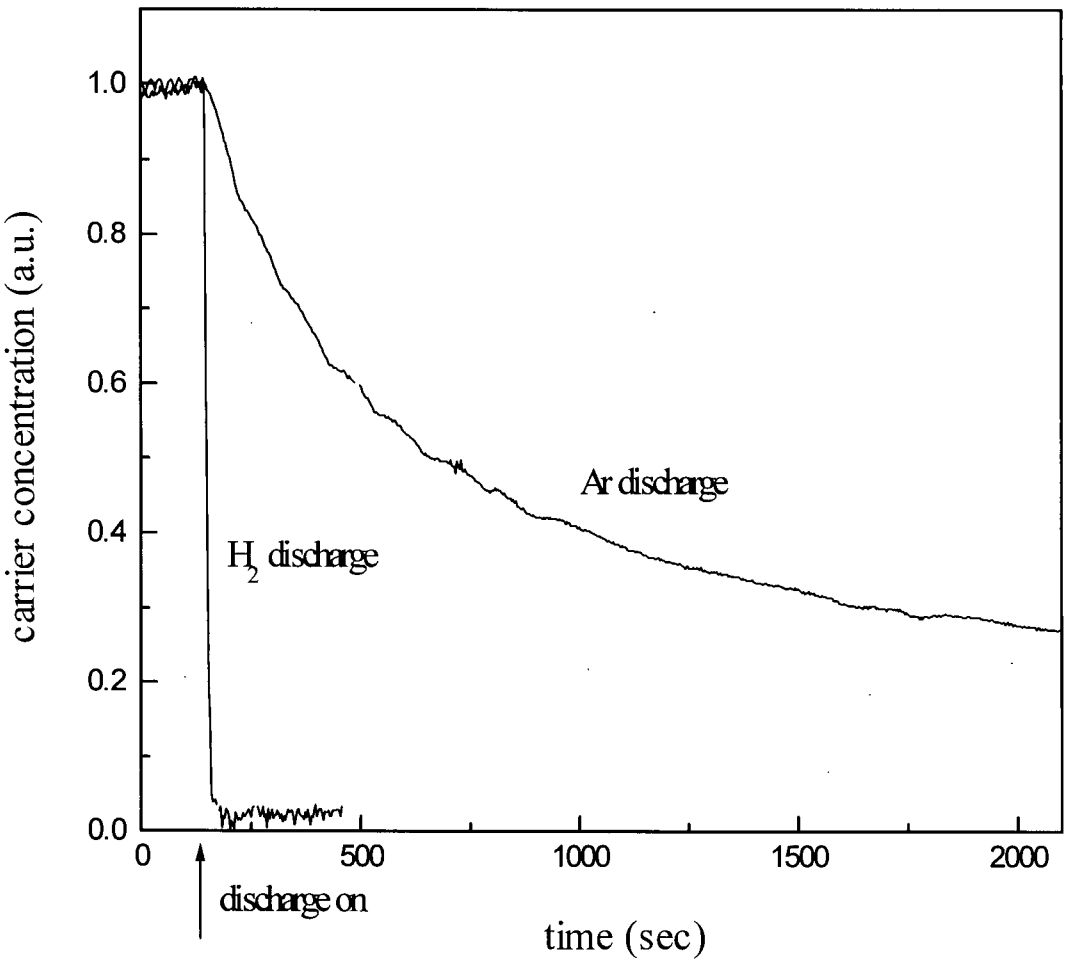

Figure 7.1 Comparison of the steady state carrier concentration loss rates for silicon sample CZ0 (p-type, 13-17 ohm·cm resistivity, with 170 Å thick thermal oxide on both sides) when exposed to the downstream products of (a) an H_2 discharge (H_2 pressure 500 mTorr, microwave power 100 W) and (b) an Ar discharge (Ar pressure 30 mTorr, microwave power 30 W) at room temperature.

with respect to the partial pressure of atomic hydrogen. The trap creation rates were measured at room temperature. Molecular hydrogen partial pressures in the reaction chamber were set at $2.9\text{x}10^{-4}$, $5.1\text{x}10^{-4}$, $7.4\text{x}10^{-4}$, and $1.6\text{x}10^{-3}$ Torr while the argon partial pressure was kept constant at 30 mTorr. The change of the measured output signal of the RF probe, which is proportional to the steady state carrier concentration in the silicon sample, during exposure to different hydrogen atom pressures is plotted in Figure 7.2. It can be seen that the rate at which the steady state carrier concentration drops becomes greater as the atomic hydrogen concentration increases.

From equation (2.13) we know that the steady state carrier concentration is determined by the density of charge carrier traps in the bulk Si and at the Si/SiO_2 interface.

$$[C]_{ss} \propto \frac{1}{k_b[t_b] + k_s[t_s]} \tag{7.1}$$

If we take the reciprocal of the steady state carrier concentration, equation (7.1) becomes

$$k_b\,[t_b] \;+\; k_s\,[t_s] \;\propto\; \frac{1}{[C]_{ss}} \tag{7.2}$$

At a fixed temperature, k_b and k_s are constants. If the density of bulk traps $[t_b]$ of the silicon sample is not affected by the exposure to hydrogen atoms, the interfacial state (trap) density is linearly related to the reciprocal of the steady state carrier concentration,

$$[t_s] + A \;\propto\; \frac{1}{[C]_{ss}} \tag{7.3}$$

where A is a constant.

The interfacial state density, obtained from the reciprocal of the steady state carrier concentration, is plotted against time in Figure 7.3. For a fixed hydrogen atom partial pressure, the interfacial trap density shows a linear increase with time. The slopes of these lines

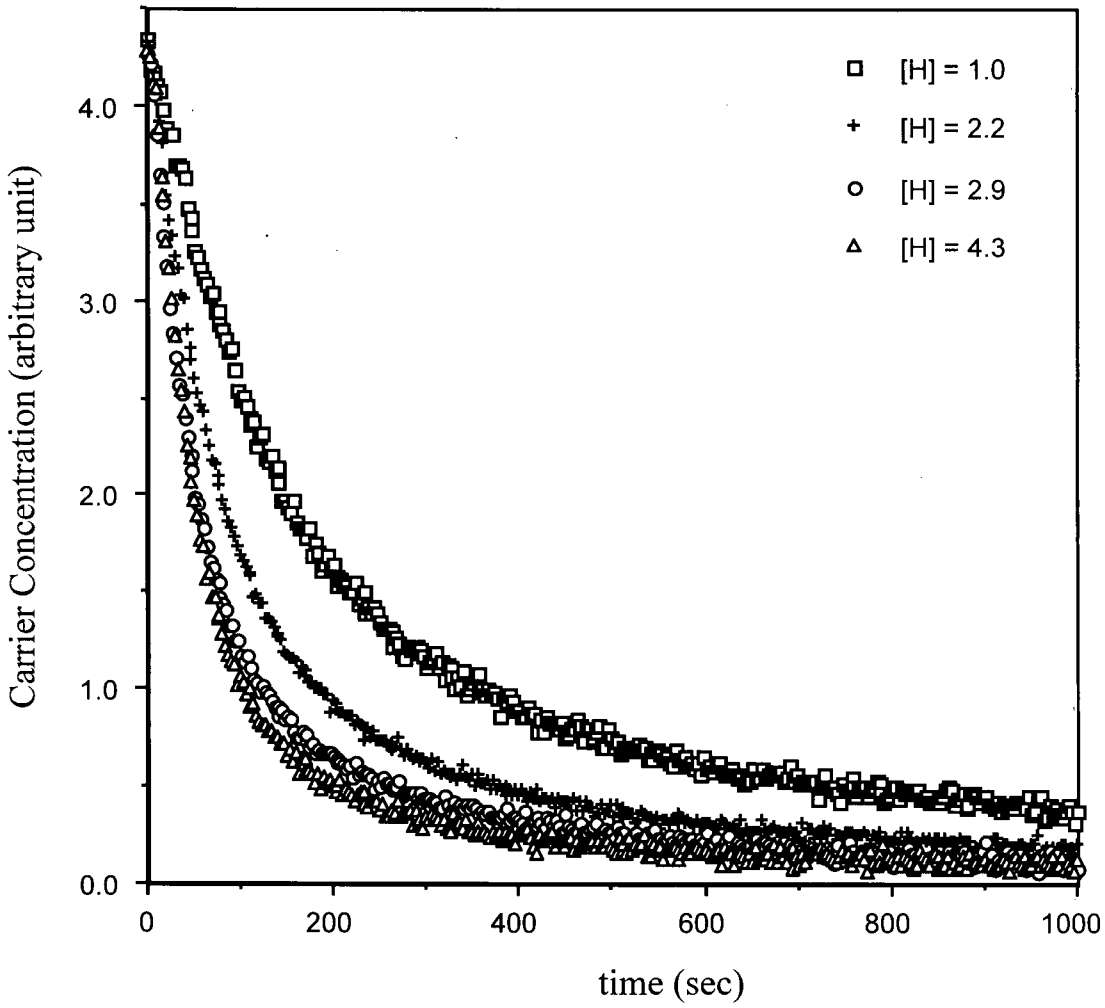

Figure 7.2 The decrease in steady state carrier concentrations with time during exposure to different atomic hydrogen pressures at room temperature. The concentrations of H-atoms are as indicated in arbitrary unit. The silicon samples were CZ0 (p-type, 13-17 ohm·cm resistivity, with 170 Å thick thermal oxide on both sides).

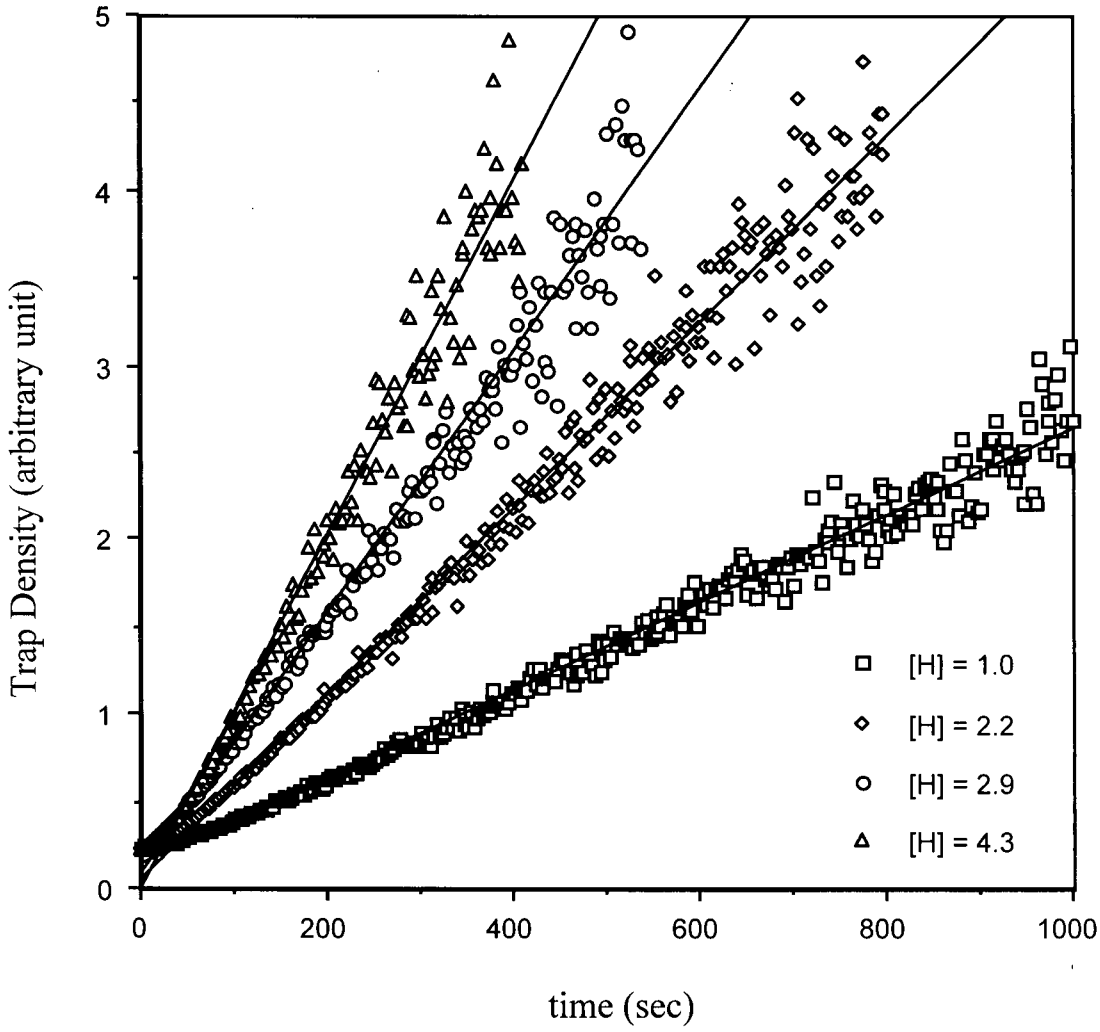

Figure 7.3 Interfacial trap densities (reciprocal of the steady state carrier concentration) as a function of time during exposure to different atomic hydrogen pressures at room temperature. The silicon samples were CZ0 (p-type, 13-17 ohm·cm resistivity, with 170 Å thick thermal oxide on both sides).

give the relative trap creation rates. These rates are listed in Table 7.1.

A plot of trap creation rate versus atomic hydrogen pressure is presented in Figure 7.4. A linear relationship indicates that the traps are formed by reaction with hydrogen atoms and the trap creation process is first order in hydrogen atoms, i.e.

$$R_{tc} = k\,(P_H)^1 \qquad (7.4)$$

where k is a rate constant and the order of the reaction is 1 with respect to the atomic hydrogen pressure.

7.2 Trap production at elevated temperatures

When silicon samples CZ0 (p-type, 13-17 ohm·cm resistivity, with 170 Å thick thermal oxide on both sides) were exposed to a very low H-atom concentration at elevated temperatures, the behavior was found to be more complex. Figure 7.5 compares the effect of a fixed H-atom flow at 22 °C, 126 °C and 206 °C. At 22 °C the steady state carrier density simply falls monotonically with time. At 206 °C, when the discharge is switched on, the steady state carrier concentration quickly drops to a low level. However, at about 100 seconds, the steady state carrier concentration goes through a minimum, then rises and plateaus at about 1/4 of the initial value. When the discharge is then switched off, the steady state carrier concentration slowly recovers to about 3/4 of the initial value. At 126 °C, the behavior is qualitatively similar to that at 206 °C, only the magnitude of the recovery is smaller. Almost no "recovery" was observed at temperatures below 100 °C.

It would appear that there are processes other than simple "trap production" occurring as a result of exposure to H-atoms at elevated temperatures. However, they have little effect on the

Table 7.1 Trap creation rates for silicon sample CZ0 (p-type, 13-17 ohm·cm resistivity, with 170 Å thick thermal oxide on both sides) during exposure to different atomic hydrogen partial pressures at room temperature.

H_2 partial pressure ($x10^{-7}$ Torr)	H atoms concentration (arbitrary unit)	Trap creation rate (arbitrary unit)
0	0	0
0.63	1.0	2.51
1.4	2.2	5.30
1.8	2.9	7.47
2.7	4.3	10.13

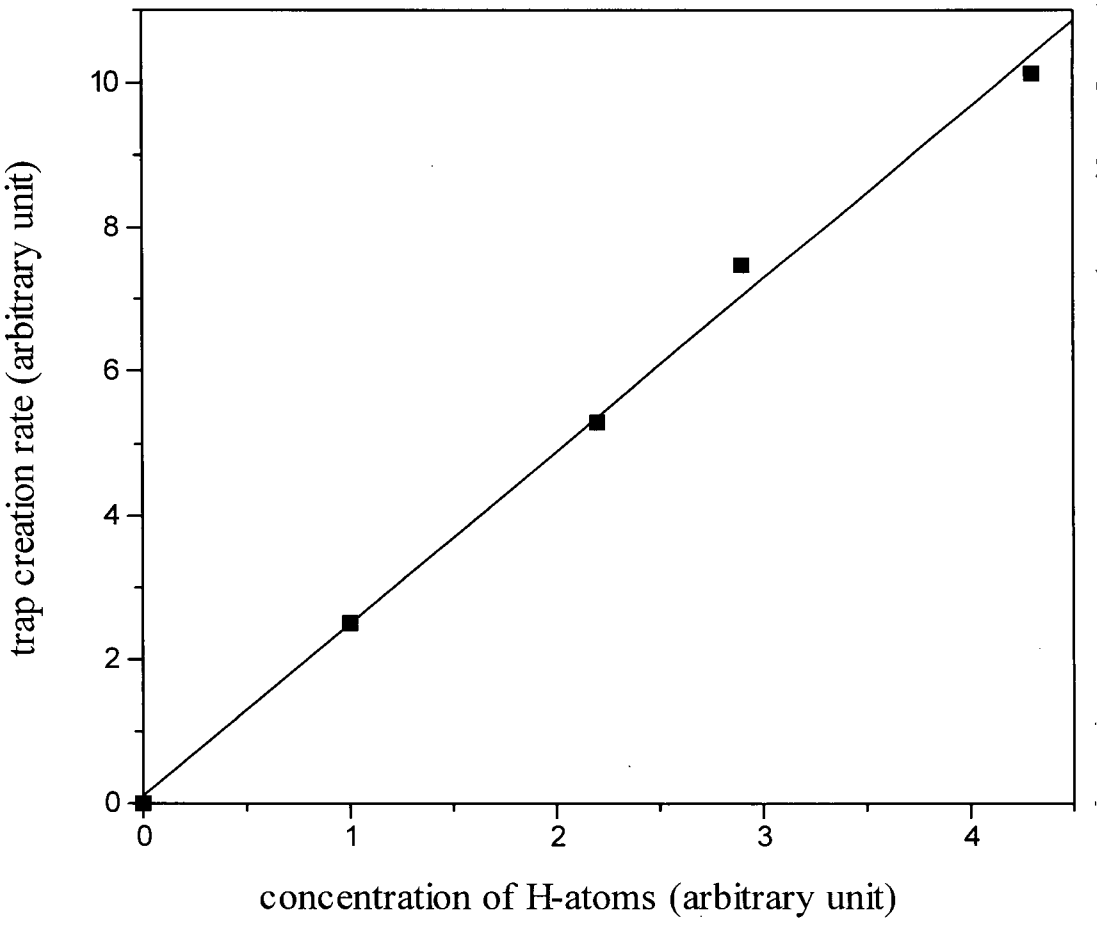

Figure 7.4 Interfacial trap creation rates for silicon CZ0 (p-type, 13-17 ohm·cm resistivity, with 170 Å thick thermal oxide on both sides) at room temperature versus atomic hydrogen pressure.

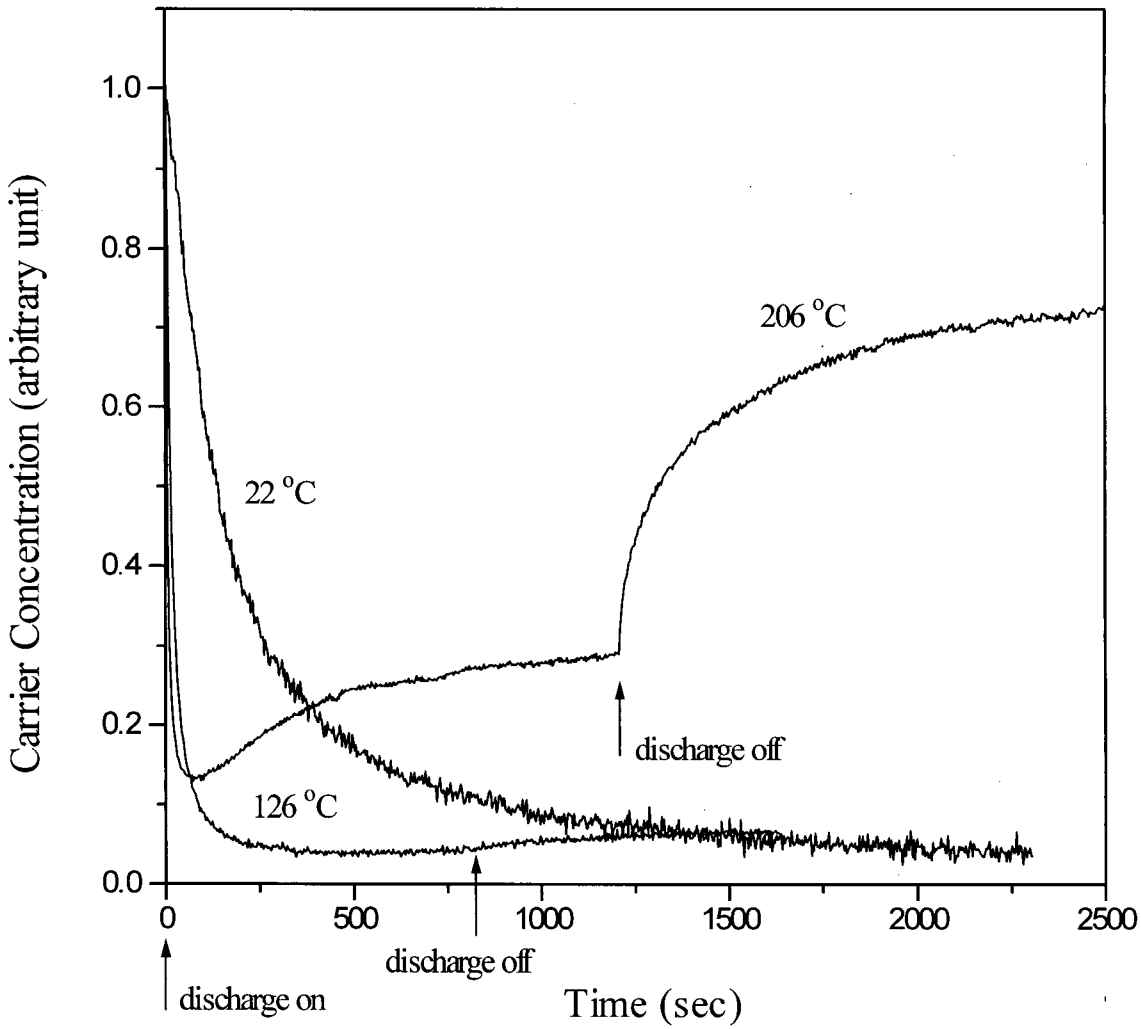

Figure 7.5 Carrier concentrations in silicon CZ0 (p-type, 13-17 ohm·cm resistivity, with 170 Å thick thermal oxide on both sides) as a function of time during exposure to hydrogen atoms at room temperature, 126 °C, and 206 °C. The hydrogen atom concentration at room temperature was half of that at 102 °C and 206 °C.

initial portion of the trap creation reaction, since they are much slower. Therefore the trap creation rate at several temperatures can be determined from the initial rate at which traps are formed when the H-atoms are first turned on.

To determine the initial trap creation rate as a function of temperature, silicon sample CZ0 (p-type, 13-17 ohm·cm resistivity, with 170 Å thick thermal oxide on both sides) was exposed to hydrogen atoms at eleven temperatures between 22 °C and 220 °C. The measured trap densities as a function of H-atom exposure time at three temperatures are illustrated in Figure 7.6, and the first order rate constants obtained from all eleven curves are listed in Table 7.2. Since we have shown in section 7.1 that the reaction is first order in [H], it will be written:

$$H + P \rightarrow Tr \qquad (7.5)$$

where P is a Si/SiO_2 interfacial trap precursor and Tr is a carrier trap created by H-atoms. An Arrhenius plot of these rate constants is presented in Figure 7.7. This plot yields an activation energy of 0.15 ± 0.02 eV for reaction of hydrogen atoms at the SiO_2/Si interface to produce carrier recombination sites (traps).

7.3 Processes generated by atomic hydrogen at elevated temperatures

In an attempt to identify more of the reactions that occur at higher temperatures, the hydrogen discharge was switched on and off a few times after the first hydrogen atom exposure. The result of exposing a thermal oxide covered silicon sample to H-atoms twice at 185 °C is presented in Figure 7.8. When H-atoms were first switched on, initially the trap density rose quickly, then the rate slowed down and the trap density reached a maximum. Continuing this exposure to H-atoms made the trap density drop and finally approach a plateau which was about

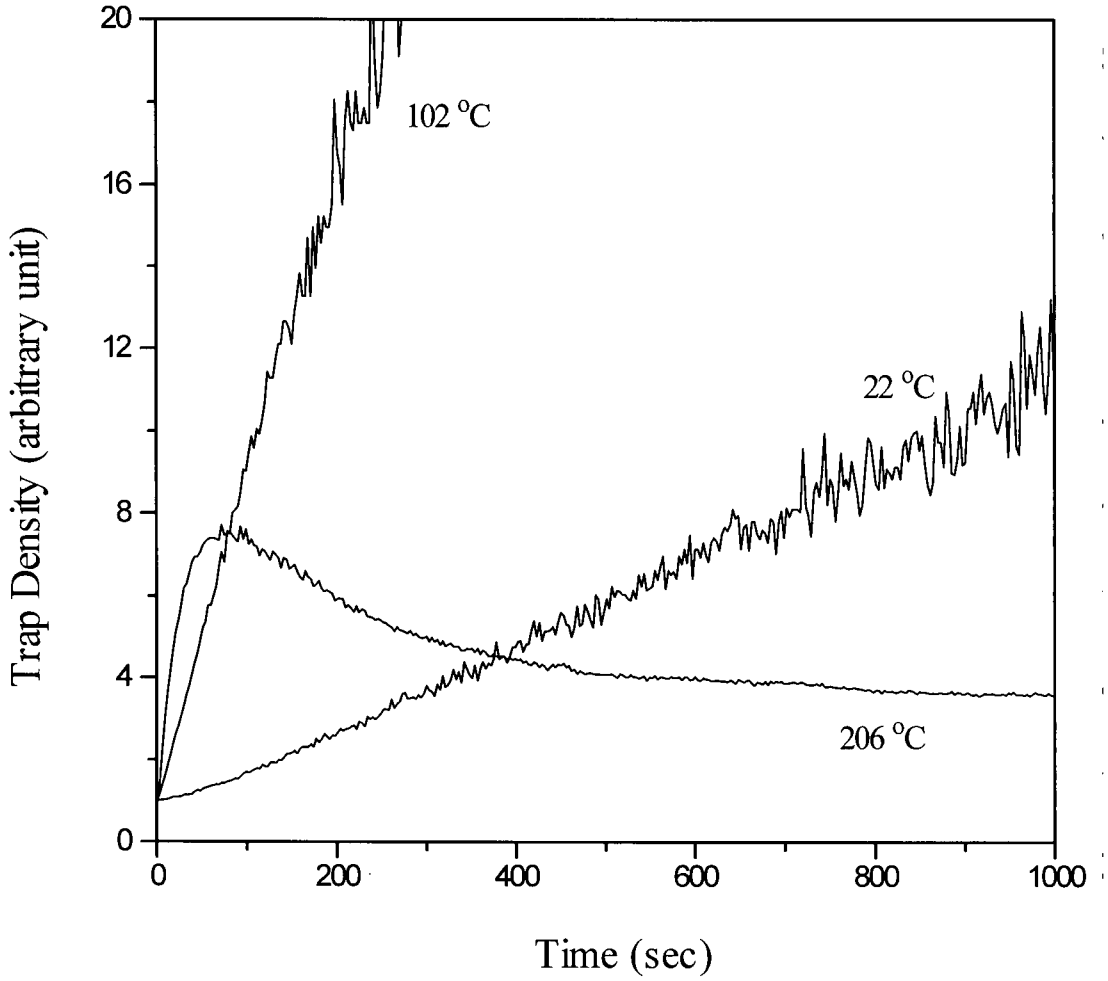

Figure 7.6 Trap concentrations in silicon CZ0 (p-type, 13-17 ohm·cm resistivity, with 170 Å thick thermal oxide on both sides) as a function of time during exposure to hydrogen atoms at room temperature, 102 °C and 206 °C. The hydrogen atom concentration at room temperature was half of that at 102 °C and 206 °C.

Table 7.2 Rate constants for initial trap creation during exposure to H-atoms at eleven temperatures.

temperature (°C)	trap creation rate constant k (arbitrary unit)
22	0.022
55	0.053
102	0.080
126	0.092
128	0.089
153	0.240
157	0.207
185	0.242
198	0.172
206	0.269
219	0.171

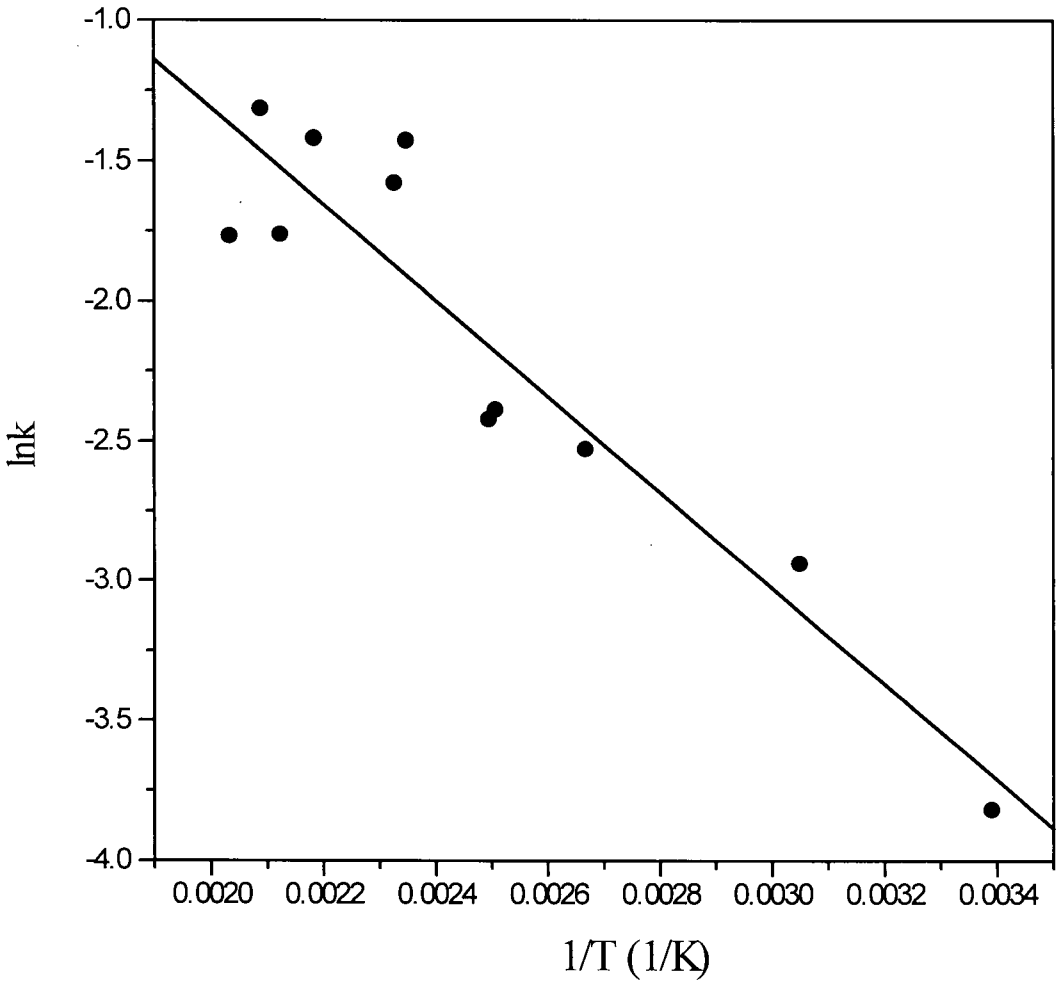

Figure 7.7 Arrhenius plot for the trap creation rate constants.

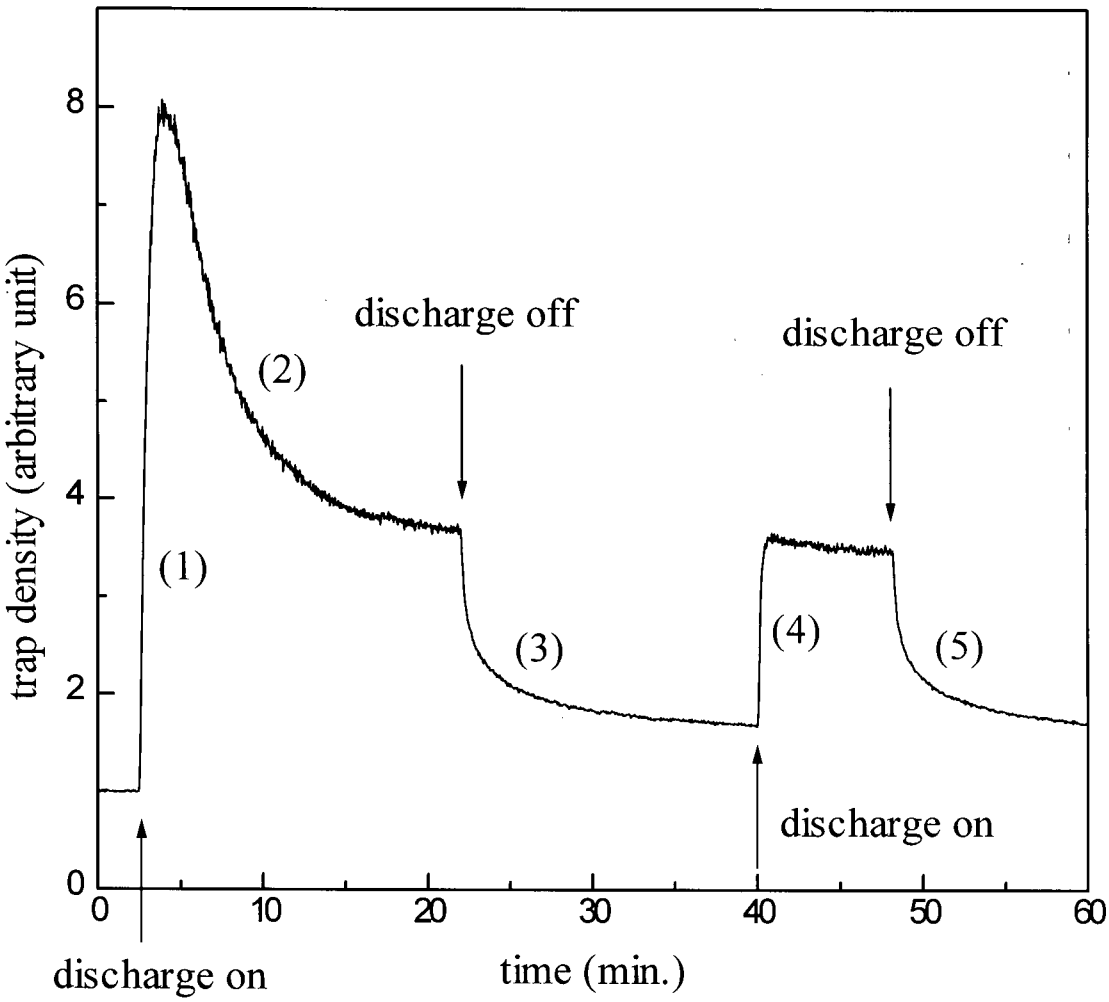

Figure 7.8 The trap density of silicon CZ0 (p-type, 13-17 ohm·cm resistivity, with 170 Å thick thermal oxide on both sides) as a function of time when the hydrogen discharge is turned on and off twice at 185 °C.

half the value of the peak maximum. When the H-atoms were shut off, the trap density dropped to a level that was always higher than the initial trap density. The second time that the sample was exposed to H-atoms, the trap density did not go through a high peak as it did during the first exposure. The trap density rose almost monotonically to about the same plateau height that it reached after the first exposure. The third time H-atoms were exposed, which is not shown in Figure 7.8, the trap density retraced to values that was passed through during the second exposure.

For the purpose of this discussion it is convenient to label certain regions of this figure by the numbers 1-5.

Process (1) is the fast trap creation reaction when the discharge is switched on for the first time.

Process (2) makes the trap density pass through a maximum and then fall to a plateau.

Process (3) is the trap decay when the discharge is switched off.

Process (4) is the very rapid rise in trap density that occurs when the discharge is switched on again. The rise times for process (4) and process (1) are comparable.

Process (5) is a trap decay process which occurs whenever the H-atoms are removed, after process (2) has been given time to go to completion.

From the simple measurement of the time constants of these five processes and the final levels at which they plateau, we can conclude that process (5) is the same as process (3), and process (4) is the same as the initial portion of process (1). Process (5) is the reverse reaction of process (4), and process (3) is the reverse of process (1). There is at least one more reaction in process (2) besides trap creation process (1) and its reverse process (3). This follows from the fact that if only the reaction in process (1) and its reverse reaction in process (3) were involved

in process (2), the steady state carrier concentration would reach its equilibrium value asymptotically and the trap density would not pass through a maximum.

From the above analysis, we identify a minimum of three reactions that result from exposing thermal oxide covered silicon (100) to gaseous H-atoms. They are

(a) the trap creation reaction,

(b) its reverse reaction after the H-atoms are removed, and

(c) a reaction which slowly makes the trap density fall to a plateau while the H-atoms are still present. This reaction almost completes during the first exposure to the H-atoms. Its effect is permanent and irreversible when the H-atoms are removed from the system.

In order to better characterize the three sets of reactions presented above, the experiment illustrated in Figure 7.8 was repeated at 153 °C, 185 °C, 206 °C and 219 °C with a constant H-atom flow. The results, which are shown in Figure 7.9, will be analyzed by considering the three reactions described above. The kinetics of the trap creation reaction (a) has already been presented in sections 7.1 and 7.2. We will examine the reverse reaction (b) next, since only this reaction occurs in process (3). Reaction (c) is always accompanied by reactions (a) and (b), and will be considered last in section 7.5.

7.4 Decay of the carrier traps produced by H-atoms

Logarithmic plots of the trap decay when the H-atoms are shut off (process (3) in Figure 7.8) are presented in Figure 7.10 for four temperatures. The infinity trap density values, which were obtained by trial and error to make the plots straight lines at long times, were subtracted from the trap density values. If only one type of trap is formed by exposure to H-atoms, then,

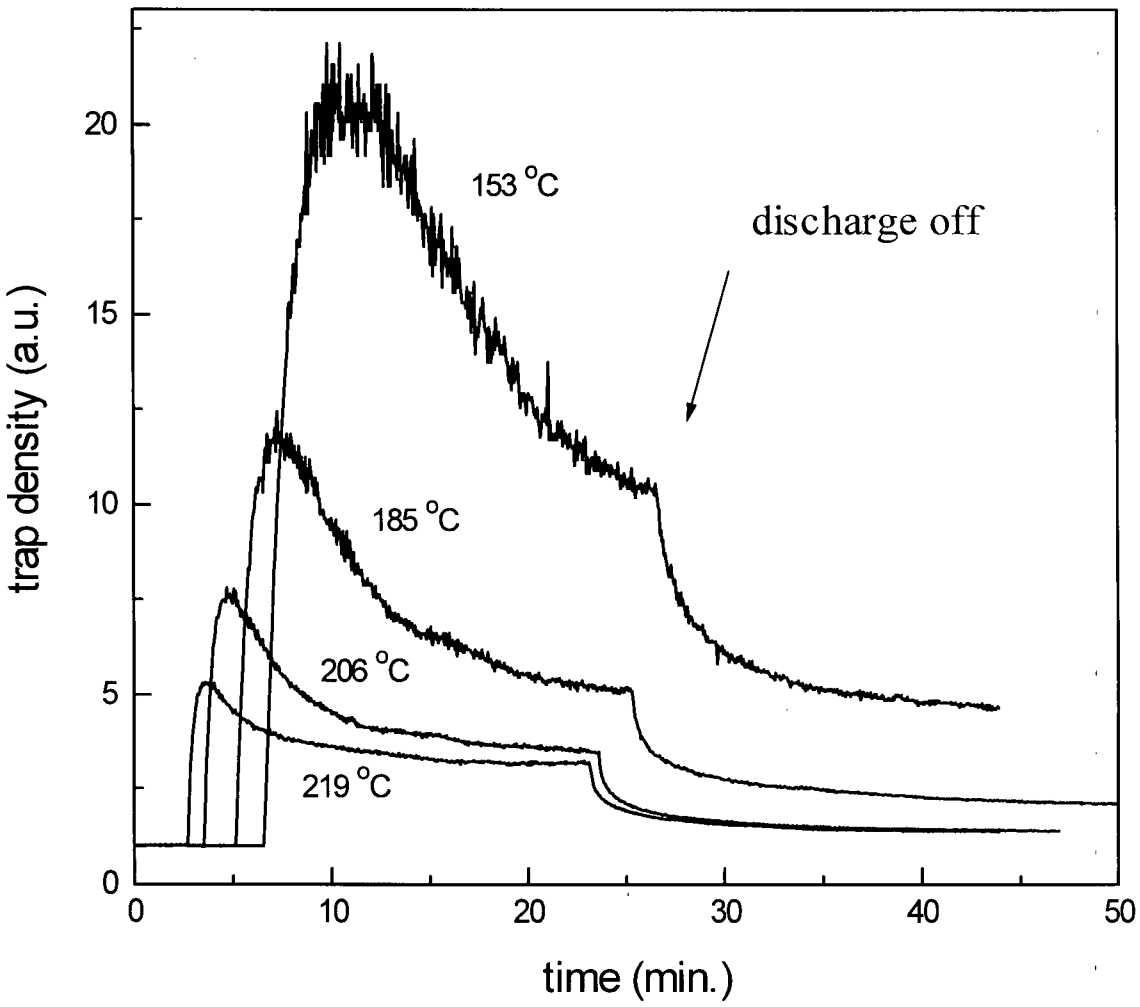

Figure 7.9 The trap density change with time during and after exposure to identical atomic hydrogen pressures at the temperatures indicated. The silicon samples were CZ0 (p-type, 13-17 ohm·cm resistivity, with 170 Å thick thermal oxide on both sides).

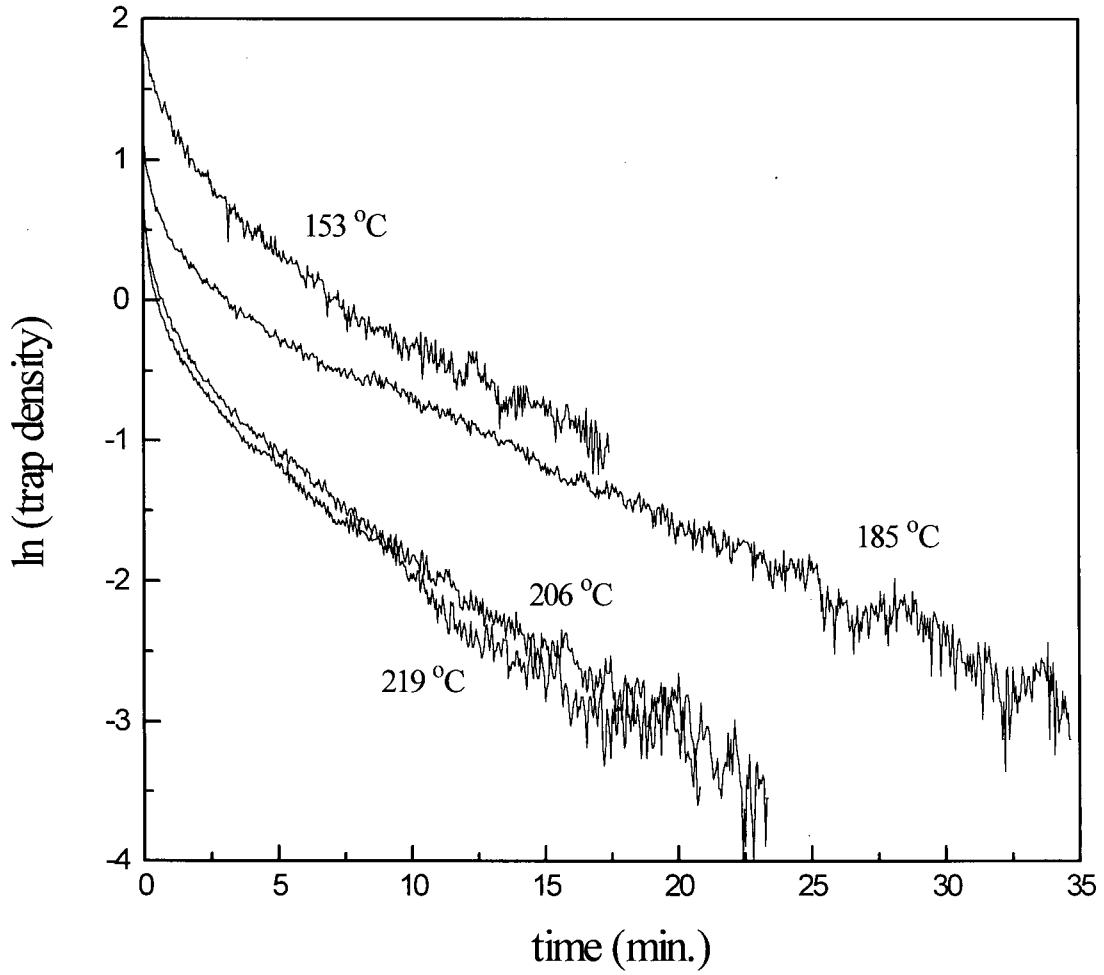

Figure 7.10 Logarithmic plots of the trap density against time when the H-atoms are shut off (later portion of Figure 7.9).

when the H-atoms are removed, the decay of this trap should follow a simple first order decay law if the process is described by reaction (7.5):

$$Tr \xrightarrow{k_p} ? \qquad (7.6)$$

The non-linearity of these curves indicates that the process does not obey a simple first order rate law unless there are two or more traps with different decay rates.

The same trap decay data were plotted in Figure 7.11 with the initial trap density values before exposure to H-atoms subtracted. The dotted curves are the best fits of the data with the assumption of two traps, each with a simple exponential decay. The curve fitting was done using software "MicroCal Origin". Superficially the fit looks acceptable, however careful examination of the fit leads us to observe that the fit is poor in reproducing both the rapid drop near t = 0 and the trend which occurs at long times. The initial trap densities of these two traps at various temperatures and their decay rate constants are listed in Table 7.3. An Arrhenius plot of the rate constants are shown in Figure 7.12. The points are scattered unacceptably.

It has been shown by Stessmans[17] that this kind of decay can be explained by the introduction of a Gaussian distribution of activation energies. If Tr_0 is the total number of traps, E_a^0 is the mean activation energy for the reaction removing traps, and σ is the standard deviation of the Gaussian distribution, then the number of traps with an activation energy in the range E_a - - E_a+dE_a is

$$Tr_{Ea} = \frac{Tr_0}{\sqrt{2\pi}\sigma}\exp\left(-\frac{(E_a - E_a^0)^2}{2\sigma^2}\right)dE_a \qquad (7.7)$$

The decay of traps in this activation energy range is described by

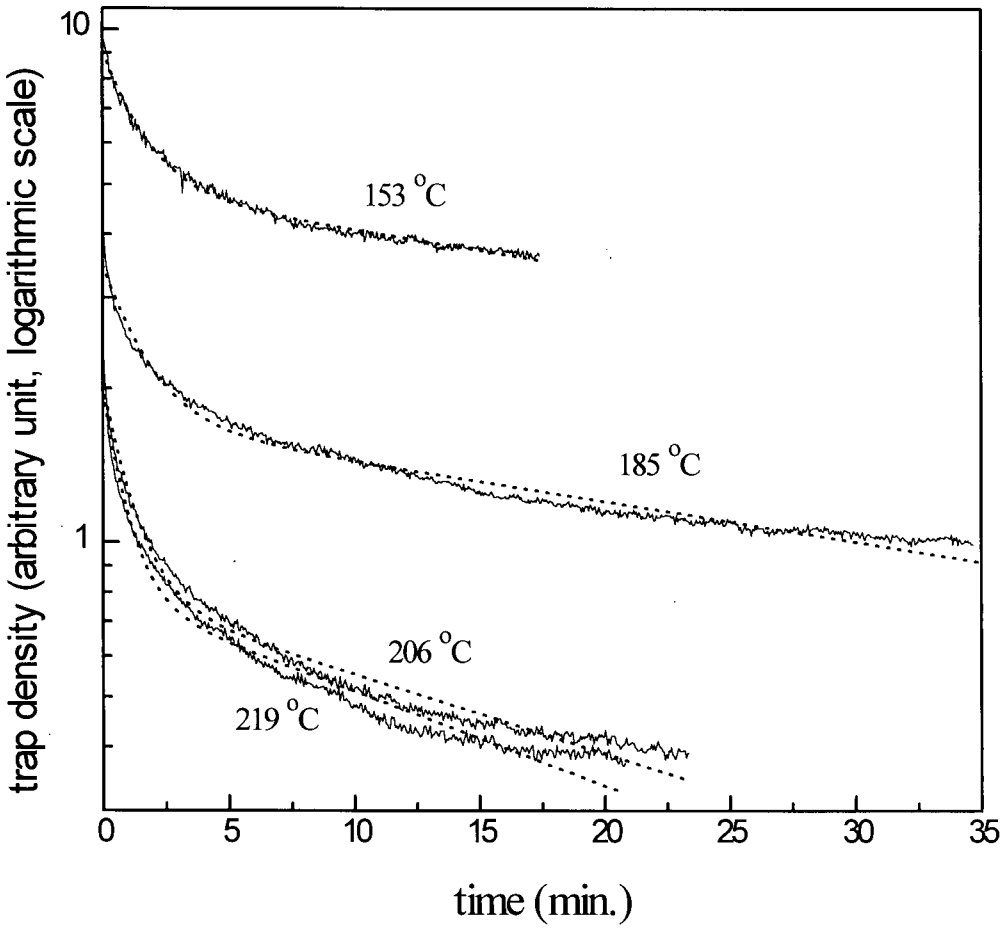

Figure 7.11 Logarithmic plots of the trap density against time when the H-atoms are shut off (later portion of Figure 7.9). The dotted curves are the best fits of the data with the assumption of two traps, each with a simple exponential decay.

Table 7.3 The initial trap densities and the rate constants of two exponentially decaying traps.

Temperature (°C)	Initial density of trap 1	Initial density of trap 2	Decay rate constant of trap 1 (min^{-1})	Decay rate constant of trap 2 (min^{-1})
153	4.19	4.90	0.653	0.0183
185	1.75	1.72	0.608	0.0179
206	1.22	0.776	0.850	0.0344
219	1.16	0.770	1.06	0.0410

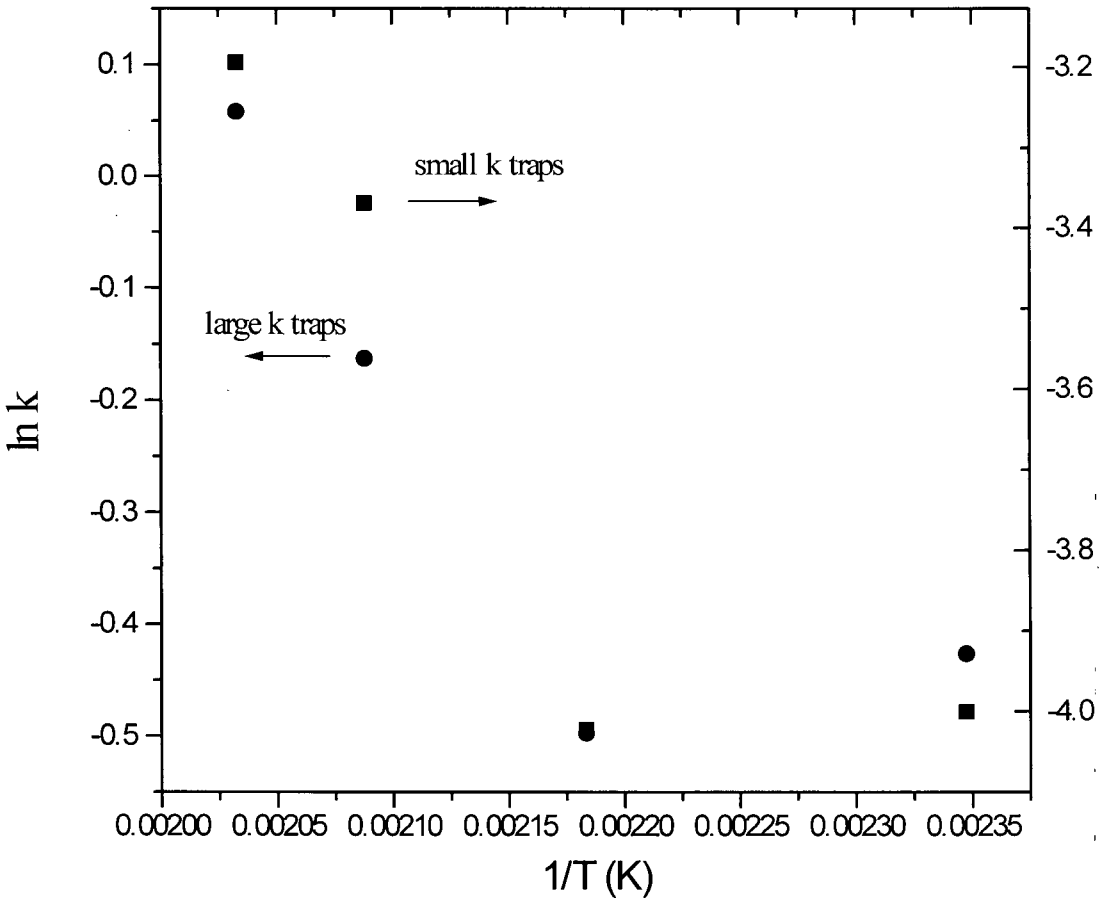

Figure 7.12 Arrhenius plot for the rate constants of two exponentially decaying traps.

$$Tr_{Ea}(t) = Tr_{Ea} * \exp(-A \exp(-\frac{E_a}{kT})\, t) \qquad (7.8)$$

where t is the decay time and A is the pre-exponential constant for the decay rate. Combining equations equation (7.7) and (7.8), the decay of all the traps with all the possible activation energies can be calculated from the equation:

$$Tr(t) = \frac{Tr_0}{\sqrt{2\pi}\sigma} \int_0^\infty \exp(-\frac{(E_a - E_a^0)^2}{2\sigma^2}) \exp(-A \exp(-\frac{E_a}{kT})\, t)\, dE_a \qquad (7.9)$$

Equation (7.9) was used to fit the trap decay curves shown in Figure 7.11 which were observed when the H-atom source has been shut off. Nine energy levels from $E_a - 2\sigma$ to $E_a + 2\sigma$ with a spacing of $\frac{1}{2}\sigma$ were used to approximate the Gaussian distribution. Tr_0 is determined by the initial trap level at the moment that the H-atoms are turned off. The initial trap density before the exposure to H-atoms is subtracted from all trap density values. The curve fitting was done using MicroCal Origin.

The dispersion of the activation energies (σ) is completely determined by the curvature of the trap decay curves shown in Figure 7.11. Its value is calculated to be in the range from 0.12 to 0.14 eV with an average of 0.13 eV.

The decay curve at any particular temperature does not determine unique values for E_a^0 and A. It is not difficult to show that what is determined is an average rate constant:

$$k = A * \exp(-\frac{E_a^0}{kT}) \qquad (7.10)$$

which corresponds to a "family" of A and E_a^0 values, each pair of A and E_a^0 evaluated to a constant k according to equation (7.10). Values of k (in arbitrary units) obtained from curve fitting at four temperatures, are listed in Table 7.4.

Table 7.4 The initial trap densities created by H-atoms at different temperatures, their decay rate constants, the mean activation energy and pre-exponential constants. The dispersion of the activation energy is 0.13 eV.

Temperature (°C)	153	185	206	219
Initial trap density	10.6	5.2	3.5	3.2
k (average) (min^{-1})	0.10	0.19	0.69	0.60
E_a^0 (eV)	0.55			
A (10^5) (au)	3.3	2.2	4.4	2.7
A average (au)	$3.2x10^5$			

Figure 7.13 shows an Arrhenius plot for these values of k. Although the value of E_a^0 is not well determined, we obtain a value of 0.55 ± 0.13 eV. The calculated values of A and its average are also listed in Table 7.4. Since k is in arbitrary units, A is also.

The fitting of the trap decay data using values $E_a^0 = 0.55$ eV and $A = 3.2 \times 10^5$ is shown in Figure 7.14 for the decay curves shown in Figure 7.9. There are at least three possible reasons for the discrepancy between theory and experimental data, (i) A Gaussian distribution is not correct, (ii) a different distribution of traps is created at different temperatures, (iii) experimental error. Since some of the fitting curves lie above the experimental points and others lie below, the most likely answer is (iii), i.e. the discrepancy between this theory and the data is due to some poorly controlled experimental parameter such as temperature.

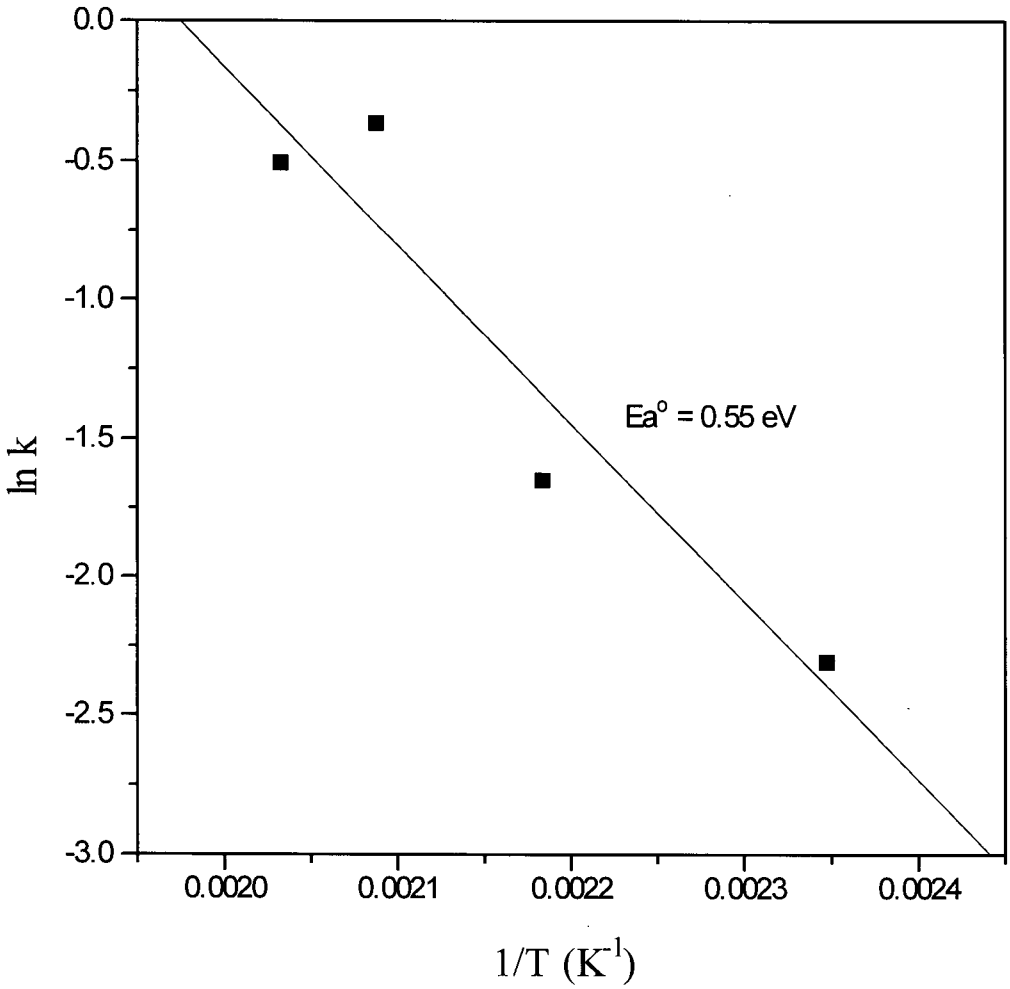

Figure 7.13 Arrhenius plot for the trap decay rate constants.

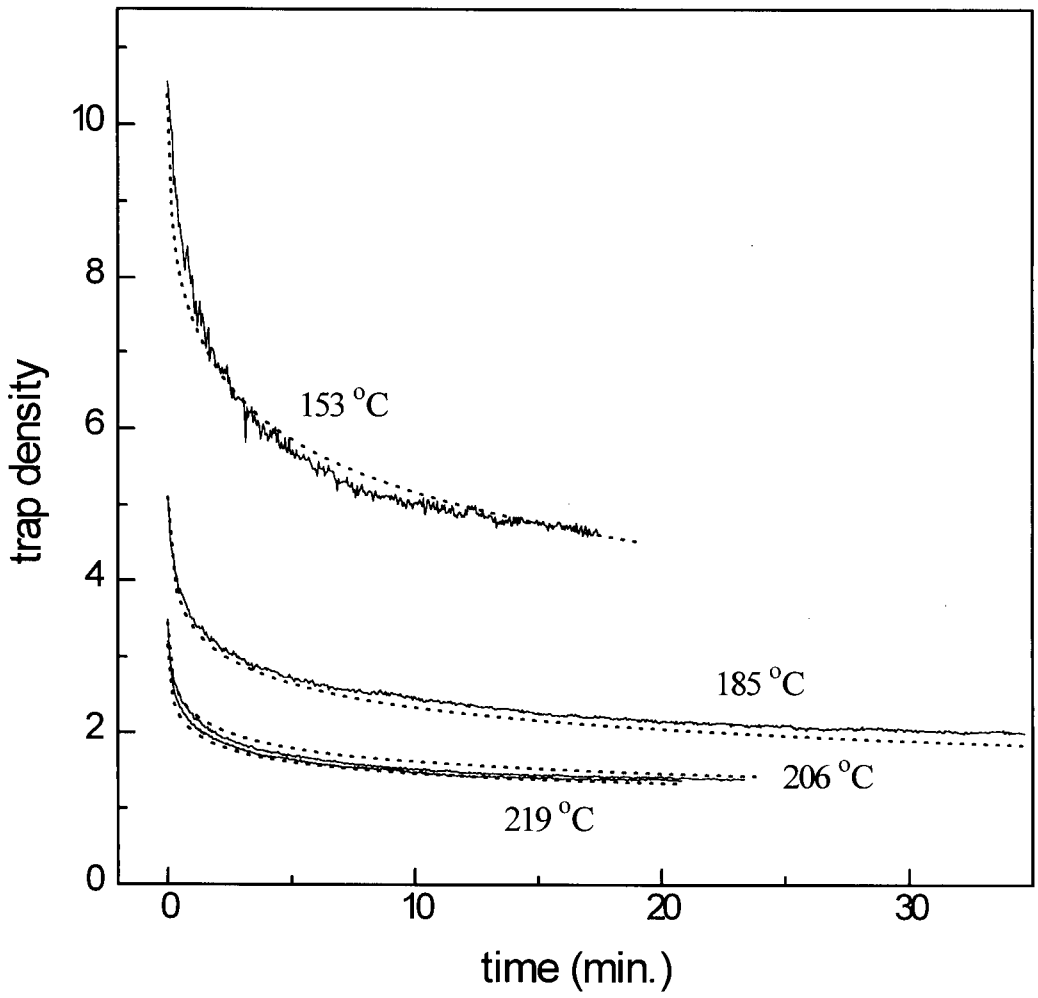

Figure 7.14 The fitting of the trap density decay results shown in Figure 7.9 with the assumption of a Gaussian distribution in the activation energy centered at 0.55 eV with a standard deviation of 0.13eV. The pre-exponential constant is 3.2×10^5.

7.5 The irreversible change created by H-atoms at elevated temperature

As mentioned earlier, in addition to the trap production that occurs when the Si/SiO_2 interface is exposed to H-atoms and its reverse reaction when the H-atoms are removed from the system, a third process occurs at elevated temperatures during the first H-atoms exposure which causes the initial large trap density, which forms during the first exposure to H-atoms, to slowly drop towards a plateau, to which it returns whenever the H-atoms are again turned on (as shown in Figure 7.8). The change in the sample is permanent and the peak does not recur after a couple of exposures to H-atoms. This falling trap density may be due to any of the following phenomena: (i) The passivation (deactivation) of the p-type dopant could be increasing the RF probe sensitivity, which then produces only an apparent drop in the trap density. (ii) Consecutive reactions that form and then remove traps could be occurring. (iii) H_2 could be accumulating at the SiO_2/Si interface repassivating the traps formed by reaction (7.5). We will show that none of these three models provide a consistent description of the observations shown in Figure 7.8. However, A modification of model (iii) in which the H_2 which accumulates at the Si/SiO_2 interface occupies and hence removes some H-atom trap sites, provides the only explanation that is at least semi-quantitative and self consistent.

7.5.1 The boron passivation model

Rationale:

It has been shown by some earlier workers[62] that boron, in a layer of Si that is a few micrometers thick, is passivated when a thermal oxide covered silicon chip is exposed to H-atoms. Since the sensitivity of the rf probe that we are using is inversely proportional to the

conductivity of the silicon sample, and the conductivity is proportional to the dopant density, the carrier concentration measured by the rf probe needs to be corrected if there is any change in the concentration of electrically "active" dopant.

When boron passivation is considered equation (2.13) must be modified:

$$[Tr_a] \quad \propto \quad \frac{1}{[C]} \quad \propto \quad [Tr]\,[B] \qquad (7.11)$$

where $[Tr_a]$ is the apparent trap density, [C] is the carrier concentration, [Tr] is the carrier trap density, and [B] is the density of active boron atoms.

To explain the apparent drop in trap density after the initial rapid rise, we will assume that although the trap density continues to rise exponentially towards some plateau, the simultaneous passivation of boron reduces the conductivity of the silicon, producing an apparent decrease in trap density.

It can be seen in Figure 7.9 that the time it takes to reach that maximum is shorter at higher temperatures. At higher temperatures, if boron is passivated more rapidly, the effective dopant density is decreased more rapidly, i.e. the correction factor [B] in equation (7.11) drops more rapidly. Thus at higher temperatures, the same trap density level will result in a lower signal from our probe because of this correction for dopant changes expressed by equation (7.11). This could drive the "apparent" trap density down to the plateau that occurs at the end of process (2) in Figure 7.8. Provided the passivation of boron is faster at higher temperature, the dopant correction will make the time it takes for the apparent trap density to reach its peak shorter at high temperatures.

<u>The model:</u>

Assume both trap and boron densities change exponentially when the substrate is exposed to H-atoms, i.e.

$$[Tr] = Tr_0 + (Tr_\infty - Tr_0)\,(1 - \exp(-k_T t)) \quad (7.12)$$

$$[B] = B_\infty + (B_0 - B_\infty)\exp(-k_B t) \quad (7.13)$$

where Tr_0 and Tr_∞ are the initial and final trap densities, B_0 and B_∞ are the initial and final boron densities, respectively. Fitting of the results shown in Figure 7.9 using equations (7.11), (7.12) and (7.13) is presented in Figure 7.15. "Fitting values" of the constants Tr_0, Tr_∞, k_T, B_0, B_∞, and k_B are list in Table 7.5.

Problems:

Although the fit is quite acceptable, the fitting constants B_∞ is inconsistent with its assumed significance, since the final boron density should decrease with increasing temperature to be consistent with the shift of the peak described above. It does not. A second piece of evidence against this model is found in the fact that there is no measurable change in the sample resistivity measured with a four-point probe before and after H-atoms exposure. These two observations lead us to conclude that boron passivation can not account for the observations in Figure 7.9. There are two additional observation that argue against this model. First, earlier experiments[65] have shown that boron passivation occurs only in a small temperature window around 100 °C. Secondly, as shown in Figure 7.16, exposure of H-atoms to intrinsic (resistivity 20000 - 50000 Ω·cm) and n-type (resistivity 5 - 10 Ω·cm) silicon samples produces the same effect as seen with p-type silicon. Since the effect is qualitatively similar for p-doped, n-doped and undoped material we conclude that dopant passivation does not play any role in the irreversible drop in trap density caused by H-atoms at elevated temperatures.

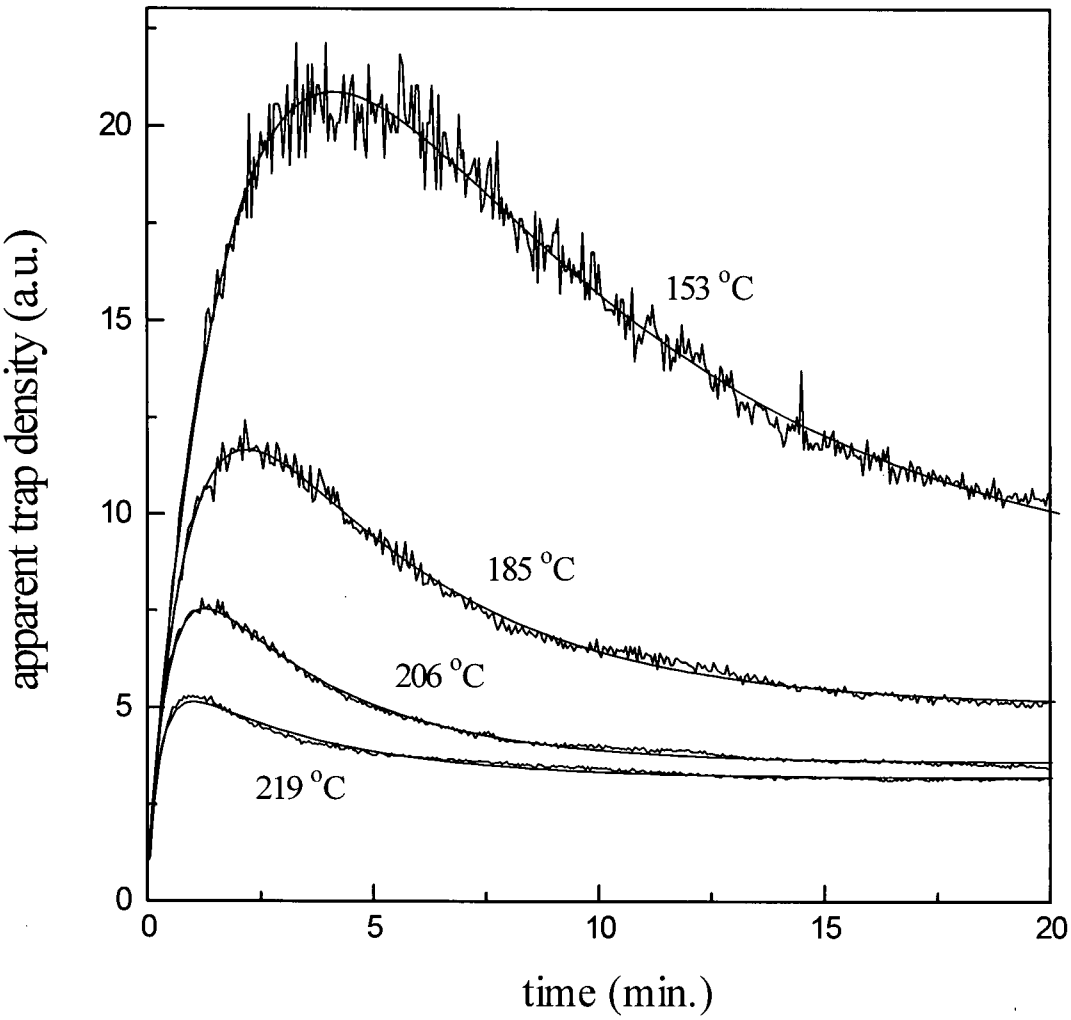

Figure 7.15 The "apparent" trap density as a function of time when the silicon sample is exposed to H-atoms at the temperatures indicated (early portion of Figure 7.9). The smooth solid curves are the fitting results of the boron passivation model.

Table 7.5 The initial, final trap and boron densities, and their rate constants for the boron passivation model.

Temperature(°C)	T_0	T_∞	k_T	B_0	B_∞	k_B
153	0.14	5.52	0.393	7.14	1.47	0.137
185	0.14	2.70	0.859	7.14	1.87	0.231
206	0.14	1.46	1.90	7.14	2.47	0.305
219	0.14	0.850	3.16	7.14	3.77	0.288

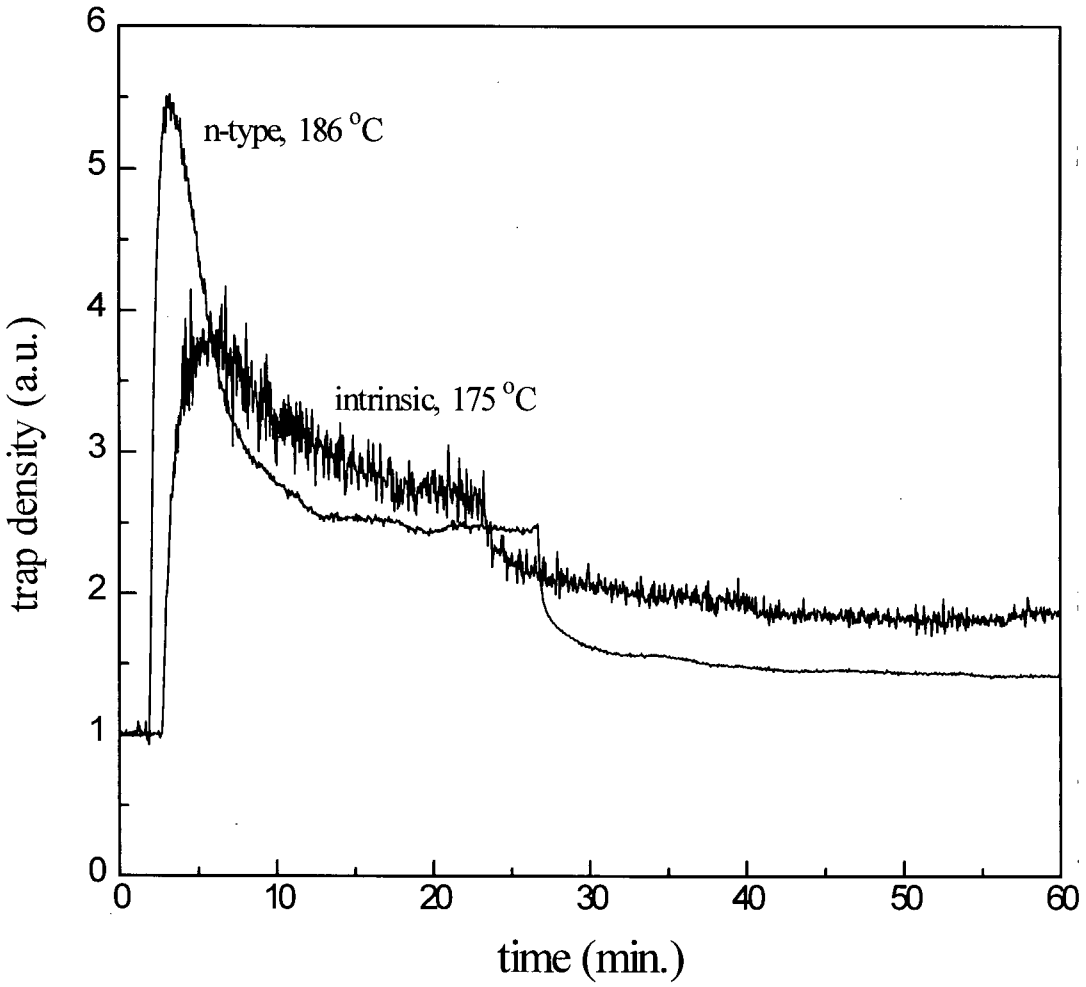

Figure 7.16 Exposure of H-atoms to intrinsic (resistivity 20000 - 50000 Ω·cm) and n-type (resistivity 5 - 10 Ω·cm) silicon samples.

7.5.2 The consecutive reactions model

Rationale:

The shape displayed by the trap density in the top region of Figure 7.8 resembles the concentration profile of an intermediate species in the classical sequence of consecutive reactions in which the first reaction forms traps and the second reaction removes them. The combination of this trap with the one that is formed by reaction (7.5) and removed by reaction (7.6) could have a trap density profile shown in Figure 7.8.

The model:

$$H + P \xrightarrow{k''} Tr \qquad (7.14)$$

$$Tr \xrightarrow{k'} N \qquad (7.15)$$

or

$$Tr + H \xrightarrow{k'} N \qquad (7.15')$$

where P is the trap precursor, Tr is the carrier trap, and N is the final product, which is not a trap. The rate constants for the two reactions are k″ and k' respectively. The first reaction is associated with H-atoms, because traps are created by exposure to H-atoms. Whether the second reaction is associated with H-atoms is still to be determined.

From reactions (7.14) and (7.15) we have the following kinetics:

$$\frac{d[Tr]}{dt} = k[P] - k'[Tr] \qquad (7.16)$$

(where $k = k''[H]$, and [H] is assumed constant at the interface.) Solving these equations with the initial conditions:

$$[P] = P_0 \text{ and } [Tr] = 0 \text{ at } t = 0 \qquad (7.17)$$

where P_0 is the initial precursor density, we have

$$[Tr] = \frac{kP_0}{k' - k}\left(\exp(-kt) - \exp(-k't) \right) \qquad (7.18)$$

If $k < k'$, when the time t is long enough so that $\exp(-kt) >> \exp(-k't)$, equation (7.8) becomes

$$[Tr]_{t\to\infty} = \frac{kP_0}{k' - k} \exp(-kt) \qquad (7.19)$$

Taking the logarithm of both sides of this equation:

$$\ln\left([Tr]_{t\to\infty} \right) = \ln \frac{kP_0}{k' - k} - kt \qquad (7.20)$$

This means that the later portion of a logarithmic plot of trap density against time will yield a straight line with a slope equal to -k.

If $k > k'$, the slope at long times is -k', the rate constant for the second reaction. In general the slope at long times is always determined by the smaller rate constant. When $k = k'$, the slope at long time = $-k = -k'$.

A logarithmic plot of [Tr] against time for the experimental results shown in Figure 7.9 is presented in Figure 7.17. The plateau height reached at long times when exposed to H-atoms was subtracted from the trap density in order to separate Tr from the other trap which determines the plateau height during exposure to H-atoms. The plateau heights were obtained by trial and error to make the portions of the curves after the peaks yield good straight lines. The calculated rate constants at various temperatures obtained from the slopes are listed in Table 7.6. An Arrhenius plot of this data is shown in Figure 7.18. The activation energy for the

smaller rate constant is 0.60 eV. In view of the discussion above we equate this to k or k', depending on which is smaller.

The "larger" rate constant can be obtained from the time required to reach the peak in trap density observed in Figure 7.9. To get an expression for the "peak time" t_p take the time derivative of equation (7.18) and set it to zero,

$$\frac{d[Tr]}{dt}\Big|_{t = t_p} = 0 \qquad (7.21)$$

Solving this equation, we have

$$t_p = \frac{\ln k - \ln k'}{k - k'} \qquad (7.22)$$

where t_p is the peak time, which is determine only by the two rate constants. The values of the "larger" rate constants calculated with equation (7.22) are also listed in Table 7.6. An Arrhenius plot for this rate constant is shown in Figure 7.18. This yields an activation energy of 0.14 eV for the larger rate constant.

The initial trap precursor density can be obtained from equation (7.18) at the trap density maximum, if we know which rate constant is the larger one. The trap precursor density values (P_0) are listed in the second last column of Table 7.6 for the assumption that k is the larger rate constant and in the last column when it is assumed that k′ is the larger rate constant. Since all the silicon samples were cut from the same wafer, the initial trap precursor density should be similar for each experiment. From the distribution of P_0 it can be seen that the assumption that k is the larger rate constant leads to an unacceptable trend in P_0. This conclusion is supported by the activation energy for k, which is 0.14 eV obtained from the Arhenius plot in Figure 7.18 and compares favorably with the trap creation activation energy of 0.15 eV obtained at lower

temperatures (see section 7.2). The activation energy for the second reaction rate constant k′ is then 0.60 eV.

In order to determine whether H-atoms are involved in the second reaction, two silicon samples were exposed to different concentrations of H-atoms at 188 °C. The concentration of H-atoms in the reaction chamber was increased by passing a greater flow of H_2 through the discharge. The partial pressures of H_2 in these two experiments were 0.41 and 4.1 mTorr respectively. The trap density changes with time are shown in Figure 7.19 and the logarithmic plots are presented in Figure 7.20. The rate constants obtained are listed in Table 7.7. k is increased to 5.2 times its original value when H_2 pressure is increased from 0.41 to 4.1 mTorr. k′ is increased by a factor of 4.5, which is comparable to the increase in k. Hence it would appear that H-atoms are also involved in the second reaction and reaction (7.15) can be rewritten as:

$$Tr + H \xrightarrow{k'} N \qquad (7.15)$$

Additional Testing of the Consecutive Reaction Model:

If both reactions require H-atoms to occur, removing H-atoms when the trap density reaches its peak should stop both reactions, leaving [Tr] at its maximum level. However, the experimental results shown in Figure 7.21 do not support such a prediction. For these experiments, which were performed at 168, 184, 201, and 222 °C, the hydrogen atoms (20 mTorr H_2 + 10 mTorr Ar, 30 Watt microwave power) were switched off after the sample had been exposed to it for 15 seconds. A careful inspection of these decay curves, and a comparison with the curves generated by a 25 minute exposure (Figure 7.9) leads us to conclude that the

decay of the trap density from its peak value to the plateau value, which occurs when the H-atoms are turned off, is comparable whether the substrate is exposed to H-atoms for 15 seconds or for 25 minutes. Although a simple comparison is difficult because of the differences in the temperatures of the various experiments, consider the curve at 219 C in Figure 7.9. The peak lies at about 5.2 and this is reduced to about 1.2 after 25 minutes of H-atoms and 20 minutes with the H-atoms off. This can be compared to the curve at 222 °C in Figure 7.21 where the concentration reached a peak of 5.6 and also fell to about 1.2 when the H-atoms were shut off after only 15 seconds. This behavior is not consistent with the "consecutive reaction model" which requires continuing H-atoms exposure to drop the trap density.

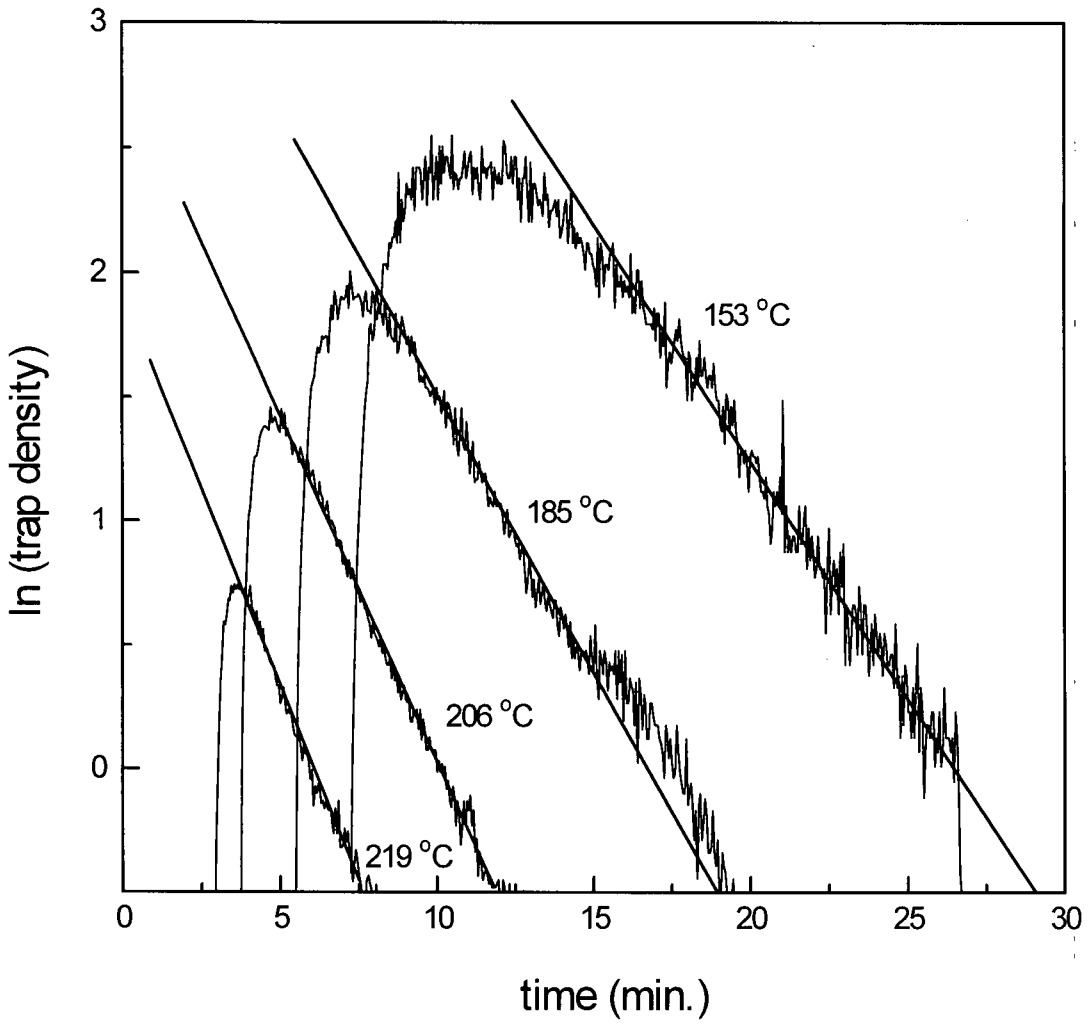

Figure 7.17 Logarithmic plot of the trap density against time for the experimental results shown in Figure 7.9. The portions after the peaks yield good straight lines.

Table 7.6 Constants for the consecutive reactions model.

T_0 is the initial trap density.

temperature (°C)	plateau height (a.u.)	k (1/min)	peak time (min.)	k′ (1/min)	P_0/T_0 if $k < k'$	P_0/T_0 if $k > k'$
153	9.3	0.19	4.2	0.29	38	25
185	4.9	0.22	2.1	0.88	42	11
206	3.5	0.28	1.3	1.6	33	5.8
219	3.2	0.32	0.9	2.7	26	3.1

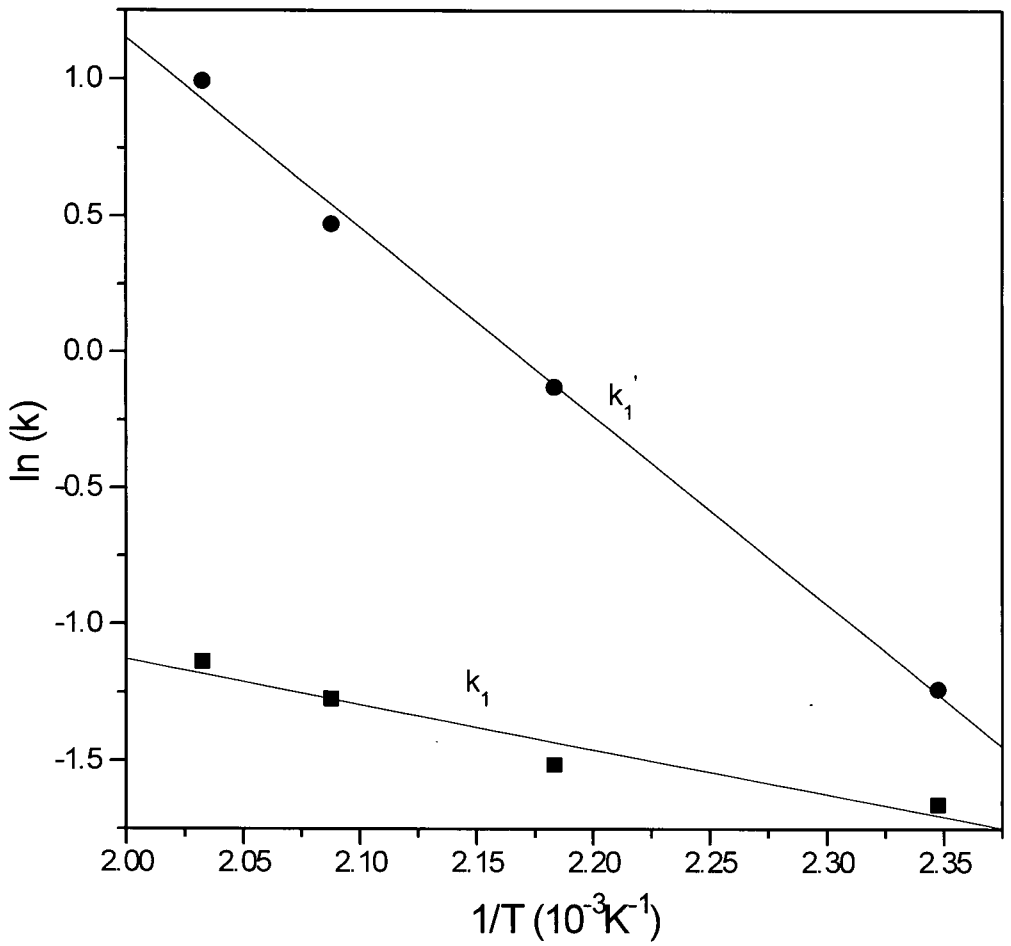

Figure 7.18 Logarithmic plots of the reaction rate constants against the reciprocal of the temperature for the consecutive reaction model.

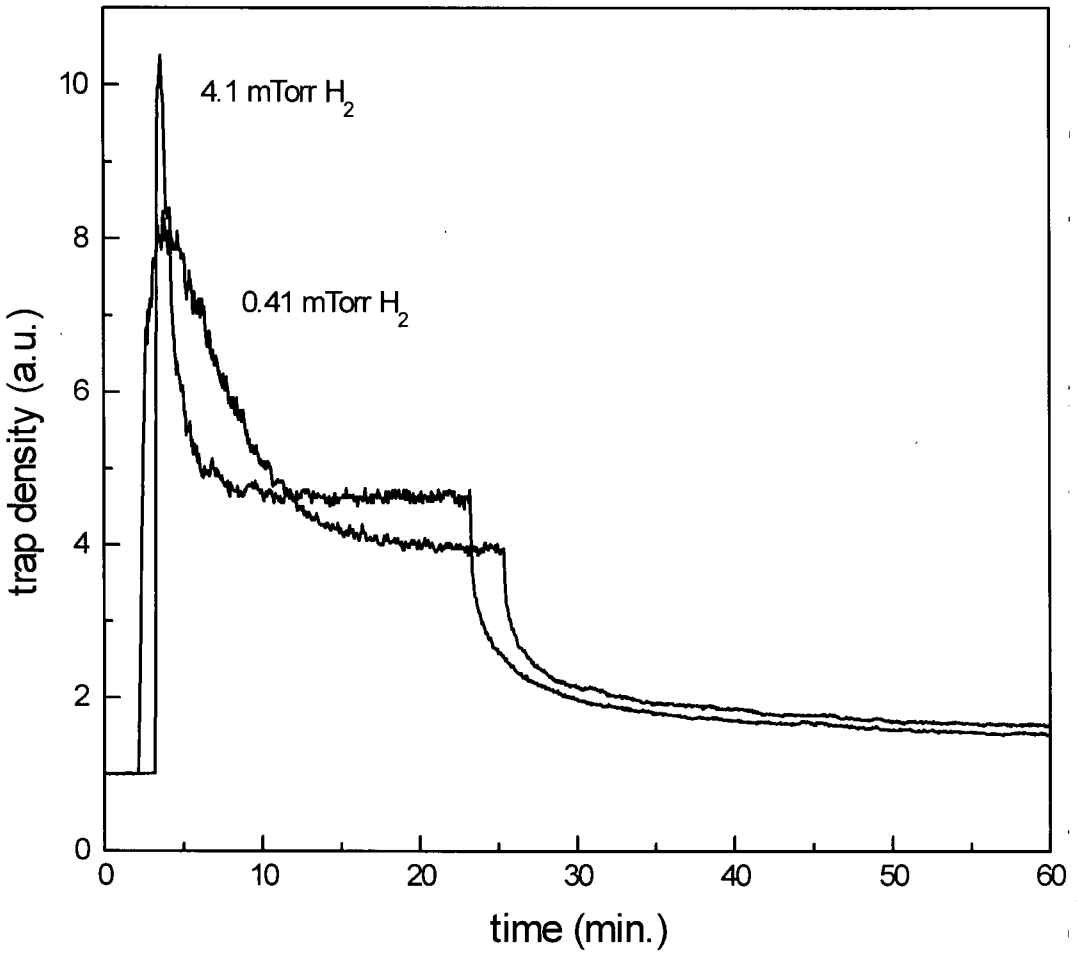

Figure 7.19 The trap density changes with time in p-type silicon samples when exposed to different concentrations of H-atoms at 188 °C. The pressure of H_2 passed through the discharge are as indicated.

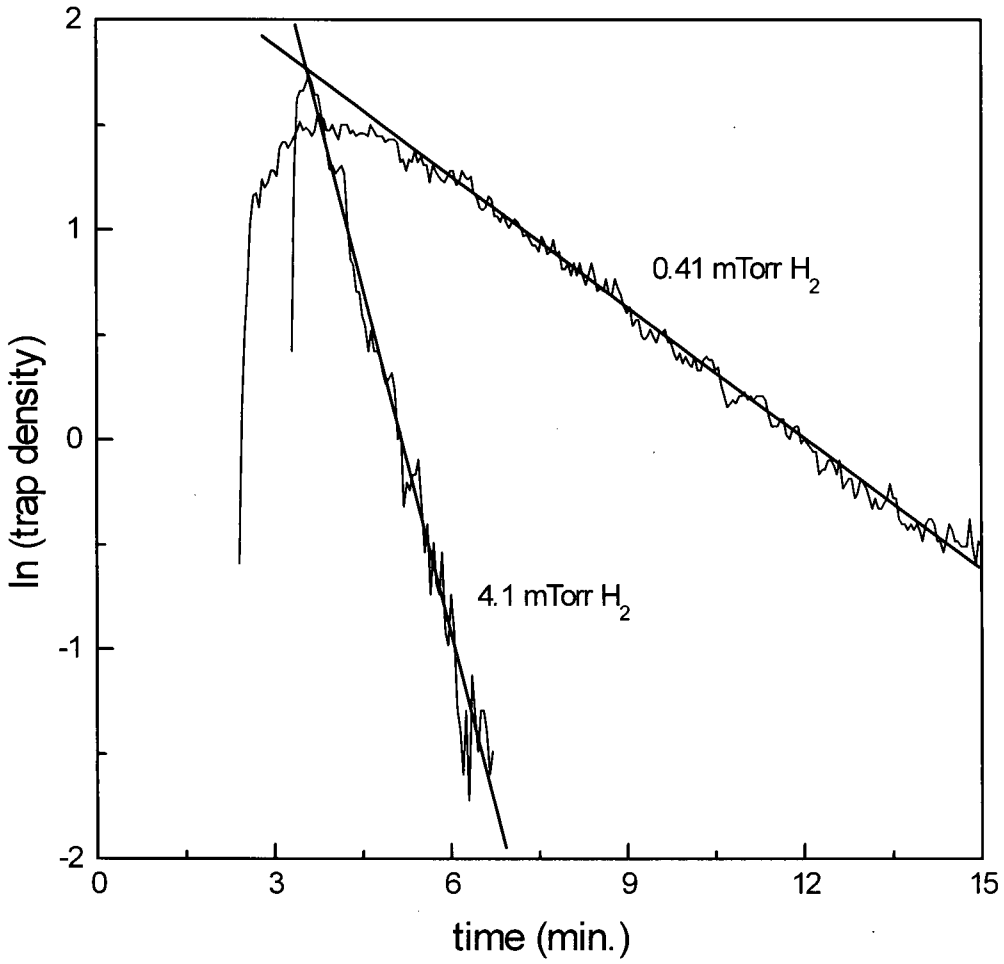

Figure 7.20 Logarithmic plot of the trap density against time for the experimental results shown in Figure 7.19.

Table 7.7 The rate constants and peak time for two different H-atom concentrations.

Temperature (°C)	H_2 pressure (mTorr)	k	peak time (min.)	k'
188	0.41	0.21	0.35	1.3
188	4.1	1.1	1.65	5.9

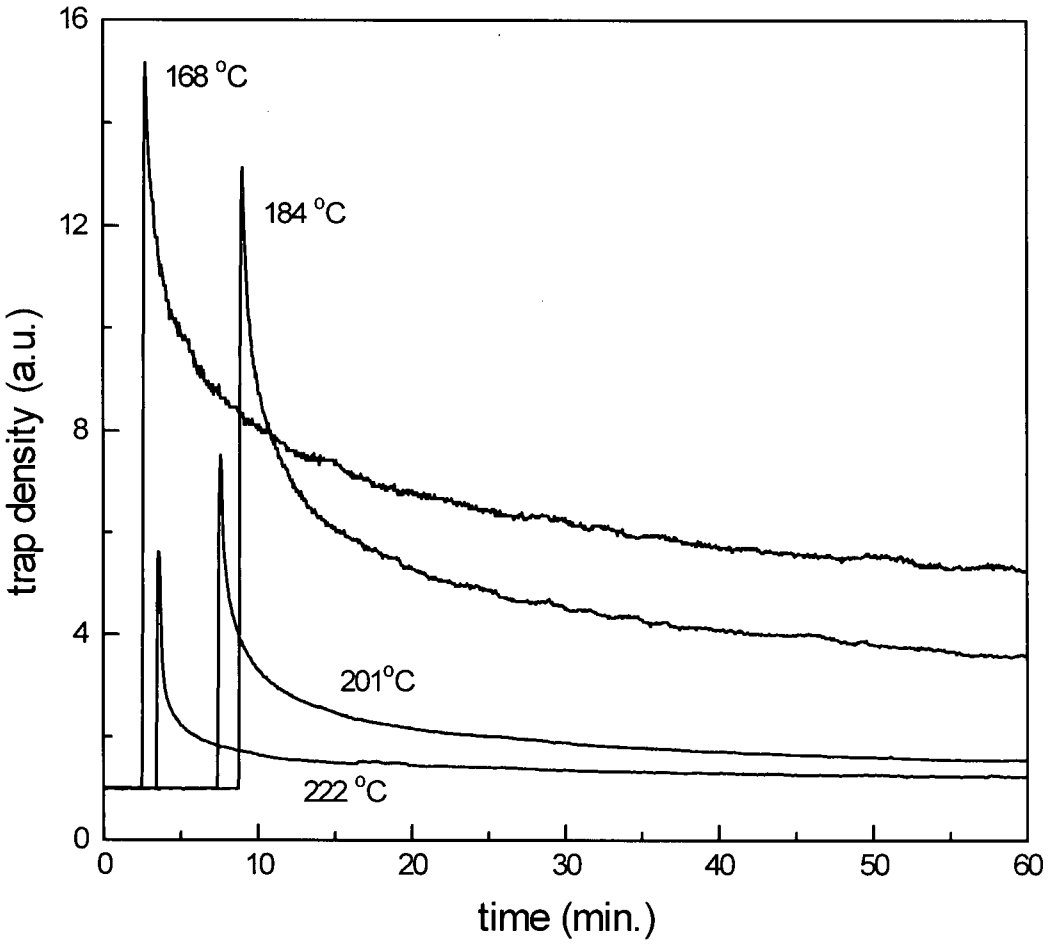

Figure 7.21 The trap density change with time during and after a 15 seconds exposure to the same atomic hydrogen concentration at the temperatures indicated.

7.5.3 H_2 accumulation model

Rationale:

If we assume that potential carrier traps are initially passivated and in the form: H-Tr, then the initial depassivation that occurs when these species are exposed to H-atoms may occur through the reaction:

$$H_{(i)} + HTr \xrightarrow{k_{dp}} Tr + H_2 \qquad (7.23)$$

where HTr is the trap precursor, $H_{(i)}$ is the H-atoms at the SiO_2/Si interface, k_{dp} is the rate constant for the depassivation (trap creation). The reverse reaction:

$$H_2 + Tr \xrightarrow{k_p} HTr + H \qquad (7.24)$$

where k_p is the rate constant for the passivation reaction of interfacial traps, would then make the passivation level eventually reach a plateau monotonically, not pass through a peak. The trap density could go through a maximum if the H_2 accumulates through a catalyzed or simple recombination reaction of H-atoms at or near the SiO_2/Si interface:

$$H + H \rightarrow H_2 \qquad (7.25)$$

When H_2 reaches its maximum "solubility" at the interface, the trap formation and passivation assume a steady state value, which is represented by the plateau after a peak.

If this assumption regarding the accumulation of H_2 is correct, when H-atoms are removed, the H_2 concentration cannot decrease significantly with time. Otherwise, exposure to H-atoms again would result in a repetition of the passage through a maximum in the trap density. It can

be seen in Figure 7.8 that the effect of the second H-atoms exposure is different from the first time. The trap density approaches the same plateau level without passing through a peak.

The model:

For a process that is governed by the elementary steps described in equations (7.23) and (7.24), the rate of change of the interfacial trap density is given by

$$\frac{d[Tr]}{dt} = k_{dp}[HTr][H_{(i)}] - k_p[Tr][H_2] \tag{7.26}$$

Assuming a fixed number of trap sites (HTr_0):

$$[Tr] + [HTr] = HTr_0$$

equation (7.26) becomes

$$\frac{d[Tr]}{dt} = k_{dp}(HTr_0 - [Tr])[H_{(i)}] - k_p[Tr][H_2]$$

$$= k_{dp}HTr_0[H_i] - (k_{dp}[H_{(i)}] + k_p[H_2])[Tr] \tag{7.27}$$

Assume H_2 accumulation is slow and integrating equation (7.27):

$$d\ln(k_{dp}HTr_0[H_{(i)}] - (k_{dp}[H_{(i)}] + k_p[H_2])[Tr]) = -(k_{dp}[H_{(i)}] + k_p[H_2])dt$$

$$k_{dp}HTr_0[H_{(i)}] - (k_{dp}[H_{(i)}] + k_p[H_2])[Tr] = B\exp(-(k_{dp}[H_{(i)}] + k_p[H_2])t) \tag{7.28}$$

where B is a constant and can be determined from the initial condition:

$$[Tr]_{t=0} = 0$$

we get

$$B = k_{dp}\, HTr_0\, [H_{(i)}] \tag{7.29}$$

Substituting the constant B in equtaion (7.28):

$$[Tr] = \frac{k_{dp}HTr_0[H_{(i)}]}{k_{dp}[H_{(i)}] + k_p[H_2]}(1 - \exp(-(k_{dp}[H_{(i)}] + k_p[H_2])t)) \tag{7.30}$$

If the H_2 build up is exponential and is slower than the forward and backward reactions (7.23) and (7.24), then:

$$[H_2] = H_2^{\infty}(1-\exp(-k_a t)) \qquad (7.31)$$

where H_2^{∞} is the final H_2 level and k_a is the first order accumulation rate constant.

The interfacial trap density in our samples was electrically measured to be about $3x10^{10}$ $cm^{-2}eV^{-1}$. After exposure to H-atoms for about one hour at room temperature, the trap density increases to $9x10^{12}$ $cm^{-2}eV^{-1}$, about 300 times the initial level. For this reason, the trap precursor concentration is set to be 300 times the initial value in the fitting calculations at elevated temperatures. The fitting of some experimental profiles is presented in Figure 7.22. The magnitudes of some of the fitting constants are listed in Table 7.8 and are plotted as a function of temperature in Figure 7.23.

Problems:

1. It can be seen from Figure 7.23 that the activation energy for the initial depassivation by H-atoms is very low, agreeing with the low temperature experimental results described in section 7.2. However, the data in Figure 7.23 yields an activation energy of 0.30 eV for the reaction in which H_2 passivates the traps. This is much lower than the value of 1.6 eV obtained by Brower[16] for the H_2 passivation reaction of P_b centers(7.24).
2. The activation energy for the accumulation of H_2 is 0.45 eV. This is very high for a hydrogen atom recombination reaction (7.25).

For these reasons, we conclude that the chemical reaction that have been shown (see section 1.2) to occur with P_b center cannot account for the observations at elevated temperatures shown in Figure 7.8 and Figure 7.9. As mentioned in section 1.2, there is evidence that traps

Table 7.8 The rate constants for the H_2 accumulation model. $HTr_0 = 300$.

temperature (°C)	k_{dp} H	H_2^{∞} k_p	k_a
153	0.033	1.26	0.076
185	0.032	2.38	0.13
206	0.033	3.65	0.24
219	0.027	3.42	0.43

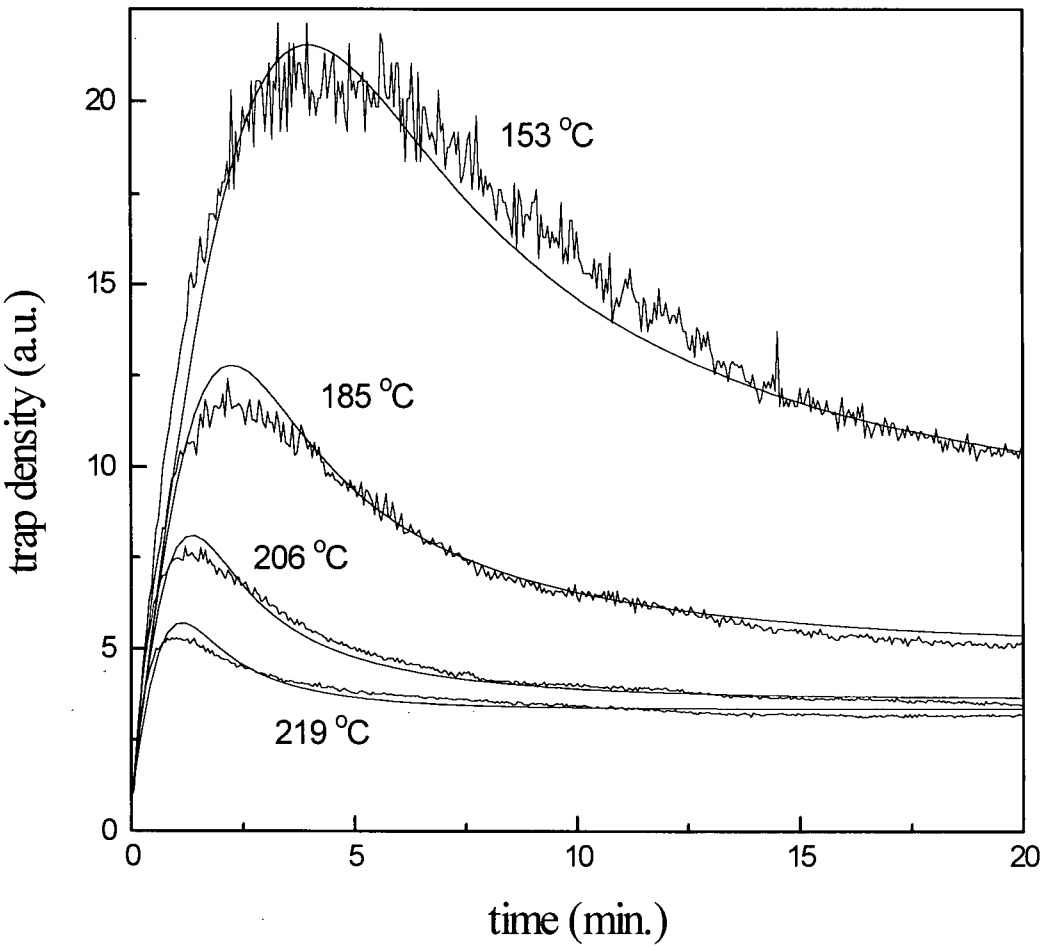

Figure 7.22 The trap density as a function of time when the silicon sample is exposed to H-atoms at the temperatures indicated (early portion of Figure 7.9). The smooth solid curves are the fitting results for the H_2 accumulation model.

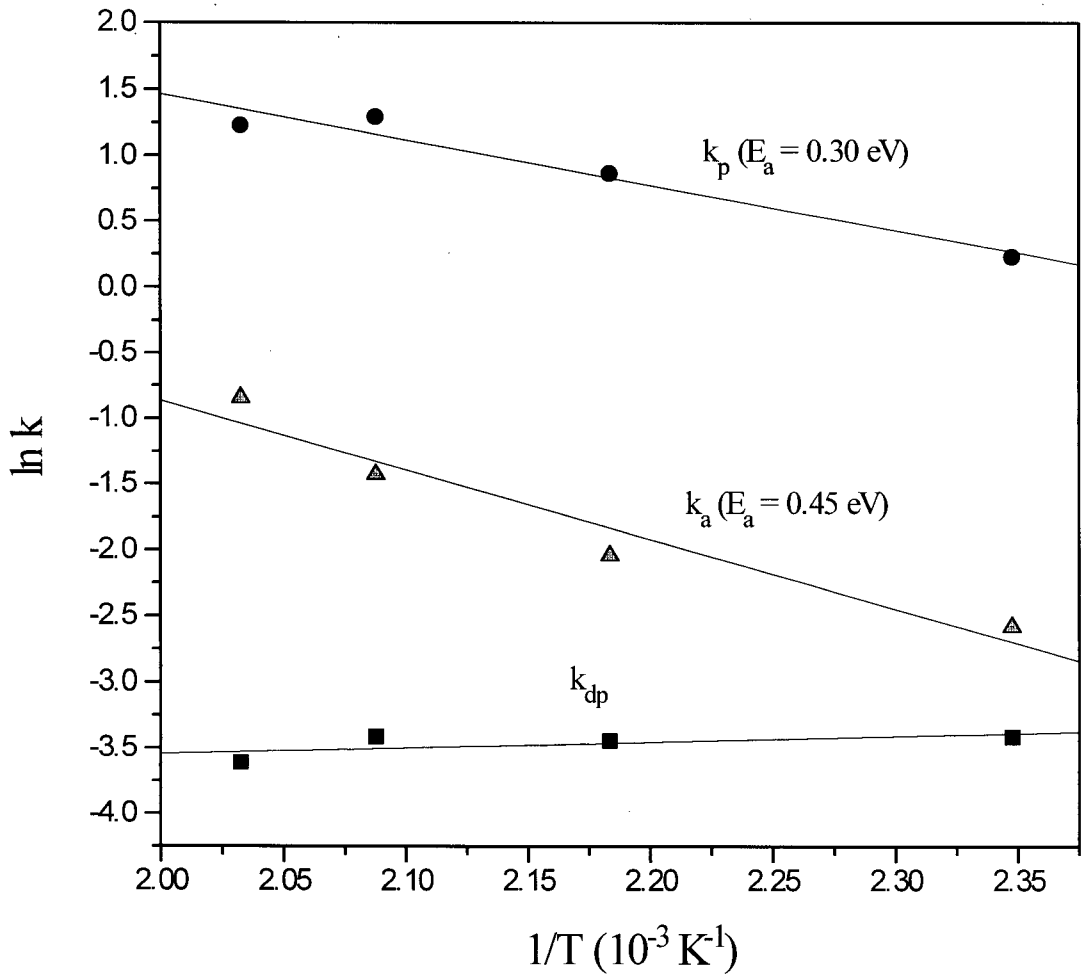

Figure 7.23 Logarithmic plots of the rate constants k_{dp}, k_p, and k_a against the reciprocal temperature for the H_2 accumulation model.

other than P_b centers are produced by exposing SiO_2/Si samples to H-atoms[23]. However these traps were found to be stable for long periods of time. In the following section, we will explore a possible mechanism for their formation by exposure to H-atoms and their disappearance when the H-atom source is removed.

7.5.4 Trap precursor site occupation by H and H_2

Rationale:

If traps are produced by the occupation of some trap precursor sites by atomic hydrogen then the process can be described by the reaction - a special case of reaction (7.5):

$$H\bullet + \text{Site} \xrightarrow{k_{dp}} \text{H-Site}\bullet \qquad (7.32)$$

where "Site" is the trap precursor site, H• is the H-atom at the SiO_2/Si interface, H-Site• is a carrier recombination catalyst (trap) because of the presence of an unpaired electron, and k_{dp} is the reaction rate constant for trap creation (depassivation). Its reverse reaction:

$$\text{H-Site}\bullet \xrightarrow{k_p} \text{Site} + H\bullet \qquad (7.33)$$

where k_p can be considered the rate constant for the passivation of interfacial traps. These reactions would make the trap density eventually reach a plateau, but it would not cause it to pass through a maximum. The trap density could go through a maximum if H_2 can also occupy the trap precursor sites through a reaction such as:

$$H\bullet + \text{H-Site}\bullet \rightarrow H_2\text{-Site} \qquad (7.34)$$

where H_2-site is not a carrier trap. The loss of trap precursor sites to H_2 will decrease the rate of reaction (7.32) lowering the steady state trap density as it does so. Like the H_2 accumulation model in section 7.5.3, when H_2 reaches its maximum "solubility" at the interface, the trap formation and passivation assume a steady state value, which is represented by the plateaus seen at long exposure times in Figure 7.9. It remains possible that H_2 cannot occupy all the sites that can be occupied by H, and hence the steady state plateau do not occur at zero trap density.

When H-atoms are removed, the H_2 in interfacial states must not change significantly with time because of the requirement that this process be irreversible. Otherwise exposure to H-atoms would result in the passage of the trap density through a maximum again, which does not occur.

Kinetic analysis:

In this analysis we will let H-Site• = tr and Site = S to decrease the complexity of the equations. From reaction (7.32) and (7.33), the rate of change of the interfacial trap density

$$\frac{d[Tr]}{dt} = k_{dp}[S][H] - k_p[Tr] \tag{7.35}$$

Assuming the conservation of trap precursor sites,

$$[Tr] + [S] = S_t$$

where S_t is the sum of the free trap sites (S) and trap sites occupied by H-atoms (Tr), we can eliminate [S] from equation (7.35):

$$\frac{d[Tr]}{dt} = k_{dp}(S_t - [Tr])[H] - k_p[Tr]$$

$$= [H]k_{dp}S_t - ([H]k_{dp} + k_p)[Tr] \tag{7.36}$$

Integrating equation (7.36) between the limits $[Tr]_{t=0} = 0$ and $[Tr]_{t=t} = [Tr]$:

$$[Tr] = \frac{[H]k_{dp}S_t}{[H]k_{dp} + k_p}(1 - \exp(-([H]k_{dp} + k_p)t)) \tag{7.37}$$

Assume the occupation of the trap precursor sites by H_2 is initially slower than the rate of reactions (7.32) and (7.33), and the accumulation of H_2-site is exponential, we have

$$[H_2\text{-site}] = S_{H2}\,(1-\exp(-k_{H2}t)) \qquad (7.38)$$

where S_{H2} is the final "H_2-Site" density and k_{H2} is the first order accumulation rate constant. Assume also that there is a conservation of total traps, we have

$$S_t + [H_2\text{-site}] = S_0 \qquad (7.39)$$

where S_0 is the initial trap precursor sites.

The fitting of some experimental profiles using equations (7.37), (7.38) and (7.39) are presented in Figure 7.24. The magnitudes of some of the fitting constants are plotted as a function of temperature in Figure 7.25 and listed in Table 7.9.

Comments:

The Arrhenius plot in Figure 7.25 yields an activation energy of 0.01 eV for the depassivation reaction. The value obtained in section 7.2 from the independent trap decay data is 0.15 eV. The activation energy for the passivation reaction is 0.54 eV. This is very close to the value of 0.55 eV obtained from the trap decay analysis in section 7.4. The activation energy for the H_2 occupation of the trap precursor sites is 0.27 eV.

It should be noted that the fit requires that the maximum trap site occupation by H_2 (S_{H2}) be different at different temperatures. At lower temperature, the level of H_2 occupation of trap precursor sites is higher.

7.5.5 Summary

To summarize the above discussions, the effects of exposing an Si/SiO_2 interface to H-atoms can be explained reasonably well by assume that H-atoms can be reversibly bound to

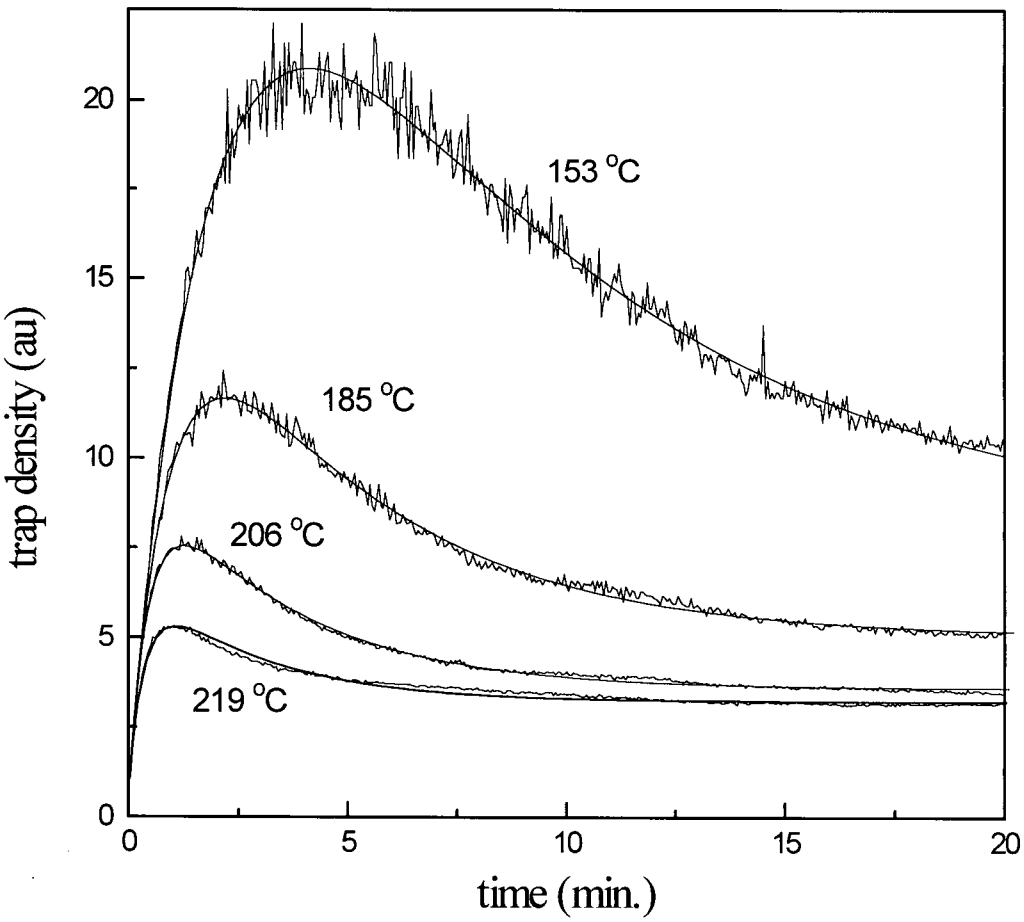

Figure 7.24 The trap density as a function of time when the silicon sample is exposed to H-atoms at the temperatures indicated (early portion of Figure 7.9). The smooth solid curves are the fitting results for the trap precursor site occupation by H-atom and H_2 model.

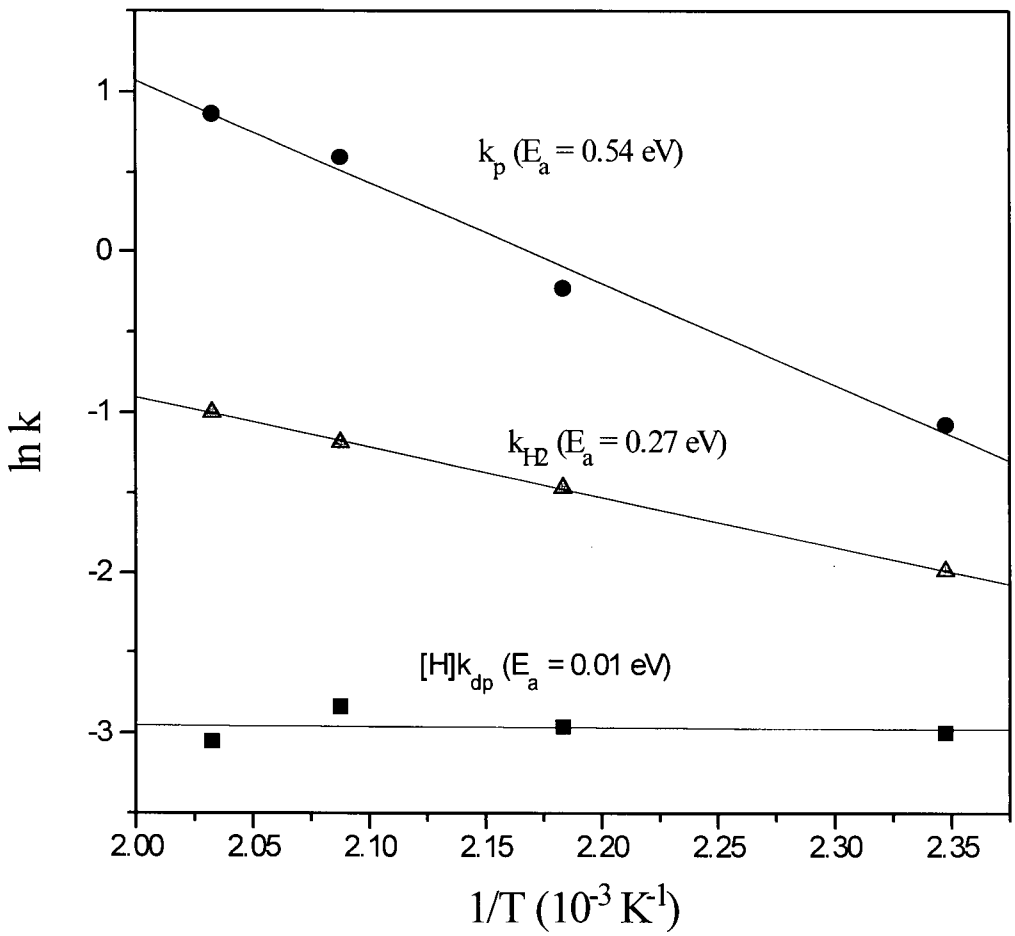

Figure 7.25 Logarithmic plots of the rate constants against the reciprocal temperature for the trap precursor site occupation by H-atom and H_2 model.

Table 7.9 The rate constants and the final H_2-site density for the trap precursor site occupation by H-atom and H_2 model. The total trap precursor sites $S_0 = 300$.

Temperature (°C)	$[H]k_{dp}$	k_p	k_{H2}	S_{H2}
153	0.0499	0.341	0.137	244
185	0.0518	0.798	0.231	234
206	0.0587	1.82	0.305	217
219	0.0472	2.38	0.368	185

certain sites found at the Si/SiO_2 interface. Once the H-atoms occupy these sites, which then have an unpaired electron, they can effectively recombine charge carriers. When H-atoms are removed from the system, the H-atoms can be lost from these carrier-trapping sites. H_2 which is formed by recombination of H-atoms at the interface, can also occupy the same sites that H-atoms do, but irreversibly, removing some of the sites available to H-atoms.

The trap sites must have different binding energies and therefore, the activation energies for the release of H-atoms from their occupation sites have a range of values, which can be described as a Gaussian distribution represented by equation (7.7). Such a distribution could be a result of a varying environment for the trapped hydrogen atom. This could be the consequence of the amorphous structure of silicon dioxide. At any given temperature, weakly bound H-atoms disappear first. On the other hand, traps that have a high activation energy for their release, decay more slowly. If the H-atoms are very tightly bound, the trap decay will be too slow to be measured in our experimental time scale. This explains the "remnant" trap density levels observed in Fig. 7.9 when the H-atoms are shut off.

Chapter 8 Conclusion

Ultra-large scale integration (ULSI) of microelectronic devices has resulted in aggressive scaling of device dimensions into the submicron range. The trend toward even smaller device dimensions has increased concern over the reliability of materials used to fabricate these devices. Of particular concern is the reliability of the Si/SiO_2 interface which is vital to metal-oxide-semiconductor (MOS) device operation. To better understand the chemistry at the Si/SiO_2 interface, a real-time probe is needed to monitor the interfacial states while the material is being processed.

For this purpose, a radio frequency technique was developed for measuring the steady state free carrier density in indirect-bandgap semiconductors. This *in situ* technique is the first of its kind. The essential element in this technique is an RF coil with a resonance frequency at about 240 MHz, that is coupled to a silicon wafer, whose photo-induced free carrier concentration changes can shift that frequency. The frequency change is detected with an RF bridge which consists of three commercially available minicircuit elements. To detect small changes in the photo-induced carrier concentrations the exciting radiation is chopped at a frequency of 200 Hz, and the signal output from the RF bridge is detected with a lock-in amplifier.

At low level photo-injection, the output voltage signal of the RF probe, detected with a lock-in amplifier, was determined experimentally to be proportional to the minority free carrier concentration induced by the radiation, and inversely proportional to the conductivity of the silicon sample. Therefore, the RF probe is effective in measuring changes in both the surface and bulk carrier recombination sites.

Low thermal budget gate oxide growth was achieved by exposing silicon samples to oxygen atoms produced in a remote molecular oxygen discharge at temperatures below 450 °C. The steady state carrier concentration, which is inversely proportional to the carrier trap densities at the Si/SiO_2 interface, was monitored with the RF probe during the oxide growth and subsequent annealing in H_2. The following steps were performed for gate oxide growth: (1) The thermal oxide coating of the standard silicon sample was removed with an HF wash, which produced a well passivated H-terminated surface. (2) The surface was oxidized with O-atoms. Exposure to O-atoms rapidly dropped the steady state carrier concentration below the detection limit of the RF probe due to the formation of P_b centers. The maximum thickness of the oxide that can be formed at below 450 °C was measured to be less than 20 Å with a FTIR absorption spectrometer. (3) The oxidized surface was annealed in the presence of H_2 for 30 minutes at 450 °C. The P_b centers created during the oxidation process were passivated to a level comparable to the thermal oxide by the reaction:

$$P_b + H_2 \rightarrow P_b\text{-}H + H$$

Boron in p-type silicon was also found to be passivated and depassivated during annealing by the formation and dissociation of a B-H complex. Hydrogen did not need to be added because it is already present in the bulk. The B-H complex started to form at about 360 °C, the formation rate increased as the annealing temperature rose. Between 450 and 500 °C, B-H complexes formed and then dissociated, reaching a maximum B-H density in about 85 minutes. More than 95% of the boron could be passivated in this way. Above 520 °C, only dissociation of the B-H complex was observed.

Adsorption of O_2 on a freshly HF washed silicon surfaces can also be detected with the RF probe. The photo-induced steady state carrier concentration was decreased by the adsorption

of O_2 at temperatures up to 200 °C. The adsorbed O_2 on the surface is postulated to draw additional electron density into surface states, therefore, increases band bending and the width of the depletion layer of a p-type silicon. The result of an increase in the width of the depletion layer, or "dead-layer" in which carriers are depleted, is to decrease the photo-induced carrier concentration in the sample. Similar results were observed when a freshly washed surface was exposed to H_2. However, the larger decrease in carrier concentration that is observed is difficult to explain in terms of "dead-layer" theory, and much work is still needed to elucidate the mechanism.

H-atoms can rapidly diffuse through a 170 Å SiO_2 layer and create carrier traps other than P_b centers at the Si/SiO_2 interface by the reaction:

$$H\bullet + Site \rightarrow H\text{-}Site\bullet \qquad (8.1)$$

where "Site" is the trap precursor site, H• is the H-atom at the SiO_2/Si interface and H-Site• is a carrier recombination catalyst (carrier trap) because of the presence of an unpaired electron. At temperatures below 100 °C the trap formation rate is first order in H-atoms with an activation energy of 0.15 ± 0.02 eV. At temperatures over 100 °C its reverse reaction occurs

$$H\text{-}Site\bullet \rightarrow Site + H\bullet \qquad (8.2)$$

Kinetic analysis indicates that this trap passivation reaction does not obey a simple first order rate law. The decay of these traps can be explained by the introduction of a Gaussian distribution of the activation energies that are centered around 0.55 ± 0.13 eV, with a dispersion of 0.13 eV.

At temperatures higher than 100 °C, another process was also detected during the exposure to H-atoms. It slowly reduces the carrier traps created by reaction (8.1). We believe it

is the competition of H_2 with H-atoms for the trap precursor sites that removes some of the trap precursor sites that could be occupied by H-atoms.

Appendix Some Additional experimental Correlation

In Figure A.1, several quantities taken from the curves in Figure 7.9 are plotted against the reciprocal temperature. These are the logarithm of (1) the peak height, (2) the plateau height in the presence of H-atoms, (3) the plateau height when H-atoms are removed, and (4) the time it takes to reach the peak. The slopes of the straight lines drawn through these points, which are listed in Table A.1, are very similar. If we take the peak heights and the final plateau heights that were presented in Figure 7.9, Figure 7.19, and Figure 7.21 and plot their logarithm against reciprocal temperature, we get the lines shown in Figure A.2. Their slopes are listed in Table A.2.

It seems that the final plateau, which the trap density approaches when H-atoms are removed, is the same, no matter how high the H-atoms concentration is or how long the H-atoms exposure is. The final trap density is only dependent on temperature. It can be seen from Figure A.2 that it is higher at lower temperature. This can be explained by the fact that the activation energy for the release of H-atoms from the trap sites is determined only by the structure of the trapping sites. The different environments produce a dispersion in the activation energy. As mentioned above, some traps could have such a high activation energy that their decay is too slow to be measured. If the temperature is raised, more H-atoms will be released from the high activation energy trap sites, making the apparent trap "plateau" density lower than it is at low temperatures.

To test this theory, an SiO_2/Si interface was exposed to H-atoms at room temperature for 10 minutes so that a large concentration of H-atoms could be trapped in the precursor sites. Then

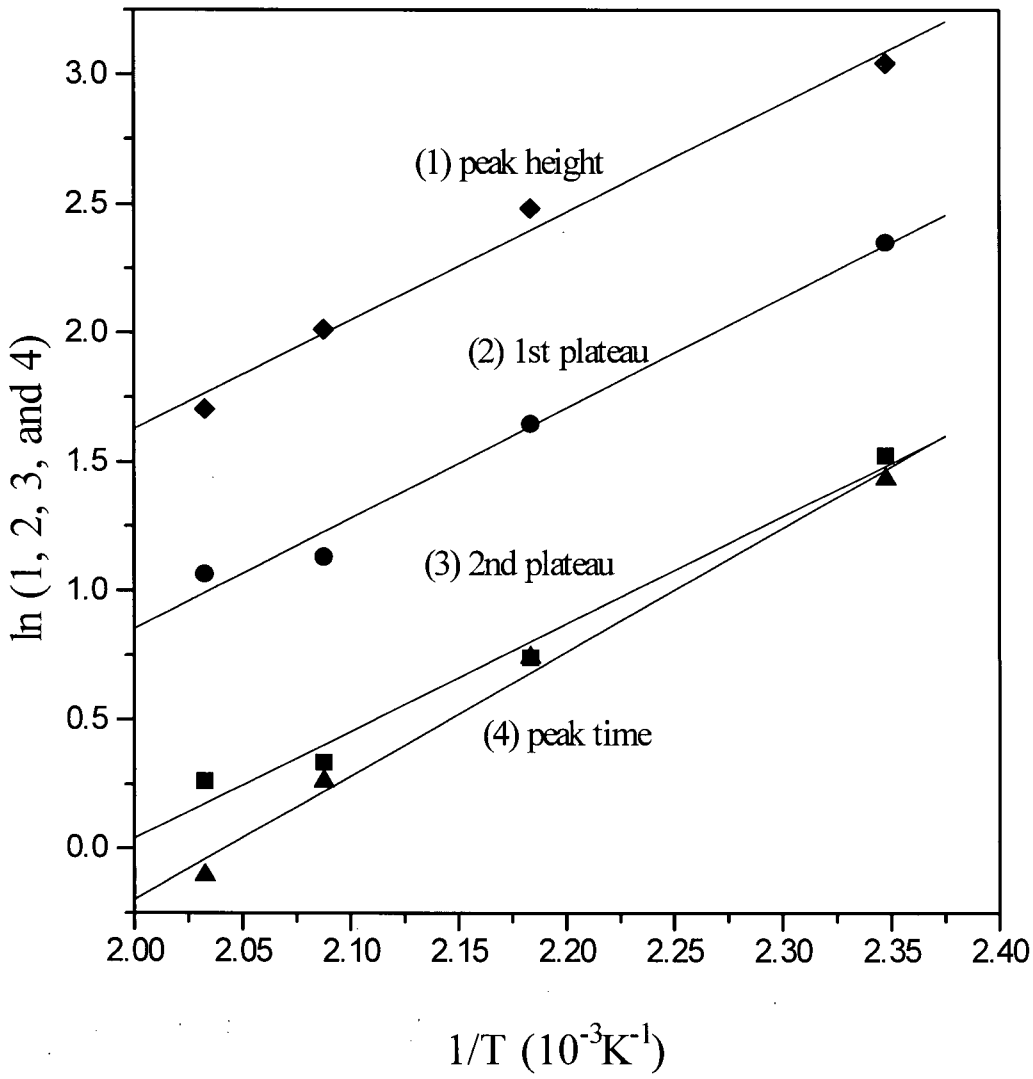

Figure A.1 Logarithmic plots of the peak heights, the plateau heights, and peak time of the curves in Figure 7.9 versus the reciprocal temperature.

Table A.1 The slopes of logarithmic plot of peak height, peak time, plateau height, and plateau height in H-atoms versus reciprocal temperature.

	slope of logarithmic plot against 1/T
peak height	4.2
time to peak	4.8
plateau height in H-atoms	4.3
plateau height	4.2

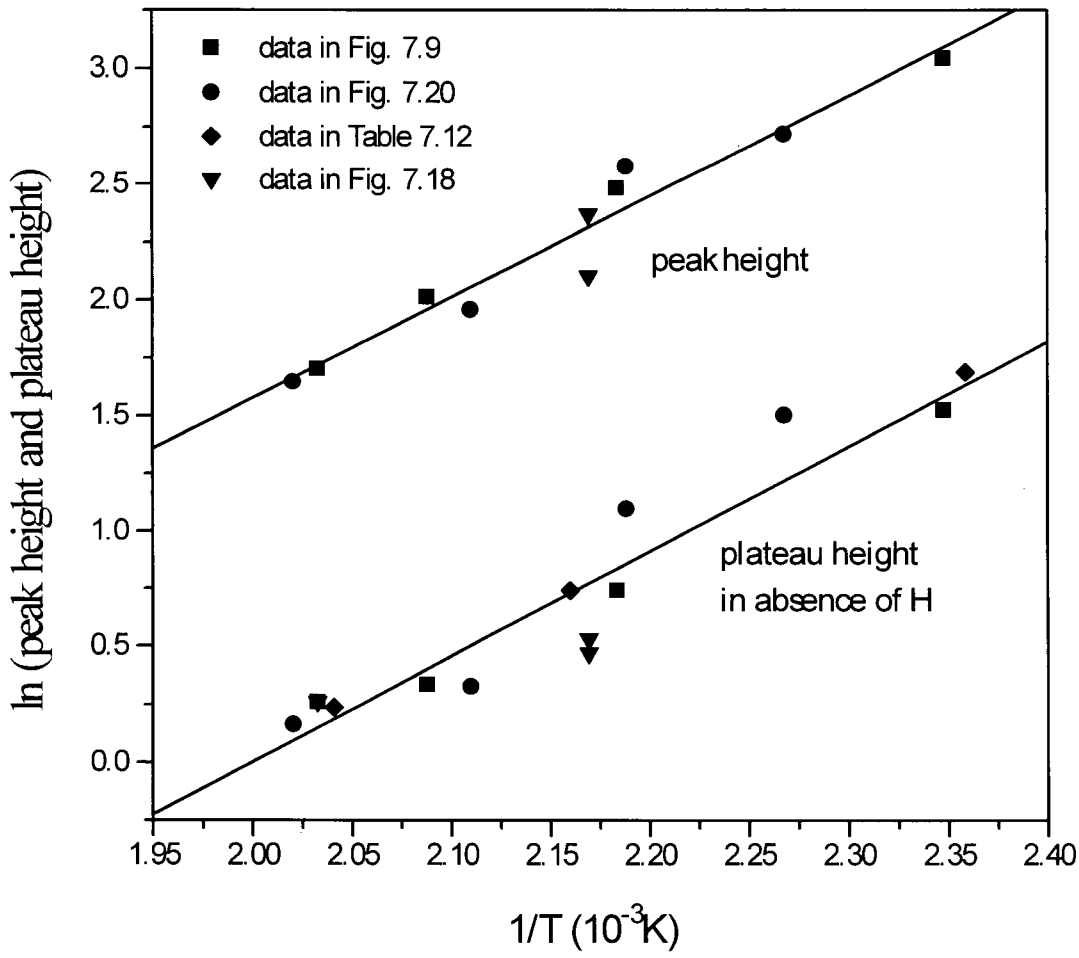

Figure A.2 Logarithmic plots of the peak height and the plateau height taken from Figure 7.9, Figure 7.19, and Figure 7.21, against the reciprocal temperature.

Table A.2 Values of peak height, plateau height, and time to peak obtained from data in Figure 7.9, Figure 7.19, and Figure 7.21.

temperature (°C)	peak height (a.u.)	time to peak (min.)	plateau height in H-atoms (a.u.)	plateau height (a.u.)
Sample was exposed to H-atoms for 20 minutes at temperature indicated (from Figure 7.9)				
153	21.0	4.2	10.5	4.6
185	12.0	2.1	5.2	2.1
206	7.5	1.3	3.1	1.4
219	5.5	0.9	2.9	1.3
Sample was exposed to H-atoms for 15 seconds at temperature indicated (from Figure 7.21)				
184	13.2			3.0
201	7.1			1.39
168	15.2			4.5
222	5.2			1.18
Sample was exposed to H-atoms for 20 minutes at 188 °C then annealed at 219 °C (from Figure 7.19)				
188	10.7	0.35		1.6
188	8.2	1.65		1.7
219				1.3

the sample was annealed for two hours at each of the temperatures: 151, 190, and 217 °C. The trap densities after each annealing step are listed in Table A.3. When the annealing temperature is higher, the trap density is lower. The levels of the final trap density after each annealing is also plotted in Figure A.2 where it can be seen that the trend is the same as it was in the earlier data shown in the same figure.

The trap densities of some samples that we exposed to H-atoms, were measured again at room temperature. The trap density remained at the high temperature value as shown in Figure A.3. This can be understood in the context of the present model. Since H-atoms are released only at higher temperatures, the decrease of the trap density that occurs when the sample is annealed at some higher temperature can not be reversed by decreasing temperature to its original value.

If the trap density is determined by reactions (7.32) and (7.33), the trap density would be higher in the presence of a higher concentration of H-atoms. This is qualitatively consistent with the data in Figure 7.19 in which two samples are exposed to different H-atoms concentrations at the same temperature. With the higher concentration of H-atoms, the steady state trap density is higher. When the external source of H-atoms is shut off, trap densities in both samples decrease to about the same level, because the rate at which the residual traps decay is only a function of temperature.

Additional experimental evidence is presented in Figure A.4. This experiment was performed at 193 °C, and the H_2 flow through the discharge was changed back and forth to vary the H-atoms concentration over the silicon sample. Qualitatively the trap density changed with

Table A.3 The trap density level after annealing at the temperature indicated. The sample was exposed to H-atoms for 10 minutes at room temperature.

annealing temperature (°C)	trap density level
151	5.42
190	2.1
217	1.27

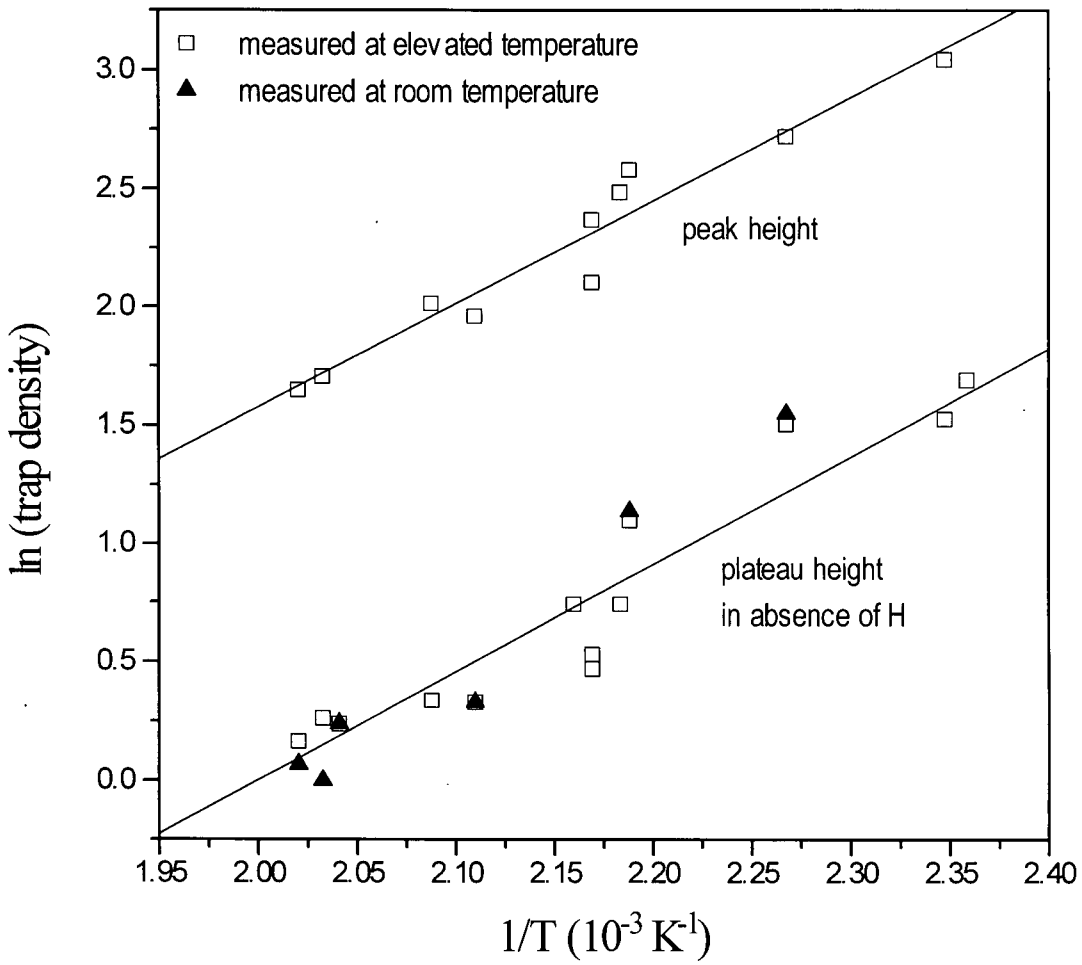

Figure A.3 Trap densities measured when the sample was cooled down to room temperature compare with the high temperature densities that were measured after H-atom exposure.

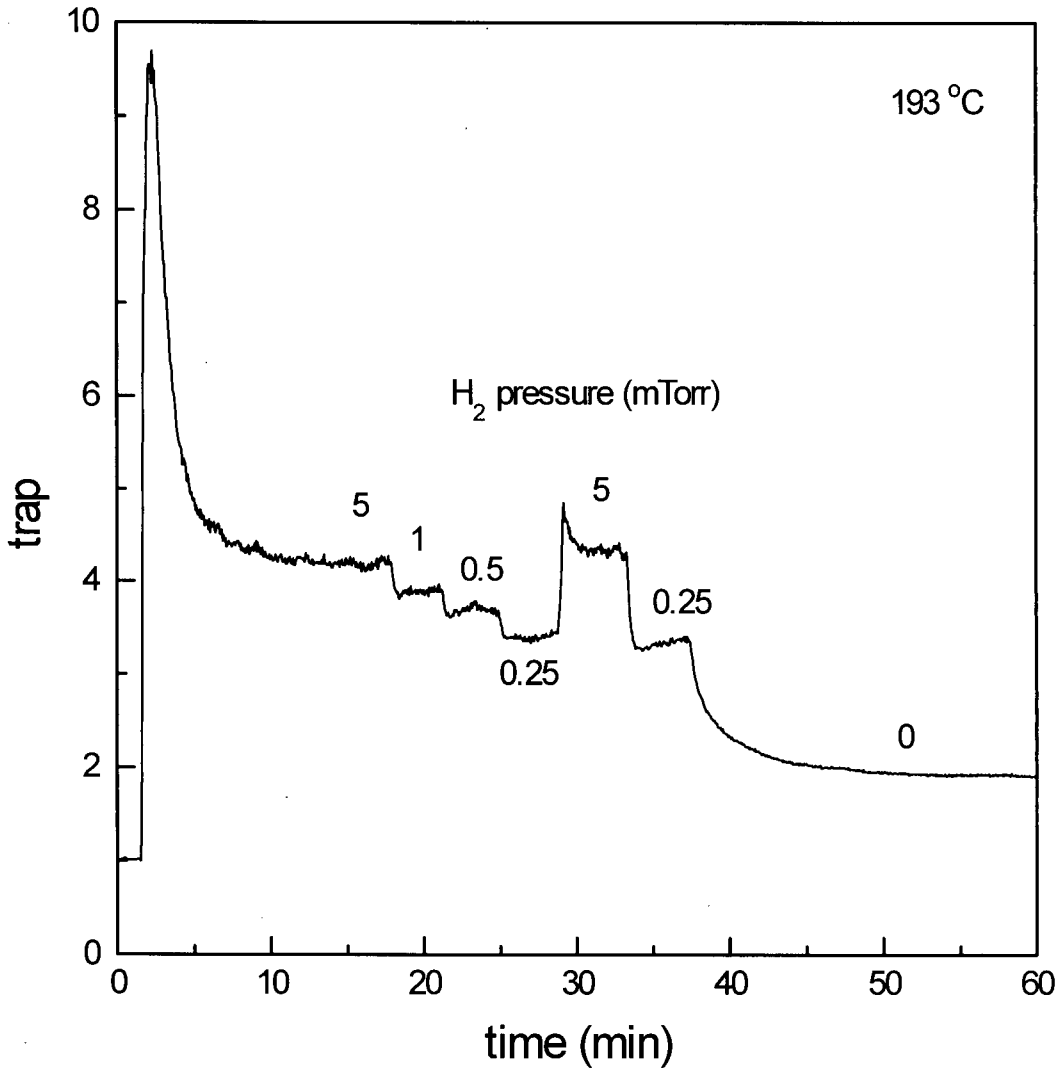

Figure A.4 The steady state trap density changes with different concentrations of H-atoms at 193 °C. The pressure of H_2 passed through the discharge is as indicted.

H-atoms concentration according to the steady state predicted if the process is governed only by reactions (7.32) and (7.33).

References

[1] Max Born, Atomic Physics, 5th ed., Hafner, New York, Chapter VIII, p.261 (1935).

[2] Y. P. Varshni, "Band-to-Band Radiative Recombination in Groups IV, VI and III-V Semiconductors (I) and (II)," Phys. Stat. Sol. **19**, 459 (1967).

[3] J. G. Fossum, R. P. Mertens, D. S. Lee, and J. F. Nijs, "Carrier Recombination and Lifetime in Highly doped Silicon," Solid-state Electron. **26**, 569 (1983).

[4] W. Schottky, "On the Semiconductor Theory of Blocking and Point Contact Rectifiers (in German)," Z. Phys. **113**, 367 (1939).

[5] Sze S.M., Physics of semiconductor devices, 2nd Ed., chapter 5, Wiley-Interscience, New York (1981).

[6] J. Bardeen, "Surface States and Rectification at Metal-Semiconductor Contact," Phys. Rev. **71**, 717 (1947).

[7] W. E. Spicer, I. Lindau, P. R. Skeath, and C. Y. Su, Appl. Surf. Sci. **9**, 83 (1981); W. E. Spicer, S. Eglash, I. Lindau, C. Y. Su, and P. R. Skeath, Thin Solid Films **89**, 447 (1982); A. M. Cowley and S. M. Sze, J. Appl. Phys. **36**, 3212 (1965); R. H. Williams, "The Schottky Barrier Problem," Contemp. Phys. **23**, 329, (1982).

[8] L. J. Brillson, Thin Solid Films **89**, L27-L33, 1982; J. Tersoff, J. Vac. Sci. Technol. **B3**, 1157 (1985); I. Lindau and T. Kendelewicz, CRC Crit. Rev. in Solid State and Mat. Sci. **13**, 27 (1986).

[9] Robert W. Keyes, The physics of VLSI systems, Addison-Wesley, p. 46 (1987).

[10] J. Mavor, Introduction to MOS LSI design, Addison-Wesley, p.127 (1983).

[11] W. Shockley and G. L. Pearson, Phys. Rev. **74**, 232 (1948).

[12] H.-M. Muhlhoff and D. V. McCaughan, in Handbook on Semiconductors, Vol. 4, p282, editor T. S. Moss.

[13] Y. Nishi, Jpn. J. Appl. Phys. **10**, 52 (1971).

[14] J. H. Stathis and E. Cartier, Phys. Rev. Lett. **72**, 2745 (1994).

[15] E. H. Poindexter, G. J. Gerardi, M.-E. Rueckel, P. J. Caplan, N. M. Johnson and D. K. Biegelsen, "Electronic traps and P_b centers at the Si/SiO_2 interface: Band-gap energy distribution", J. Appl. Phys. **56**, 2844 (1984).

[16] K. L. Bower and S. M. Myers, Appl. Phys. Lett. **57**, 162 (1990).

[17] A. Stesmans, Appl. Phys. Lett. **68**, 2076 (1996).

[18] K. L. Brower, Phys. Rev. B **38**, 9657 (1988).

[19] K. L. Brower, Phys. Rev. B **42**, 3444 (1990).

[20] D. J. DiMaria and E. Cartier, J. Appl. Phys. **78**, 3883 (1995).

[21] N. S. Saks and D. B. Brown, "Interface trap formation via the two-stage H+ process", IEEE Trans. Nuclear Sci. **36**, 1848 (1989); R. E. Stahlbush, B. J. Mrstik, and R. K. Lawrence, "Post-irratiation behavior of the interface state density and the trapped positive charge", IEEE Trans. Nuclear Sci. **37**, 1641 (1990).

[22] E. Cartier, J. H. Stathis and D. A. Buchanan, Appl. Phys. Lett. **63**, 1510 (1993).

[23] E. Cartier and J. H. Stathis, Microelec. Eng. **28**, 3 (1995).

[24] Michael L. Reed and James D. Plummer, "Chemistry of $Si-SiO_2$ interface trap annealing", J. Appl. Phys. **63**, 5776 (1988); A. Stesman and G. Van Gorp, Appl. Phys. Lett. **57**, 2663 (1990).

[25] J. M. M. de Nijs, K. G. Druijf, V. V. Afanas'ev, E. VanderDrift, and P. Balk, Appl. Phys. Lett. **65**, 2428 (1994).

[26] A. E. Edwards and G. Germann, Nucl. Instrum. Methods **B32**, 238 (1988).

[27] E. Cartier, D. A. Buchanan, J. H. Stathis, and D. J. DiMaria, J. Non-crystalline Solids **187**, 244 (1995).

[28] Sze S.M. Semiconductor Devices Physics and Technology, John Wiley & Sons (1985).

[29] J. J. Ebers and J. L. Moll, "Large-Signal Behavior of Junction Transistors," Proc. IRE, **42**, 1761 (1954).

[30] W. Shockley and W. T. Read, "Statistics of the Recombination of Holes and Electrons," Phys. Rev. **87**, 835 (1952).

[31] R. Castagne and A. Vapaille, Surface Sci. **28**, 557, 1971; C. R. Acad. Sci. (Paris), **270**, 1347 (1970).

[32] A. R. Gerhard and C. W. Pearce, "Measurement of Minority Carrier Lifetime in Silicon Crystals by the Photoconductive Decay Technique," Lifetime Factors in Silicon (R. D. Westbrook, ed.), Am. Soc. Test. Mat., Philiadelphia, pp. 161 (1980).

[33] T. Tiedje, J. I. Haberman, R. W. Francis, and A. K. Ghosh, "An RF Bridge Technique for Contactless Measurement of the Carrier Lifetimes in Silicon Wafers", J. Appl. Phys., **54**, 2499 (1983).

[34] E. Yablonovitch and T. Gmitter, Appl. Phys. Lett. **49**, 587 (1986); E. Yablonovitch and T. Gmitter, IEEE Elec. Dev. Lett. **11**, 597 (1985); E. Yablonovitch, D. L. Allara, C. C. Chang, T. Gmitter, and T. B. Bright, Phys. Rev. Lett. **57**, 249 (1986); E. Yablonovitch, R. M. Swanwon, W. D. Eades, and B. R. Weinberger, Appl. Phys. Lett. **48**, 245 (1986).

[35] M. Kunst and G. Beck, J. Appl. Phys. **60**, 3558 (1986).

[36] J. A. Hoerni, IRE Electron Devices Meeting, Washington, D.C. (1960); U.S. Patents 3,025,589 (1962) and 3,064,167 (1962).

[37] C. J. Froth and L. Derrick, J. Electrochem. Soc. **104**, 547 (1957).

[38] G. Q. Lo, W. C. Ting, D. K. Shih and D. L. Kwong, Appl. Phys. Lett. **56**, 979 (1990).

[39] X.-L. Ku, R. T. Kuehn, J. J. Wortman and M. C. Ozturk, Appl. Phys. Lett. **60**, 3063 (1992); J. Batey and E. Tierney, J. Appl. Phys. **60**, 3136 (1986).

[40] T. Yasuda, Y. Ma, and G. Lukovski, Appl. Phys. Lett. **60**, 432, (1992).

[41] F. J. Feigl, R. Gale, H. Chew, C. W. Magee and D. R. Young, Nucl. Instr. and Meth. **B1**, 348 (1984); D. A. Buchanan, A. D. Marwick, D. J. DiMaria and L. Dori, in: The Physics and Chemistry of SiO_2 and the Si-SiO_2 interface, ed. C. R. Helms and B. E. Deal, Plenum, New York, p.481 (1993).

[42] R. A. Gottscho, B. L. Preppernau, S. J. Pearton, A. B. Emerson, and K. P. Giappis, J. Appl. Phys., **68**, 440 (1990); E. Yoon, R. A. Gottscho, V. M. Donnelly, and H. S. Luftman, Appl. Phys. Lett., **60**, 2681 (1992).

[43] George. Gu, Hongjun Li, and E. A. Ogryzlo, J. Chem. Soc. Faraday Trans., **91**, 3021 (1995).

[44] H. Li, E. A. Ogryzlo, T. Tiedje and J. G. Cook, Proceeding of the 22nd International Conference on Semiconductors in "The Physics of Semiconductors", D. J. Lockwood Editor, 1, 514, (1995), World Scientific.

[45] W. W. MacAlpine, and R. O. Schildnecht, "Coaxial Resonators with Helical Inner Conductors", Proc. of the IRE, **47**, 2099 (1959)

[46] J. G. Fossum, R. P. Mertens, D. S. Lee, and J. F. Nijs, "Carrier Recombination and Lifetime in Highly doped Silicon," Solid-state Electron. **26**, 569 (1983).

[47] Sorab K. Ghandhi, VLSI Fabrication Principles, Silicon and Gallium Arsenide, Wiley, New York (1982), Chapter 3, P86.

[48] W. G. Pfann, Zone Melting, Wiley, New York (1958).

[49] Dieter K. Schroder, Semiconductor Material and Device Characterization, Wiley, New York (1990), Chapter 1, P5.

[50] T. Yasuda, Y. Ma, Y. L. Chen, G. Lucovski, and D. Maher, J. Vac. Sci. Technol. A, **11**, 945 (1993).

[51] L. Ling, S. Kuwabara, T. Abe, and F. Shimura, Multiple Internal Reflection Infrared Spectroscopy of Silicon Surface Stricture and Oxidation Process at Room Temperature, J. Appl. Phys., **73**, 3018 (1993).

[52] Kohei Kavamura, Shuichi Ishizuka, Hiroyuki Sakaue, and Yasuhiro Horiike, Jap. J. Appl. Phys., Part 1, **30**, 3215 (1991); Hiroki Ogawa, Kenji Ishikawa, Carlos Inomata, and Shuzo Fujimura, J. App. Phys., **79**, 472 (1996).

[53] M. A. A. Clyne, in Physical Chemistry of Fast Reactions, volume 1, Gas Phase Reactions of Small Molecules, edited by B. P. levitt (Plenum Press, London and New york, 1973), Chapter 4, P259.

[54] J. A. Bardwell, K. B. Clark, D. F. Mitchell, D. A. Bisaillion, G. I. Sproule, B. MacDougall, and M. J. Graham, J. Electrochem. Soc. **140**, 2135 (1993); M. L. W. van de Zwan, J. A. Bardwell, G. I. Sproule, and M. J. Graham, Appl. Phys. Lett. **64**, 446 (1994).

[55] Paul F.A. Meharg, Alkane-based Reactive Ion Etching of III-V Semiconductors, Ph.D. Thesis (1992).

[56] Fumio Shimura, Semicondutor Silicon Crystal Technology, p97, Academic Press (1989).

[57] J. I. Pankove, P. J. Zanzucchi, and C. W. Magee, Appl. Phys. Lett. **46**, 421 (1985).

[58] I. A. Veloarisoa, M. Stavola, D. M. Kozuch, R. E. Peale, and G. D. Watkins, Appl. Phys. Lett. **59**, 2121 (1991).

[59] R. A. Gothscho, B. L. Preppernau, S. J. Pearton, A. B. Emerson and K. P. Giapis, J. Appl. Phys. **68**, 440 (1990).

[60] R. A. Street, R. H. Williams, and R. S. Bauer, J. Vac. Sci. Technol. **17**, 1001 (1980).

[61] R. E. Hollingsworth and J. R. Sites, J. Appl. Phys. **53**, 5357, (1982).

[62] E. Cartier, D. A. Buchanan, and G. J. Dunn, Appl. Phys. Lett. **64**, 901(1994).